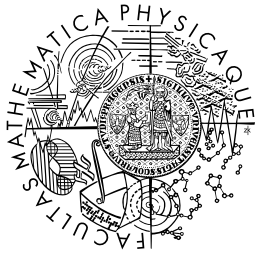

FACULTY
OF MATHEMATICS
AND PHYSICS
Charles University

DOCTORAL THESIS

Ing. Karel Bernášek

Applications of spectrally and spatially resolved NMR: induced anisotropy and phase transition in hydrogels; new relaxation probes for imaging

Department of Low Temperature Physics

Supervisor of the doctoral thesis:	doc. RNDr. Jan Lang, Ph.D.
Study programme:	Physics
Study branch:	Biophysics, Chemical and Macromolecular Physics

Prague 2021

I declare that I carried out this doctoral thesis independently, and only with the cited sources, literature and other professional sources.

I understand that my work relates to the rights and obligations under the Act No. 121/2000 Sb., the Copyright Act, as amended, in particular the fact that the Charles University has the right to conclude a license agreement on the use of this work as a school work pursuant to Section 60 subsection 1 of the Copyright Act.

In ..... date ..... signature of the author

Title: Applications of spectrally and spatially resolved NMR: induced anisotropy and phase transition in hydrogels; new relaxation probes for imaging

Author: Ing. Karel Bernášek

Department: Department of Low Temperature Physics

Supervisor: doc. RNDr. Jan Lang, Ph.D.

Abstract: Nuclear magnetic resonance is a non-invasive way to observe material properties on a molecular level. Magnetic resonance imaging is an important diagnostic tool in medicine. Molecules of several metabolites in muscle tissue show similar interactions as molecules partially oriented in orienting media. These interactions could provide new information about processes *in vivo*, this can serve for diagnostics of metabolism. New insight into the function is gained by observation of metabolites in orienting media. Observable anisotropic interactions in muscle tissue in vivo could be used for diagnostic purposes. Anisotropic NMR interaction of solvent as a new method for observation of phase transition of hydrogel with temperature change or change of solvent composition. Use of magnetic resonance imaging in slices to observe the collapse of polyacrylamide in water-acetone mixtures. Use of diffusion-weighted magnetic resonance imaging to observe phase transition of PNIPAM-based semi-interpenetrating polymer.

Keywords: NMR spectroscopy, NMR imaging, Hydrogel, Partial orientation

Acknowledgements

I want to thank my supervisor Jan Lang. I am the most grateful to Helena Štěpánková for her support during my study and an opportunity to start my own research projects regarding MRI. I want to thank my coworkers, namely Pavel Srb for consultations about NMR in general and especially partial orientation, to Marián Grocký for cooperation on partial orientation, to Hana Kouřilová for discussions about hydrogels, to Petr Dvořák for useful discussion about the measurement of pure water and to Petr Křišťan, Karel Kouřil, Václav Římal, Martin Adamec, and Vojtěch Chlan for discussions regarding study and NMR research. I want to thank my consultant Antonín Škoch for providing an overview of literature about localized NMR spectra of muscle tissue, the study of partial orientation was originally his idea. Experience with polyacrylamide sample preparation was provided by Jiří Vlach. I am grateful to Jan Blahut and Petr Hermann for their cooperation in imaging their magnificent ^{19}F molecular probe that restarted my interest in MRI. I want to thank Martin Burian and Vít Herynek for advice about ParaVision software and discussions regarding MRI. I am grateful to Lenka Kubíčková, Denisa Kubániová, and Jaroslav Kohout for cooperation on study of magnetic nanoparticles as MRI contrast agents. I also appreciate the work of all people at the Faculty of Mathematics and Physics and Charles University that enabled my study and research.

Project of partial orientation of muscle metabolites was supported by grant No. 2010/251272 of the Grant Agency of the Charles University. Investigation of volume phase transition of hydrogels was supported by grant No. 13-23392S of the Czech Science Foundation.

Contents

Introduction **3**

1 Nuclear magnetic resonance **5**
1.1 NMR Basics . . . 5
1.2 Interactions observable in NMR spectra . . . 5
1.3 NMR and partial orientation . . . 7
1.4 NMR with spatial resolution . . . 9

2 Partial orientation of muscle metabolites **14**
2.1 Muscle anatomy and physiology . . . 14
2.2 NMR spectra of muscle tissue . . . 14
2.3 Carnosine . . . 18

3 Hydrogels **21**
3.1 Gelatin as orienting media . . . 21
3.2 Polyacrylamide (PAM) as orienting media . . . 22
3.3 VPT of Polyacrylamide . . . 23
3.4 VPT of poly(*N*-isopropylacrylamide) . . . 24

4 Sample preparation **27**
4.1 Gelatin samples . . . 27
4.2 Polyacrylamide (PAM) samples . . . 27
4.3 Poly(*N*-isopropylacrylamide) samples . . . 29

5 Partial orientation of carnosine **31**
5.1 Setting of NMR measurements . . . 31
5.2 Remarks on sample preparation . . . 32
5.3 Properties of the orienting media for NMR . . . 37
5.4 Determination of RDCs and partial orientation . . . 37
5.5 Comparison of *in vitro* model and *in vivo* data . . . 40
5.6 Summary of chapter . . . 41

6 Response of hydrogel by localized NMR **43**
6.1 Setting of NMR measurement . . . 43
6.2 Remarks on sample preparation . . . 44
6.3 Partial orientation and stimuli-responsive hydrogels . . . 46
6.4 VPT of PAM by localized partial orientation . . . 49
6.5 MRI of PNIPAM response to temperature stimuli . . . 54
6.6 Summary of chapter . . . 60

7 MRI of ^{19}F molecular probe and IONPs **62**
7.1 Setting of NMR measurement . . . 62
7.2 MRI of ^{19}F molecular probe . . . 63
7.3 Measurement of novel IONPs . . . 66
7.4 Summary of chapter . . . 68

Conclusion **70**

Bibliography **73**

List of Figures **82**

List of Tables **83**

List of Abbreviations **84**

List of Conference Contributions **86**

List of Publications **87**

A Attachments **88**
A.1 First Attachment 88

Introduction

Presented thesis focus on method of nuclear magnetic resonance (NMR) [1], [2]. NMR can provide unique knowledge about molecules of interest on a molecular level up to a macroscopic scale in a non-destructive way. An exciting option is utilizing the NMR signal spatial resolution by gradients of the magnetic field, known as magnetic resonance imaging (MRI).

MRI has become very important diagnostic tool in medicine that enables non-invasive observation of water, fat, and even individual metabolites in tissue *in vivo*. The information gained from *in vivo* NMR measurement corresponds to density and properties of ^{1}H containing molecules with a high degree of motion in the human body, mainly water, fat, and small molecules. The ratio of the most abundant metabolites can be estimated by localized NMR and use for the diagnostic of pathologies. An interesting phenomena was observed in muscle tissue *in vivo* [3], [4]. Signals of metabolites showed additional splitting that was dependent on the orientation of muscle fibers in the magnetic field of an MRI machine. The observed phenomenon is caused by residual dipolar coupling (RDC) introduced by a partial orientation of observed molecules. A fit of alignment tensor evaluates RDCs derived from the proposed structure to experimental values [5]. Specific molecular orientations are less probable than others due to steric hindrance induced by a media, in this case, structures of muscle cells. The actual state of particular molecules *in vivo* is complicated to determine as several compartments with different properties can be present in the observed volume. Interpretation of *in vivo* data could be made by comparison to *in vitro* model where RDCs of a given metabolite can be measured for almost all possible RDCs. Such an approach would be to determine as much RDCs *in vivo* as possible and compare values with *in vitro* model based on stretched hydrogel where all signals of the selected molecule can be observed. NMR has been used for a long time as an interesting method for the study of macromolecular materials in general [6].

Hydrogels are an important class of materials with potential for utilization in medicine and manufacturing [7]. NMR spectroscopy and imaging have already been proven methods for characterizing macromolecular systems [6]. Some hydrogels can respond to certain stimulus, such as adding a different solvent or change of temperature. The first observation was a collapse of polyacrylamide (PAM) in water-acetone mixtures [8]. Change of interactions between polymer fibers and solvent cause phase transition. At a specific condition, the interaction between polymer fibers is preferable to interaction with the solvent. Linear polymers are in the state of a random coil, but globular structures are created from polymer fibers in case of phase transition. In cross-linked polymers, the process is more complicated due to the entrapment of solvent molecules in collapsing fibers. The initial aim was to characterize cross-linked poly(*N*-isopropylacrylamide) (PNIPAM) hydrogel that shows volume phase transition at a specific temperature by detection of partial orientation. The response of PNIPAM based hydrogel to temperature stimuli can be considered reversible. Data from a partial orientation of a suitable molecule could gain new insight into processes during the collapse and swelling of the polymer network.

Acquisition of new equipment enabled imaging in three dimensions. Solvent

hindrance effects were reported for cross-linked PNIPAM, and semi-interpenetrating networks were polymerized to obtain hydrogels with a faster response to stimulus. The response of a polymer network is heavily dependent on the morphology and dimensions of a sample. Detection of bound water by diffusion-weighted imaging (DWI) provides a way to characterize hydrogel response to temperature stimulus. Effects of solvent hindrance by a collapsed network with gradual proliferation from the surface to the core of hydrogel could be observed by diffusion-weighted imaging (DWI). MRI is a great tool to observe reversible changes in a temperature-responsive hydrogel cylinder, where changes can be characterized on a slice in the middle of the cylinder.

NMR is the primary spectroscopic method in the presented work. A brief introduction to this wonderful method is in Chapter 1. Current state of knowledge about partial orientation in muscle tissue *in vivo* with focus on carnosine is in Chapter 2. The basic description of orienting media used to introduce partial orientation and the volume phase transition for PAM and PNIPAM is provided in Chapter 3. The preparation of samples for partial orientation and volume phase transition is showed in Chapter 4. Measurements and results of partial orientation of carnosine in *in vitro* model with comparison to data *in vivo* are in Chapter 5. Utilization of partial orientation for localized NMR measurement of volume phase transition of PAM after acetone addition is in Chapter 6. Measurement of MRI on new ^{19}F molecular probe and IONPs is shown and discussed in Chapter 7.

1. Nuclear magnetic resonance

1.1 NMR Basics

Nuclear magnetic resonance (NMR) spectroscopy and imaging [1], [2] provide a way to directly observe populations of molecules in a given sample. NMR became important method for physicists, chemists, and physicians.

The essential phenomena for NMR is the Zeeman effect. A splitting of energy levels of an atomic nuclei with non-zero spin in external magnetic field. Proton and neutron have an intrinsic moment called spin, it is also valid for atoms, almost every element in the periodic table can be measured by NMR. A nucleus with a spin quantum number I has a dipolar magnetic moment μ with projections to an axis z quantised to the values $\mu_z = m\hbar\gamma$ where the quantum number $m \in \{-I, -I+1, ..., I-1, I\}$, $\hbar$ is the reduced Planck constant and γ is the gyromagnetic ration for the given isotope. In a static magnetic field B_0 collinear with $z(\mid B_0 \mid = B_0 = B_z)$, the stationary magnetic energy levels of a nucleus, $E_m = -B_0 \cdot \mu = -B_0\mu_z = -m\hbar\gamma B_0$ belonging to particular values of m, are not equal, which is known as Zeeman effect. The individual levels are differently populated in a sample containing N nuclei in a thermodynamic equilibrium according to the Boltzmann distribution, leading to a macroscopic nuclear magnetization $M = \frac{NI(I+1)\hbar^2\gamma^2}{3kT}B_0$ given that $\hbar\gamma B_0 \ll kT$, satisfied in the achievable laboratory condition The observed energy difference is proportional to an applied magnetic field. The resonance frequency at given magnetic filed is determined by product of field intensity and the gyromagnetic ratio that characterizes particular nuclei. The best candidates for NMR studies are ^{1}H, ^{2}H, ^{13}C, ^{15}N, ^{19}F, and ^{31}P. Natural abundance is very important factor, isotopic labeling is necessary to gain signal in reasonable time.

System of spins is manipulated only in case that frequency of excitation radiation fulfill resonance condition. After excitation a spin system returns to equilibrium. Energy transfer in a material is characterized by relaxation times. Two relaxation times provide a description of spin ensembles. Longitudinal relaxation, denoted as T_1, characterize energy exchange of spin system lattice, it is called spin-lattice relaxation. Transversal relaxation denoted as T_2, characterize coherence of spin magnetization, it is called spin-spin relaxation time.

1.2 Interactions observable in NMR spectra

There are four interactions that can be observed in NMR spectra: chemical shift, direct dipole-dipole interaction, indirect dipole-dipole interaction (J-coupling), and nuclei with the spin I $> \frac{1}{2}$ there is quadrupolar interaction. The focus of this work was on direct dipole-dipole interaction as partial orientation is a manifestation of the influence of orienting media. The aim is to obtain information about spatial dependencies of atomic bounds from direct dipole-dipole interaction used in solid-state measurements but still have narrow lineshapes in order to resolve individual signals as can be done in liquid-state measurements.

Chemical shift is field-dependent interaction expressed in parts per million

(ppm) of the resonance frequency of reference compound. Averaging of a local magnetic field by nearby electrons enables to elucidate the chemical environment of observed spins. Chemical shift provides information about the local environment of an observed population of atoms. In the case of continuous measurement with a change of conditions (e.g., temperature), the chemical shift can provide helpful information. Chemical shift value is averaged to a specific value influenced by the unique local environment and size of spin populations. In solid materials, other interactions cause the broadening of spectra. The chemical shift value is averaged from all contributions due to fast rotational diffusion in liquids and gases.

Direct dipole-dipole interaction can be imagined as an interaction of two bar magnets in an external magnetic field in space. The magnitude of splitting is dependent on the angle and distance of two nuclei in space. Additional energy terms (splitting of individual signals) that characterize dipole-dipole interaction could provide valuable information in solids about the orientation of spins in an external magnetic field. In the case of monocrystal changing angular dependence in magnetic field splitting magnitude dependencies are observed. The spins (atom nuclei) can be described as two interacting magnets that feel each other in space. Direct dipole-dipole interaction is distance-dependent. Dipole-dipole interaction cannot be observed directly in liquids due to fast exchange without any spatial dependence (e.g., partial orientation) is averaged to zero. Geometrical factor governs the magnitude of observed partial orientation. NMR is usually presented as a local method, but with direct dipole-dipole interaction, an effect of orientation of spin pairs in external magnetic in entire molecule can be observed.

Indirect dipole-dipole interaction, also known as J-coupling, provides direct observation of the manifestation of chemical bonds. This phenomenon is created by the fine interaction of the nucleus with valence electrons of another nucleus connected with chemical bonds. Indirect dipole-dipole interaction is one of few cases where chemical bound can be observed.

Quadrupolar interaction is present if there is a non-spherical distribution of electric charge at the atomic nucleus. If the quadrupolar interaction is present, it is the dominant interaction that determines the energy levels and observed NMR signals in spectra. It is dominant interaction for spins $I > \frac{1}{2}$. Electric interactions are a thousand times stronger than magnetic interactions.

It should be mentioned that there are also several issues associated with NMR. The most painful aspect of NMR is sensitivity, as NMR signal is detected by measurement of the induced voltage in a coil. The thermal fluctuation of circuit components causes noise. Noise can be reduced by the repeated acquisition of induced signal or cooling of the circuit used for measurement.

Simple spectra are measured by $\frac{\Pi}{2}$ or 90 deg pulse, that tilt precessing magnetization fully to the transversal plane. Information about different molecules and even different groups in one molecule can be gained from simple NMR spectra of a liquid. After excitation pulse a signal free induction decay (FID) is observed. Spin echo is a phenomena utilized for measurement of relaxation or diffusion. T_2 value can be estimated from full with at half maximum (FWHM). In case of faster repetition of excitation pulses magnetization in transversal plane is not maximal for $\frac{\Pi}{2}$ pulse but at so called Ernst angle [1]:

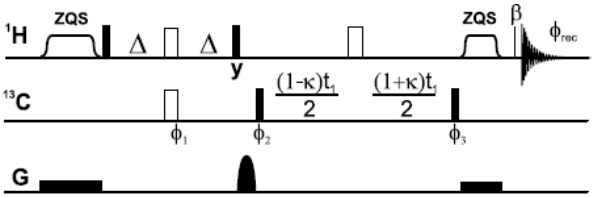

Figure 1.1: P.E.HSQC pulse sequence.
Pulse sequence used for measurement of ^{1}H-^{13}C RDCs. Version with improved appearance of multiplets [9].

$$\alpha_E = \cos^{-1}(\exp[-TR/T_1])$$

For localized measurement *in vivo* intensity of NMR signal of metabolites could be dependent on repetition time of pulse sequence. Spin 1/2 has two level transition, for higher spin numbers and spin system, energy transition diagram is complicated. Heteronuclear correlated NMR spectra such as (HSQC). Correlation of ^{1}H and ^{13}C in order to distinguish individual couplings. In case of ^{1}H-^{13}C splitting there is weak coupling, additional splitting is directly coupling.

1.3 NMR and partial orientation

An elementary derivation of key equation for RDC can be obtained from [10]. Averaging over certain orientation is described by tensor. There are four possible solutions, a mirror images by the axis system. Three Euler angles and two component of diagonalized alignment tensor provide determination of partial orientation. The magnitude of partial orientation is given by

$$(3\cos^2\theta - 1)$$

where θ refers to internuclear orientation in molecule of interest. Partial orientation can also be introduced just by insertion to a high magnetic field. Small but measurable additional splittings were observed on proteins at high magnetic fields. Partial orientation was used for the determination of molecular structure due to one director. All those orientations can be used to determine one alignment tensor in the case of rigid molecular structure.

It is about alignment tensor that describes partial orientation by a fit of proposed molecular structure and expects RDCs for given alignment tensor and structure to measured RDCs. Additional splitting by direct dipole-dipole interaction in liquids is not observed as the motion of molecules is not restricted. It is desirable to turn it on and get information about the observed system and still have NMR spectra with narrow signals that do not overlap. RDC requires introducing a uniaxial director, a force that causes averaging to be anisotropic in a suitable way. This situation is created when averaging of molecule motion is suitably anisotropic. Use for determination of molecular structure in case of rigid molecules or observe the effect of dynamic averaging of conformations of molecules of interest. Dipole-dipole interaction is the main relaxation mechanism

in liquids. Suppose we would obtain partial orientation and still a fast movement of molecules so that signal line-width is low. We can still obtain resolved signals in NMR spectra and get information about the structure of a molecule from dipole-dipole interaction. NMR provides a way to determine which parts of the molecule are rigid and which are moving in liquid. Use of RDC measurement for small organic molecules [11], [12] and for large biological macromolecules [13], [14]. Especially ^{1}H-^{15}N RDCs provide valuable information about the proposed structure of proteins.

An anisotropic environment is in this case polymer network or interacting liquid-crystalline media, that has one preferable axis created by stretching. Observed phenomena are residual dipolar coupling (RDC) and residual quadrupolar coupling (RQC). Both are observed as an additional splitting of NMR signals. Particularly interesting is the fact, that those anisotropic interactions are averaged out from all observed molecules, so the exchange of molecules between the free liquid and alignment media has to be very fast, the target molecule should not bind to orienting media. PALES [15] requires at least five independent RDCs to fit any alignment tensor to the proposed molecular structure. A coupling characterizing residual dipole-dipole interaction has to be determined from total splitting. In heteronuclear cases, e.g., ^{1}H-^{13}C RDCs, the coupling is determined as half of the additional splitting to indirect dipole-dipole interaction (J-coupling). However, in the case of ^{1}H-^{1}H RDCs, a strong coupling occurs that makes the determination of coupling from measured ^{1}H spectra more complicated. Detection of direct dipole-dipole interaction by multiple-quantum (MQ) NMR experiments. It was shown that measurement of build up of double-quantum (DQ) transitions could provide information about dipole-dipole interactions in macromolecular system. Difference between additional splitting observed in NMR spectra and coupling used for structure and alignment tensor fitting. Both measurements, narrow lines as in liquids, signals of individual molecules can be distinguished, and information about orientational dependence by dipole-dipole interaction that is dominant is solids. The information gained by NMR from liquids is averaged by rapid rotational and translational diffusion enabling discrimination and characterization of individual spin populations. There is also an influence of partial orientation that similar effect induced by orienting media is observed as chemical shift anisotropy. In heteronuclear case there is a weak coupling that enable easy extraction: 2 * RDC = Total - J-coupling. Heteronuclear J-coupling is so large that doublets are separated and do not overlap. Even very small additional splitting can be determined. For homonuclear RDCs, a situation is more complicated as signals are overlapped, J-coupling magnitude is comparable to additional splitting. Determination of splitting sign could be an issue in ^{1}H NMR spectra, where the signal overlap of additional splitting and effects of magnetic field homogeneity complicate the determination of coupling. Sign of splitting could be not certainly derived for ^{1}H-^{1}H RDCs from simple ^{1}H spectra. Measurement of ^{1}H-^{15}N HSQC type spectra provide RDCs in peptide research that can be used for the determination of structure. At natural abundance measurement of ^{1}H-^{15}N HSQC spectra are time-consuming, and larger molecules are needed to get at least five independent RDCs for the fitting of any alignment tensor. For small molecules, ^{1}H-^{13}C RDCs can be used for alignment determination. However, in the case of CH_2 or CH_3 group, motional averaging has to be considered to influence the observed

value of additional splitting. In the homonuclear case, the most easily available data are for ^{1}H-^{1}H RDCs there is a severe complication called strong coupling. The coupling constant can not be directly determined from splitting, and fitting all observed spins together is necessary. The introduction of indirect dimension by exclusive correlation spectroscopy (E.COSY) can determine the sign of coupling.

For evaluation of partial orientation, a software PALES (Prediction of ALignmEnt from Structure) for evaluation of measured RDCs and proposed structures was used, [15]. PALES has three modules for the determination of alignment from the proposed structure The most suitable method for small molecules in PALES is -bestFit. Correlation of measured RDCs with back-calculated RDCs obtained from proposed structure, alignment tensor is fitted, the magnitude of the main and the axial component can provide information about the accuracy of a fit when compared with a similar rigid molecule in the same orienting media. -bestFit option is suitable for small molecules and orienting media that are complicated to simulate. Well-defined structures of complete macromolecule or smaller fragments enable determination of alignment tensor S from the observed dipolar couplings. All five independent elements of the alignment matrix can be determined, provided a minimum of five experimental RDCs are available. The essential assumption for PALES RDCs evaluation is that molecule of interest is rigid. The effect of averaging due to several conformations influence observed values RDCs. PALES approach is suitable for larger molecules and orienting media can be simulated as planes or cylinders, although more complicated shapes can be made with more demanding calculations.

1.4 NMR with spatial resolution

In order to observe origin of NMR signal, magnetic field have to be inhomogeneous, preferably with linear dependence of intensity of magnetic field. In such conditions, the resonance frequency is dependent of position in such a magnetic field but only in one direction. Discrimination of NMR signal in space can be done by two way, frequency or phase encoding. The first one is the frequency encoding of a signal, when gradient is applied during selective RF pulse or during whole acquisition. The other is to encode position gradual change of phase, a phase of NMR signal is made spatial applying short but intensive gradient of magnetic field without RF pulse or acquisition. The resolution is given by number of changes of phase encoding. NMR image is NMR spectrum with low resolution corresponding to frequency ranges that determines voxel of origin. A very useful review about MRI with original references is provided at [16]. The use of a gradient of magnetic field enables localization of NMR signal in space. NMR provides a way to observe changes as non-ionizing radiation is used, a measurement can be repeated, and *in vivo* time series can be obtained. MRI measurement can be repeated as often as required for diagnostics.

Frequency encoding is achieved when pulse field gradient (PFG) is present during the pulse for slice selection or during the acquisition of NMR signal for spatial resolution of a given area. Frequency encoding can be utilized with a reconstruction of the image by back-calculated projection. By frequency encoding signal and measurement of FID spins with very short T_1 can be localized and characterize. The NMR signal of such spins can be enhanced by frequent

repetition using T_1 contrast. A flip angle with the highest signal at the given repetition rate and relaxation is given by Ernst angle. Frequency encoding is based on dependence of resonance frequency on local field that has linear change due to gradient. Disadvantage is a cancellation of peak near each other in chemical shift, observation of signal also in inhomogeneous fields.

A systematic change of gradient magnitude without excitation or detection achieves phase encoding. Phase is a very interesting property of NMR signal. Phase encoding can provide a way to obtain NMR spectra from a layer or individual voxels if phase encoding is used in both dimensions. A disadvantage of phase encoding is the time required, as the number of scans required is equal to spatial resolution. There are also artifacts when not enough number of phase encoding steps is set. Voxel 'bleeding' is when data from one voxel contribute to signal in surrounding voxels [17]. Phase encoding is used for chemical shift imaging.

Utilization of slice selection in three dimensions to obtain phase sensitive localized spectra. Influence of T_2 on NMR signal intensity of localized spectra as certain time is required for shaped pulses with gradients to excite spins only in given area of interest. There are two pulse sequences usually used to acquire localized NMR spectra, PRESS and STEAM. The RARE pulse sequence is a speedy way to obtain a relaxation weighted image. A long train of spin echoes creates a strong T_2 filter combined with a short repetition time to provide T_1 weighted image of long T_2 species. The pulse sequence is based on trains of echoes that enable the acquisition of multiple k-space lines after one excitation pulse.

DTIST is the abbreviation for diffusion tensor imaging standard sequence that uses spin echo with diffusion filter to acquire images. This sequence can be used to measure diffusion tensor in biological tissues for stationary samples, as one phase encoding is done in one repetition of sequence. The setting of lower resolution enables faster acquisition of image due to signal attenuation by diffusion filter. To evaluate the apparent diffusion coefficient or diffusion tensor measurement have to repeat to obtain several diffusion filter strengths, and data for several gradient orientations have to be acquired. DTIepi is diffusion tensor imaging combined with echo-planar imaging (EPI). EPI is similar to the RARE sequence, but instead of spin-echo, a train of gradient echoes is used to acquire data in k-space. The combination of EPI with diffusion filter provides a faster way to measure images. A drawback of measurement is that echo train intensity decline with T_2*. This pulse sequence is suitable for fast measurement of changes with lower resolution.

MRI have been used in soft matter research [18], [6]. A non-invasive way of measurement and the possibility to observe solutes and solvent behavior inside soft matter provide a unique description of samples. In two ways, frequency encoding can be used, selective observation of a particular layer by selective pulse or frequency dependence of position in a gradient of the magnetic field measured by gradient during the signal acquisition. Single voxel methods are used to obtain a spectrum from a particular area. There are two pulse sequences usually used to obtain localized NMR spectra from the selected volume. The PRESS pulse sequence is point resolved spectroscopy is based on three echoes that provide spectroscopic information from the rectangular area. The STEAM pulse sequence

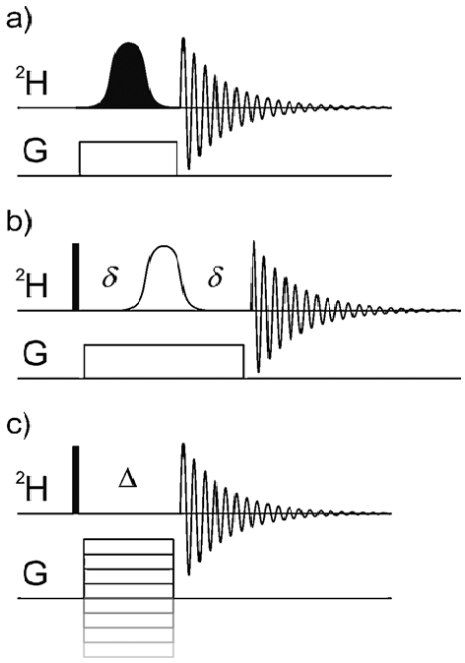

Figure 1.2: The z imaging pulse sequences.
Pulse sequences to obtain spatial resolution by (a) selective-excitation combined with gradient, (b) broadband excitation with space selective spin echo or (c) phase encoding experiment with incremented gradient strength [19].

is based on the stimulated echo approach. STEAM can start acquiring data faster. It is due to 90 deg pulses that are shorter than refocusing 180 deg pulses used for PRESS. Comparison and artifacts associated with spectroscopic imaging were described in [17]. Overlap of signal from different layers due to the low resolution of an image in case of phase encoding. Voxel 'bleeding' could occur in a case of a low number of steps for phase encoding. The signal from neighboring areas leaks to observed space, the solution is increase number of k-space lines, more steps for phase encoding.

The use of stronger gradients for frequency encoding suppresses chemical shift artifacts but also causes a signal to be spread to noise. Gradient strength should be a compromise to acquire an intense NMR signal without artifacts observable in frequency encoded dimension. Phase encoding has a limiting factor at a low number of steps, low resolution in phase-encoded direction, where 'bleeding ' can occur, information from another voxel is contained in a particular voxel. Selection of pulse sequence for imaging can influence observed NMR signal intensity, especially with the use of a higher magnitude of the gradient.

Acquisition of images focuses on spatial resolution rather than the precise determination of relaxation or diffusion. PFG used for excitation of slice and phase and frequency encoding also cause dephasing of NMR signal that affects the observation of signal. Use of PFG to encode spatial distribution of observed species. Spin echo by refocusing NMR signal after excitation using RF pulse called π pulse. Gradient echo is created by a suitable combination of the magnetic field gradients. Gradient echo provides several advantages. TE of gradient echo sequences could be shorter than in the case of spin echo. A limitation for MRI measurement *in vivo* is the heating of tissue by RF pulses. A disadvantage of

gradient echo is a dependence of signal intensity on T_2*, instead of T2 as in the case of spin echo. By gradient echo, a local fluctuation can be observed because of sensitivity to changes in magnetic field homogeneity that influence the observed signal. T_2* is dependent on the local magnetic susceptibility. In case of gradient echo there is greater spatial influence of inhomogeneities. A change of susceptibility occur on the boundary of hydrogel and solution. Determination of relaxation or diffusion directly from images is described in [20]. It is better to use block for obtaining T_1 or T_2 contrast and then repeat the same imaging block. Change of echo time in imaging sequence can introduce non-equal attenuation of NMR signal. Observation of susceptibility change in images, a properties of local magnetic field are changing after stimuli, hydrogel is more dense and magnetic properties are different. There should be the same excitation conditions for all lines of k-space. There are two main advantages of gradient echo, the first is that no shaped pulse is required for refocusing and that no RF power is induced in sample. Gradient echo can obtain image faster and with lower energy deposited to a sample, especially in case of biological samples. Multi-slice multi-echo (MSME) is spin echo based imaging sequence combining phase and frequency encoding. It is suitable for larger T_2 values, it also heavily T_1 weighted. Use of smaller flip angle is optional for maximizing magnetization in the transversal plane, see Ernst angle for further elucidation. Fast low angle shot (FLASH) is gradient echo based pulse sequence. After excitation pulse pulse a suitable gradient is applied to achieve similar effect as for spin echo. The difference is that echo amplitude does not correspond to T_2 but T_2*. Image is heavily influenced by inhomogeneity of magnetic field, especially at boundaries of two regions with different magnetic susceptibility. Rapid acquisition with relaxation enhancement (RARE) is spin echo based sequence [21]. An echo train similar to CPMG is used for obtaining k-space lines after one excitation pulse. RARE number determines number of echoes acquired after excitation pulse. It is important where is the center of k-space that determines intensity in images. In ParaVision 6.0 the middle phase encoding gradient has lowest magnitude in the middle of loop. The observed image is T_2 weighted with TE value corresponding to the middle of pulse train. Echo planar imaging (EPI) is gradient based echo train. method based on train of gradient echoes Ultrashort TE (UTE) is a method that uses radial encoding of signal in form of projections that enable back-calculation of spatial distribution of spins [22], [23]. Changes can also be evaluated for whole sample of for different levels that can be compared. Based on train of spin echoes, that enable measurement of whole image with just one excitation pulse. RARE factor determines number of echoes after excitation pulse. Train of gradient echoes that samples k-space. RARE is T_1 and T_2 weighted pulse sequence. T_2 weighting has stronger effect on a signal due to acquisition of k-space in train of echoes, where quite larger attenuation of a signal with lower T_2 value is observed. In a case of FID, the first point of time dependent voltage induction a NMR coil determines intensity of all signal in 1D NMR spectra. In case of NMR imaging this point correspond to the four points in the middle of k-space and the lowest value of gradient for phase encoding is for both polarities of applied gradient.

NMR provide unique way to study directly diffusion of solute or solvent molecules. Diffusion measurement is unique feature of NMR, self-diffusion of molecules can be obtain without addition of trace as in the case of fluorescence

measurement. Diffusion weighted imaging could be used to diagnose tissues *in vivo* without using any contrast agent. It is convenient in case of low signal-to-noise ratio to rather fit linear dependence. In case of diffusion intensity ratio of logarithmic dependence with strength of applied gradient is a quadratic function. Very important for fitting of such a dependence is SNR.

2. Partial orientation of muscle metabolites

2.1 Muscle anatomy and physiology

Muscle tissue is created from muscle fibers grouped to fascicles that are covered by ligament tissue called epimysium. A muscle fiber is made from muscle units that are in multiple cells joined together. Fibers have a diameter from 0.01 mm to 0.1 mm and length from several mm up to several cm. Muscle units are made from actin fibers (thin filament), myosin fibers (thick filament), titin, and other proteins that bind molecules together, as shown in Figure 2.1. Muscle tissue shows high compartmentation to execute the contraction of muscle units that provide movement for the entire organism. There are three types of muscle fibers: skeletal, smooth, and cardiac. There are also fast and slow muscle fibers from the point of view of energy consumption. Fast is adapted for intense and-short term load. Slow fibers provide long-term function at lower loads. The rate of energy consumption and also other biochemical processes are different for both types of muscle fibers.

The environment of cells can be described as a biphasic poroelastic medium composed of water, dissolved proteins, cytoskeleton, and organelles. A very complex situation inside living cells is referred to as molecular crowding [24]. Inside all cells, continuous electrostatic and hydrophobic interactions are affecting active transport and diffusion of molecules. The presence of muscle units influences all membrane structures inside muscle cells, such as the nucleus, mitochondria, and endoplasmatic reticulum. The most abundant material in animal cells is collagen that creates connective fibers.

2.2 NMR spectra of muscle tissue

NMR enable non-invasive and repeatable characterization of tissue *in vivo* by measurement of ^{1}H and ^{31}P localized spectra. Localized ^{1}H NMR spectra *in vivo* provide information about ratio of several muscle metabolites shown in Figure 2.2. Two signals from lipids are detected, extramyocellular lipids (EMCLs) and intramyocellular lipids (IMCLs). The difference in the resonance frequency of lipids is due to the susceptibility effect, EMCLs are long cylinders around muscle fibers, and IMCLs are tiny spherical droplets inside cells [26]. Several important metabolites are observable in ^{1}H, ^{13}C, and ^{31}P spectra of muscle tissue, as shown in Figure 2.2 [27]. The image provides information about the spatial distribution of ^{1}H containing molecules with specific mobility. The most intensive signal is water. By suppression with presaturation, signals of lipids and metabolites with fast-moving moieties can be detected. Measurement of localized ^{1}H NMR spectra is mainly utilized to diagnose brain tissue. Large and uniform skeletal muscle tissue is suitable for measurement by localized NMR [28]. The most suitable for measuring localized NMR spectra from muscle tissue is the soleus and gastrocnemius located in the calf. Those muscles are pretty large, and surface coils

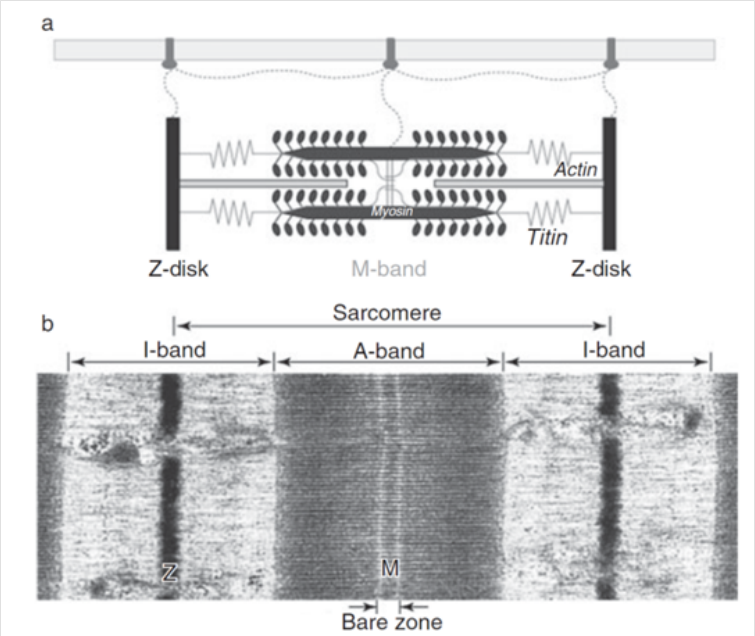

Figure 2.1: Structure of muscle unit.
Schematic (a) and photograph (b) of protein structure that creates muscle unit [25].

around the leg significantly improve NMR signal intensity. Signals originating from abundant metabolites can be observed [27]. Especially ^{31}P NMR spectra provide a unique way to evaluate the metabolism of muscle tissue *in vivo*. A partial orientation of small molecules was observed in muscle tissue indicating influence by ordered structures created by muscle units [4].

Homogeneity of magnetic field B_0 and motional artifacts are factors that could severely impact the observed NMR signal. The ratio of abundant metabolites can be estimated, although precise concentration can be determined only by biopsy. There are two essential fiber types inside muscle tissue, glycolytic and oxidative, adapted for short and long-term load, respectively. Those fibers do not have the same metabolism, and pH changes during long-term exercise were observed [29].

Additional splittings of signals of metabolites in localized ^{1}H NMR spectra *in vivo* depending on the orientation of muscle fibers were observed [4]. It is crucial to measure volume with the same orientation of muscle fibers to the external magnetic field. Characterization of muscle fiber orientation to the force-generating axis of intact muscle tissue is by pennation angle. There are three types of muscle fiber configuration suitable for localized NMR measurement: fusiform, unipennate, and bi-pennate shown in Figure 2.3. The area of interest has to have the uniform orientation of muscle fibers to observe additional splitting. There is an overlap of contributions for muscle tissue with a multi-pennate structure, and measured data provide a sum of all observed orientations.

^{31}P NMR spectra are used for characterization of metabolism of muscle tissue as macro energetic molecules contain ^{31}P with 100 % abundance and chemical shift dispersion that enable separation of NMR signals.

^{13}C is not a suitable probe as natural abundance is about 1 % and aliphatic signals overlap at low field as 1.5 T or 3 T that are commonly used in MRI machines.

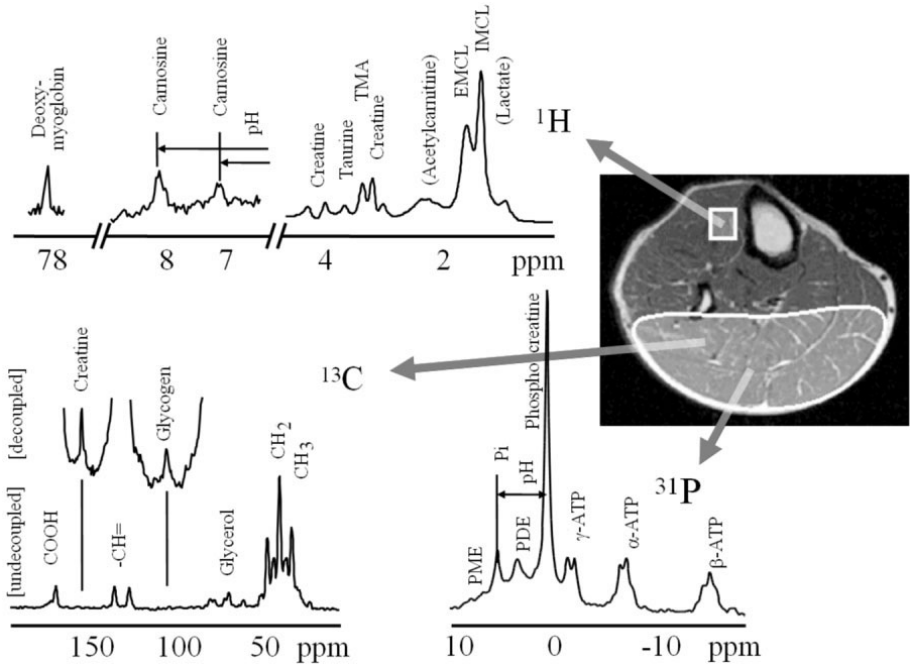

Figure 2.2: Localized NMR spectra of muscle tissue for ^{1}H, ^{13}C, and ^{31}P
Localized ^{1}H, ^{13}C, and ^{31}P NMR spectra from muscle tissue with assigned metabolites [27]. Abbreviation in ^{1}H spectra: (TMA) trimethylammonium, (EMCL) extramyocellular lipid, and (IMCL) intramyocellular lipids.

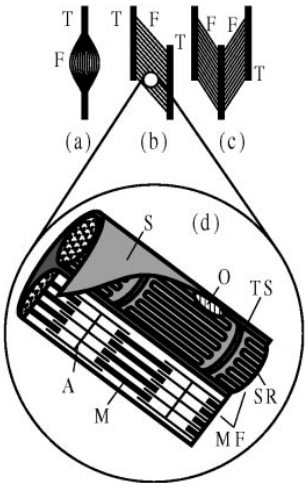

Figure 2.3: Types of muscles defined by pennation angle.
Muscle fiber orientation is described by pennation angle, there are several types suitable for localized NMR measurement: (a) fusiform, (b) uni-pennate, or (c) bi-pennate [4]. The view (d) show simplified muscle fiber with two myo-fibrils. Abbreviations: actin (A), muscle fibers (F), myosis (M), myo-fibrils (MF), organells (O), sarcolemma (S), sarcoplasmatic-reciculum (SR), tendom (T), transversal T-system (TS),

Several metabolites show additional splitting in Figure 2.2:
Creatine - Important for metabolism as energy storage in form of phosphocreatine.
Taurine - Food suplement for muscle builders, also present in bile.
Lactate - Product of metabolism, can be considered as energy storage.
TMA (trimethylammonium) - Product of choline and carnitine metabolism.
Carnosine - Function as chelator and pH buffer.

The origin of orientation was found by ^{2}H DQF NMR measurement of bovine arteries and veins *ex vivo* [30]. ^{2}H isotope was used due to quadrupole moment, which shows a much more significant energy level difference and bigger additional splitting created by partial orientation. ^{1}H splitting could be about 10 times smaller than observed ^{2}H splitting. Splitting of ^{2}H of deuterated water was calculated by fitting multiple-quantum filtered spectra and showed two components with different magnitudes. The broad component showed splitting in the range of 150 to 380 Hz depending on the specimen. The narrow component showed splitting of 85 to 111 Hz. There is no uniform fiber orientation in arteries and veins, the two observed components could also be similar to radial and transverse collagen structures in different layers of cartilage [31]. Collagen is the most abundant protein in animal tissues. Formic acid degrades the collagen network by the destruction of hydrogen bonds that create physical cross-linking. After the addition of formic acid to bovine arteries and veins, observed dependence was not detected.

Change of intensity and effects associated with partial orientation were also observed in animal *post mortem* studies [3], [32]. ^{1}H and ^{31}P NMR spectra show similar decay of observed signals of phosphocreatine, as molecules that store energy is depleted in tissue *post mortem*. Splitting disappeared within several hours after death.

Previous studies of partial orientation focus on creatine, which has a high concentration in muscle tissue and is essential in phosphocreatine, which provides temporal energy storage. Creatine and phosphocreatine CH_3 signals are overlapped in ^{1}H spectra. Indentification of CH_2 signal was done by measurement ^{1}H and ^{31}P NMR *post mortem* studies [3], [32]. Creatine CH_2 signal in ^{1}H spectra and phosphocreatine ^{31}P signal showed similar decay after death. It was assumed that the NMR detectable signal belongs only to phosphocreatine. In a study of the identification of metabolites and changes with prolong exercise [33], [34], the observed signal of CH_2 group vanishes. The signal was identified to be phosphocreatine that is depleted during exercise. In the case of CH_3 group, hydrogen atoms are rotating around the carbon-carbon axis and thus have higher mobility than CH_2 group that could be bound to some macromolecular structure, movement of creatine CH_2 is not observable.

Magnetization transfer studies were used on muscle tissue [35], [36] and show that water protons are restricted in muscle tissue and are in interaction with abundant creatine. Creatine-kinase bound effect were denied in studies [37], [32] of rat with deficient creatine-kinase. Metabolism of red blood cells in gelatin during stretching shows higher energy consumption when introducing directed anisotropy [38]. Red blood cells in stretched gelatin also show that the signals from metabolites inside cells are isotropic and signals outside cells are anisotropic. Living cells somehow consume more energy to compensate for interaction with the surrounding anisotropic environment.

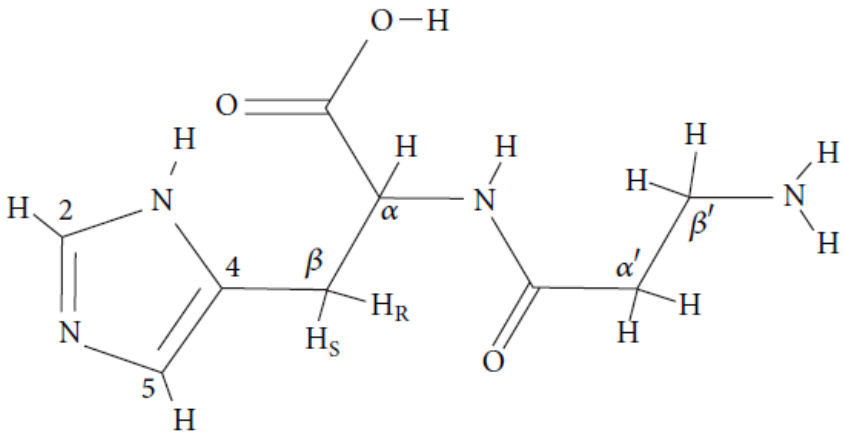

Figure 2.4: Schematic molecular structure of carnosine
Assignment of atoms in carnosine molecule [39]

2.3 Carnosine

Carnosine is a promising target for study of partial orientation in muscle tissue *in vivo* [40]. Molecular structure of carnosine with assigned atoms is in Figure 2.4. This dipeptide consists of L-histidine and β-alanine. Other observable metabolites by NMR are smaller and provide fewer RDCs. NMR study of carnosine structure in the solution described molecule geometry and populations of main rotamers of CH_2 group of L-histidine by investigation of dihedral angles [41]. L-histidine has a rigid imidazole ring that is interesting for detecting partial orientation and enables observation in localized NMR spectra. *In vivo* ^{1}H signals from the imidazole ring are shifted to a range of chemical shifts where there is no overlap with other more abundant metabolites. Carnosine is an important metabolite that has been intensively studied for utilization in diagnostic of tissue *in vivo* [42], [43]. It has an essential function in the nervous system necessary for the proper development of nerve cells. In muscle tissue, it is a chelator for scavenging ions and a buffer of intracellular pH. Carnosine is known to create complexes with divalent cations, such as Zn^{2+} and Cu^{2+} that could be present *in vivo* [44]. Measurement of paramagnetic effect on carnosine signal at 1.5 T enabled *in vivo* estimation of Cu^{2+} concentration in muscle tissue [45]. Figure 2.5 show carnosine signals in localized *in vivo* ^{1}H NMR spectra. X1, X2, X3 and X4 were interpreted as additional splitting. A sizeable intracellular pool of carnosine in skeletal muscle tissue could also serve as an extracellular signaling agent [46]. Localized NMR measurement of carnosine H2 and H5 chemical shifts in muscle tissue were used to determine pH noninvasively [47]. It can also discriminate oxidative and glycolytic muscle fibers in particular muscle [48]. Diagnostic of Duchenne muscular dystrophy was done by determining pH from carnosine ^{1}H signal [49].

Carnosine concentration in muscle tissue for untrained subjects is up to 2.8 mmol/kg and for bodybuilders up to 4.8 mmol/kg and can be determined non-invasively by NMR [50]. Dietary intake of β-alanine can increase the concentration of carnosine in skeletal muscle tissue up to 2 times [51]. β-alanine supplementation [52].

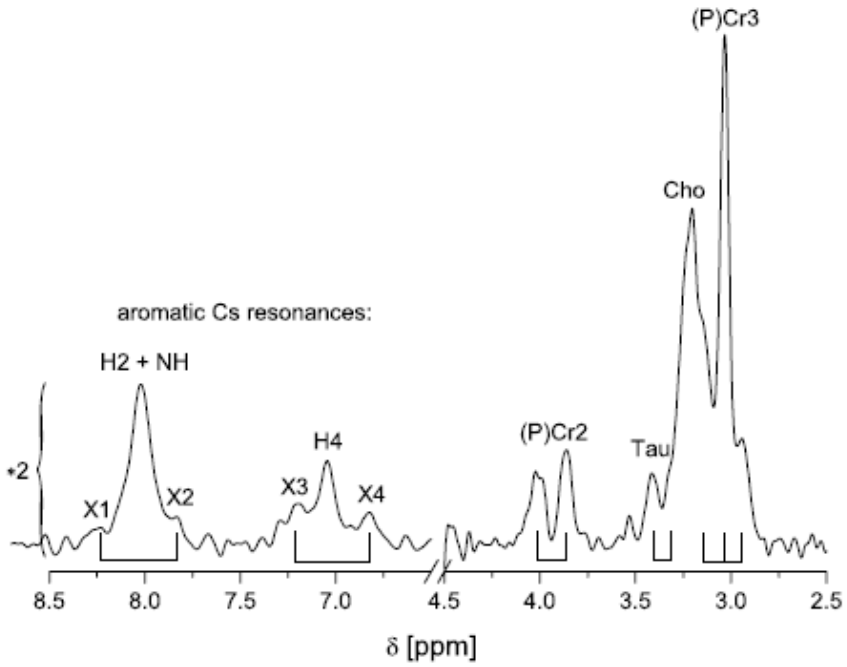

Figure 2.5: Localized NMR spectra of muscle.
Observable splitting of carnosine [45]. Influence of strong coupling effect is observed as non-equal intensity of splittied signal. In comparison to other metabolites carnosine showed much larger splitting due to partial orientation.

Model for carnosine in muscle tissue for metabolism [53].

Observation of dipolar coupled carnosine *in vivo* was reported at 1.5 T [54]. ^{1}H localized spectra were measured by 500 averages in 10 minutes. A subject should not move for the whole period. Observable splitting was about 18 Hz for both H2 and H5 signals of a low population of possibly oriented carnosine. Interaction could also be intermolecular as two imidazole rings are close in space.

Measurements of carnosine signals for evaluating exercise effects at 7 T show several NMR signals [29]. A difference of H2 chemical shift signal on local pH is shown for soleus and gastrocnemius after prolonged exercise. Additional splitting of carnosine signals was not observed, although only 20 averages of localized spectra were acquired.

Localized ^{1}H correlation spectra (L-COSY) of muscle at 3 T show cross-peak between H2 and H5 carnosine signals [55]. Figure 2.6 show cross-peak described as C6, intensity is similar to X signals in Figure 2.5. Observed cross-peak indicating coupling (direct or indirect dipole-dipole interaction) has a very low intensity that is with an agreement with measurement of localized ^{1}H NMR spectra, where the population of carnosine influenced by partial orientation is much lower [54]. ^{1}H L-COSY from soleus muscle at 7 T [56] does not show a presence of possibly oriented carnosine with coupling between H2 and H5. It has to be noted that there is a very low intensity of carnosine NMR signal, and also shorter T_2 values are observed for metabolites at 7 T.

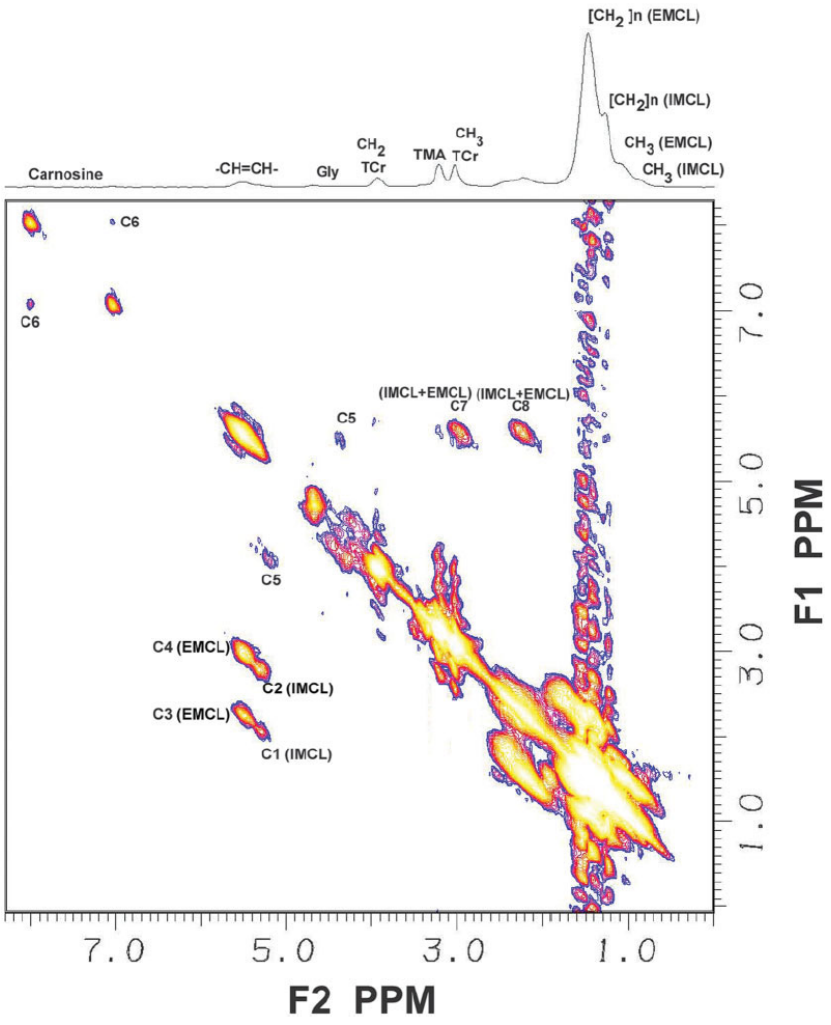

Figure 2.6: L-COSY spectra of muscle tissue *in vivo*.
Observable cross-peak of carnosine between H2 and H5 (denoted C6). Observed intensity is much lower indicating much small population of coupled system compared to monomer [55].

3. Hydrogels

3.1 Gelatin as orienting media

Gelatin is prepared by denaturation of collagen from tissues either by acid or alkali treatment. The treatment influence gelatin properties by inducing charged groups. The mechanical properties of gelatin can be influenced by selecting chains with a certain length by a suitable filter. A network from gelatin is created by physical cross-linking of triple-helixes of tropocollagen fibers by hydrogen bonds. Above the temperature of 25 °C, the gelatin will start to melt as thermal fluctuations disrupt hydrogen bonds. Gelatin was used as orienting media for small and charged molecules to create relatively large partial orientation [57]. As is made from helices, such chiral media induce different partial orientation to different enantiomers. The method is known as strain-induced alignment in gel (SAG) method.

Covalently cross-linked gelatin is also possible by using irradiation by accelerated electrons [58]. In the case of chemical cross-linking, melting does not occur, and measurement of the temperature dependence of partial orientation would be possible. Another way to chemically cross-link gelatin is to use free radicals to create chemical bonds between macromolecular chains. Irradiation by the electrons is a better option. Proper mixing of dense media is difficult to achieve. Different network morphology could occur in different parts of a sample when dense gelatin would be prepared by chemical cross-linking. Gelatin is very charged and could be prepared much denser than other hydrogels, therefore suitable for creating partial orientation even for very small molecules. Hydrogen bonds connecting molecular chains can be disrupted during stretching to such an extent that ruptures occur, and hydrogel does not provide uniform partial orientation. Gelatin is also a chiral orienting media and provides different partial orientations for a given enantiomer, as shown for alanine [57], as shown in Figure 3.1. Only a steric interaction should introduce partial orientation in orienting media. Specific interaction such as binding is not wanted.

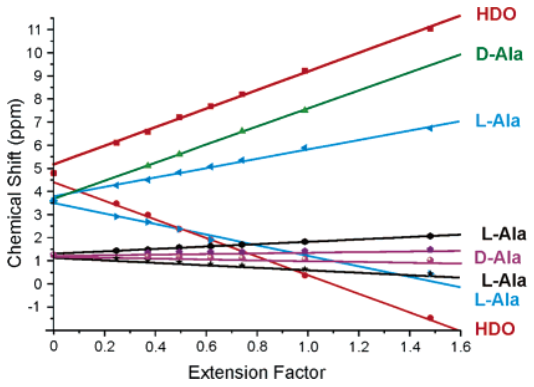

Figure 3.1: Dependence of additional splitting on stretching of gelatin. Additional splitting of L-alanine and D-alanine show linear dependence on extension factor of gelatin [57].

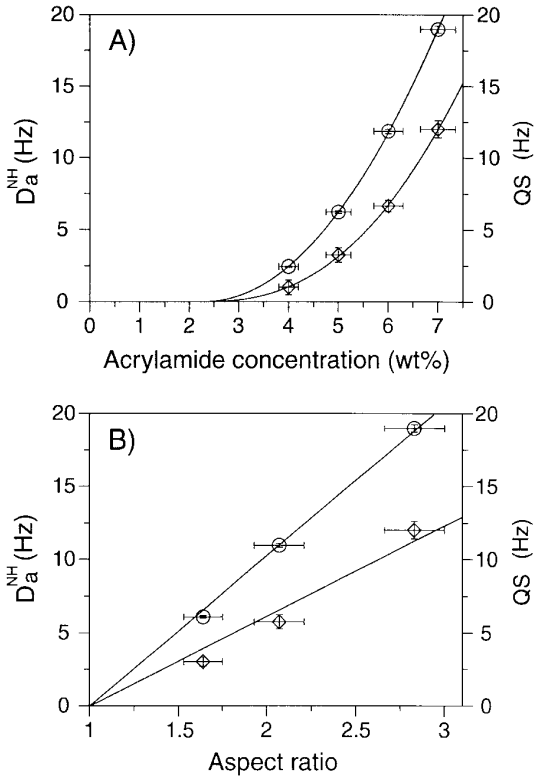

Figure 3.2: PAM alignment by composition and stretching.
Dependence of quadrupolar splitting of D_2O (diamond) and dipolar splitting of NH (circle) dependence on weight ratio of AM and stretching [59].

3.2 Polyacrylamide (PAM) as orienting media

PAM was used as orienting media for the determination of protein structure [59]. Sidechains of polyacrylamide can bound a large amount of water molecules. Chemical cross-linking by free radical polymerization. The monomer is toxic. It is a known flaw of polyacrylamide-based hydrogel that monomer units can be present in a network, a large amount of water is required to clean hydrogel. Influence of polymer network on water molecules [60]. Without suitable solvent, fibers can not move freely. A cross-linker used for creating the network is bisacrylamide, which provides a connection for four linear chains. Polymer networks from polyacrylamide could have several morphologies depending on the ratio of monomer and cross-linker. The presence of polymer networks only slightly influences solute molecules. A hydrogel containing from 3 to 8 % (w/w) of PAM is suitable for stretching in the NMR tube by the method described in [59]. Water provides lubrication for the movement of side chains and even entire polymer fibers. Morphology of created network is a key for the partial orientation of molecules of interest. The creation of cross-links by uncontrolled random polymerization depends on concentration. Above a certain limit, inhomogeneities occur in a network. In the case of a network, the movement of random coils is restricted, and a broader signal is observed. Networks are not perfect. There is a distribution of chains, and some chains are free to move faster and contribute as a narrow part of the signal.

Cross-linked macroscopic hydrogels have a response on stimulus in two kinds.

The first is the immediate response of polymer units The mobility of polymer fiber is restricted. This process is still not fully understood. Research focuses on the response of linear chains. The second type of response is associated with the entrapment of solvent when collapsed network hinders the flow of solvent out of macroscopic hydrogel.

Direct observation of polymer signal can, in some cases, discriminate chain motions [61]. A so-called tube model is used with four different time and length scales. There are four different dimensions and time dependencies to model motions of polymer fibers. Free chains are important in the case of NMR observation because the signal from the free chain would be observable. A chain with both ends incorporated in the polymer network has less freedom and would have a much broader signal in NMR spectra. The diffusion of a solute in hydrogels is a complicated phenomena and can be modeled only with severe approximation of hard sphere that does not interact with polymer fibers, for example by obstruction-scaling model [62]. Observation of average diffusion coefficient from entire populations in hydrogel. A factor in case of interaction of network with solvent are free end chains, that are more mobile. There is a difference in phase transition of polymer chains and volume phase transition of cross-linked hydrogel. In case of linear chains in solution, water exchange is much faster, for cross-linked polymer networks an exchange of water molecules is restricted by the fact that surface will collapse and hinder a flow outside macroscopic hydrogel.

Change of molecules mobility is immediate. Random coil segments are somehow interconnected, water is trapped inside, and it takes some time to get the whole network to equilibrium. Water exchange and properties between water-rich and polymer-rich regions are of interest. Network collapse from the surface as water trapped inside the hydrogel slowly gets out. A phenomenon of skin effect and barrier effect significantly influence time to reach equilibrium. A question is how to suppress or exploit such an effect with particular applications of a smart hydrogel.

PNIPAM chains of specific length exhibit sharp reversible phase transition with change of temperature. The observed phenomenon is associated with methyl groups that induce a tiny change to the interaction of PNIPAM and water at a specific temperature. As stated before, several units are required for a chain to exhibit phase transition. A process of cooperative hydration is believed to be responsible for temperature-induced phase transition. The length of a polymer required is called persistence length, several units to observe temperature-driven phase transition. PNIPAM is not entirely hydrophobic. Water molecules are observed near nitrogen and carboxyl groups. Main difference with PAM in reversibility, and the fact that temperature is changed in whole volume, in case of exchange of solvent, molecules have to diffuse. In case of temperature change on molecular level is immediate for all polymer units.

3.3 VPT of Polyacrylamide

Polymers exhibit phase transition phenomena, a change of interaction between polymer chains and solvent upon a particular stimulus. The first observation of hydrogel was on polyacrylamide (PAM) in water-acetone mixtures [8]. Understanding processes undergoing in the cross-linked network is crucial for the inter-

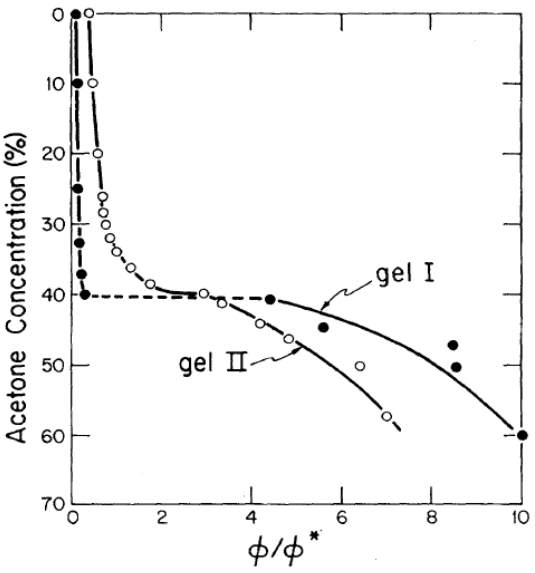

Figure 3.3: The swelling ratio for two PAM gels.
Swelling of gel I (curing) and gel II (curing) in different water-acetone mixtures [8].

pretation of measured NMR data. NMR spectroscopy and imaging are commonly utilized to characterize macromolecular systems [6] and especially hydrogels [63]. Mechanism and models of solute diffusion inside hydrogels has been of interest for long time, several mathematical models were proposed and tested [64]. PAM hydrogel undergoes collapse in water-acetone mixture [8] above 40 % (v/v) of acetone. MRI study was done to determine T_1, T_2 and diffusion coefficient in PAM with different amounts of acetone [65]. A volume phase transition occurs when water molecules interact with acetone more than with polymer. NMR study of water-acetone mixtures showed a change of rate of chemical shift difference above 40 % (v/v) of acetone [66]. Water and acetone create some cluster structures. When water and acetone are mixed, heat and bubbles are released. Molecules are assembled in more energy-efficient structures.

3.4 VPT of poly(*N*-isopropylacrylamide)

PNIPAM chains exhibit phase transition between hydrophilic and hydrophobic structures at the lower critical solution temperature (LCST) [67]. PNIPAM has been intensively studied as sharp VPT is caused only by a slight change of temperature. [68] Very interesting is the reversible temperature-induced phase transition of poly(*N*-isopropylacrylamide) (PNIPAM) that could be applied for smart materials in medicine and technology. The microscopic structure of PNIPAM by small X-ray scattering and pulsed-field gradient NMR [69]. Diffusion showed three regions of the water phase and two polymer-rich regions with different apparent diffusion coefficients. Authors concluded based on experimental data that diffusion of water molecules is not unique, there are cavities with a Gaussian distribution. The connectivity of the cavities implies that the gel structure is an irregular sponge phase with smooth interfaces and a submicrometer cross section. Authors also concluded that the absence of compartmentization of the water

phase implies that the slow deswelling rate of the gel is not due to trapping of the water. Measurement of water T_2 relaxation and average diffusion of PNIPAM by HRMAS PFG NMR at different temperatures observed unrestricted and restricted water species [70]. VPT of PNIPAM macroscopic hydrogel is dependent on temperature [71]. PNIPAM is not completely hydrophobic above LCST, the water is always bound to polymer fibers [72]. The process of VPT of PNIPAM in free swelled gels and gel under tension was described as a cooperative hydration [73]. The cooperative hydration is defiend as simultaneous dissociation of the bound water from the polymer chains in correlated sequences.

A study of PNIPAM under uniaxial elongation showed a difference of onset and sharpness of phenomena dependent on temperature [74]. Atom force microscopy showed that single-chain PNIPAM has the same stiffness for swelled and collapsed state, indicating the interchain origin of VPT [75]. A deformation of the hydrogel can influence a process of VPT [76]. NMR studies of volume phase transition of PNIPAM characterized dimensions, T_2 and apparent diffusion coefficient in the hydrogel with observable skin effect [8] and [77]. MRI study shows that in PNIPAM at a temperature above LCST, the apparent diffusion coefficient of water is smaller than at room temperature [65]. MRI study of PNIPAM collapse in D_2O and discrimination of hydrophilic and hydrophobic sites by ^{129}Xe was described in [78]. Investigation of swelling and diffusion of PNIPAM samples after adding alcohols or change of temperature was described in [79]. Solvent absorption was measured by a one-dimensional diffusion experiment by observation of time dependence of signal intensity. The macroscopic response is induced by a change of temperature in the range of several degrees. Collapse and swelling can be reversible. Although PNIPAM is not entirely hydrophobic, as water molecules are still near CO and NH groups, the observed phenomena are associated with sidechains. The influence of additional CH_3 incorporated into the network was reported. The observed phase transition and VPT are associated with some change of water interaction with CH_3 groups. The LCST is between 30 °C and 35 °C, depending on the polymer. Temperature change is much easier to establish than the exchange of solvent, where a high amount of solvent would be necessary to clear hydrogel. PNIPAM shows a shift in the onset temperature of phase transition in H_2O and D_2O of 0.7 K [80].

PNIPAM became a model system for temperature response behavior that shows reversible phase transition induced by the change of temperature. Phase transition of PNIPAM is induced by so-called cooperative hydration. Several units are necessary to observe phase transition. A small change in solvation of side chains induces stimulus observable on a macroscopic level.

In the case of PNIPAM, the primary mechanism of phase transition is cooperative hydration. Several side chains interact together somehow. It is still of the question whether observed phenomena is rather intra-chain or inter-chain. PNIPAM is not hydrophobic. There are always water molecules near hydrogel. The solvent flow rate outside of a hydrogel depends on the macromolecular network's dimensions, shape, and morphology. PNIPAM based semi-interpenetrating hydrogels were prepared to have a faster response than in the case of PNIPAM polymerized only with a cross-linker. It was reported that at least about 11 units are needed to observe coil-to-globule transition. The minimum amount of polymer units to observe a motif in the backbone is called persistence length. Isopropyl

group with two methyl groups is essential for the temperature-driven response. It was reported that there is a change of temperature onset with the presence of other methyl groups. Linear PNIPAM shows a different temperature of phase transition for light and heavy water. There was a shift of about 0.7 K [80].

There is no differentiation of water to individual populations in ^{1}H, just one averaged signal. Hydrogels can be used as orienting media for the determination of molecular structure by NMR measurement. Stimuli-responsive by temperature change - reversible after several volume phase transitions. An exciting study of volume phase transition of PNIPAM by the method used to characterize porous media was utilized [81]. Study of solvent during the sol-to-gel transition of PNIPAM by two-dimensional ^{2}H T_1-T_2 relaxation provide an insight into phase transition. Data indicate several different pools that occur after phase transition. Dependence of phase transition sharpness on stretching due to elongation. The observed phenomena are reversible for linear chains, but in the case of cross-linked hydrogels, it was shown that several cycles of heating and cooling have to be done in order to accomplish the reversibility of the observed process. Temperature cycling disrupts the network, and thus a volume response could take longer or could be faster depending on the influence by skin and barrier effects. Coil-globule transition time requirement is different in the case of linear chains and cross-linked networks.

PNIPAM was used as orienting media in study of novel compound [82]. Polymerization in DMSO (dimethyl sulfoxide). Monomer concentration 2 mol/L with 0.7 % of cross-linker (BIS). Measured solvent was DMSO.

Much faster response can be achieved by preparation of semi-interpenetrating polymer network [83]. Two polymerizations are done, the first create linear PAM and the second create networks from PNIPAM around linear PAM. By variation of linear PAM content several hydrogel with different properties were prepared. Visualization of solvent diffusion in polymers by NMR microscopy with radio-frequency field gradient [84].

4. Sample preparation

4.1 Gelatin samples

Type A gelatin from porcine skin and sodium azide were obtained from Sigma-Aldrich (item G2500). Deuterated water (D_2O) was purchased from Armar Chemicals. Carnosine (β-alanyl-L-histidine) was purchased from Acros Organics.

Dry gelatin was put into a 4 ml vial with 0.5 mol carnosine in 90 % (v/v) D_2O to get desired gelatin weight percentage. The vial was sealed by cap and inserted into a water bath of 0.5 l. The temperature was set from 50 °C up to 70 °C to melt the gelatin fully. Air bubbles have to go to the top. Melted gelatin was cooled down to room temperature and move out from the vial by tweezers. The foam at the top was removed by a knife. A hydrogel cylinder was placed into a glass funnel with an attached silicone hose. A hot air stream by a heat gun was used to melt the gelatin. The heat gun was moved around the funnel, not focused to one spot where the high temperature would create bubbles in gelatin. Gelatin was transferred this way inside the silicon hose, and a conical teflon plug was inserted to hold cooling gelatin inside. The sealed silicon tube was inserted in a water bath of about 0.5 l at 50 °C that was turned off and left to reach room temperature. In this way, homogeneous gelatin was prepared inside the silicone hose.

Set described in Figure 4.1 was used for stretching of gelatin [85]. Silicon hose was inserted to both end open NMR tube and pushed through, water was used as a lubricant, so that silicon tube would not be stuck inside NMR tube. A mold was observed at the top of a gelatin sample stored after measurement in the fridge. Several crystals of sodium azide were dissolved in carnosine solution and added at the top of gelatin to prevent mold formation and drying of a sample. At the bottom end was a conical teflon plug, and at the top, a plastic cap with two screws was put on a silicon hose. The silicone hose was stretched to desired elongation ratio, and two screws were used to fix the silicone hose. The top end of the silicone hose was sealed with parafilm to avoid drying a sample.

For an MRI machine in IKEM that can measure rodents, a larger sample of gelatin was prepared. 4.7 T spectrometer was not able to measure ^{2}H NMR spectra, and gelatin was mixed with distilled water and carnosine to get carnosine concentration 0.2 mol. Gelatin was prepared in a steel tube with 30.5 mm inner diameter. A plastic bag was put around the steel tube in a water bath at 50 °C, and aluminum foil was used to seal the bag. After cooling down top part with foam was removed by a knife. Anisotropy was introduced by pushing the gelatin cylinder inside a latex bag into a plastic tube with an inner diameter of 27 mm. Glycerol was used as a lubricant so that gelatin does not rupture during pulling and pushing.

4.2 Polyacrylamide (PAM) samples

Arcylamide and amonium persulfate (APS) were purchased from Sigma-Aldrich. *N,N"*-methylenebis(acrylamide) (BIS) and *N,N,N',N'*-Tetramethylethylenediamine (TEMED) were obtained from ACROS organics. Carnosine (β-alanyl-L-histidine)was

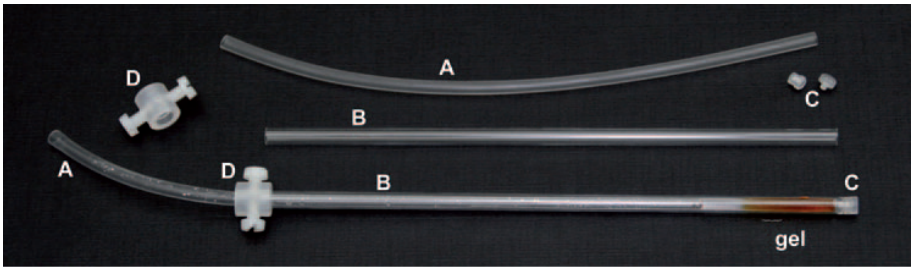

Figure 4.1: Stretching apparatus for 5 mm NMR tubes.
Silicone hose (A) is placed in open 5 mm NMR tube (B) with cone-shaped plug at the bottom (C) and fixed by plastic srews in cap (D) to get desired elongation factor [85].

purchased from Acros Organics. Deuterated water (D_2O) was purchased from Armar Chemicals.

Acrylamide was mixed with bisacrylamide in a molar ratio of 50:1 in a 5 ml volumetric flask to get a 20 % stock solution. Polymerization was not initiated without free radicals. Stock solution can be stored in the fridge for a prolonged time. A filtration through at least μm filter was recommended to obtain more homogenous hydrogel. An adequate amount of acrylamide solution was mixed with distilled water and 10 % (w/w) APS and 10 % (v/v) TEMED solutions in a plastic laboratory tube. Immediately after the addition of APS and TEMED, efficient mixing of the solution was required to obtain homogeneous hydrogel. A 1 ml pipette tip cut by scissors to get a wider opening was used to mix several times and then transport polymerizing solution into teflon chamber. A commercially available set described in Figure 4.2 [59] was purchased from [86]. The solution was left for at least 5 hours to polymerize fully. After polymerization, samples were moved to at least 250 ml of distilled water and cleared from chemicals and polymer chains not incorporated in the network for about 12 hours.

Hydrogel in distilled water swelled to such an extent that can not be placed into teflon chamber where it was polymerized. To replace H_2O with D_2O and fit hydrogel into teflon chamber, partial drying on parafilm was used. D_2O is used for lock and splitting of water signal to estimate the magnitude of partial orientation and evaluate the uniformity of prepared orienting media. Complete drying of hydrogel could also be used, although the author was concerned about cracks in a thoroughly dried hydrogel. During drying, hydrogel changes from symmetrical cylinder to barrel shape cylinder due to higher evaporation at the bases of the hydrogel. Manipulation with hydrogel can be done only with parafilm it will stick to other materials, and it could rupture when force was applied. The hydrogel was partially dried in about 5 hours at room conditions to fit inside teflon chamber. 200 μl of D_2O with the desired molecule was added, both ends of teflon chamber were sealed with parafilm, and the hydrogel is left for at least 12 hours to swell in teflon chamber fully.

Introduction of directed anisotropy was done by pushing a hydrogel from teflon chamber with an inner diameter of 5.6 mm through a funnel to a special open NMR tube with an inner diameter of 4 mm. The NMR tube from the set [59] has a thinner wall than an ordinary NMR tube, and the edge is ground to smooth sharp glass edge. In case a flame is used to smooth sharp glass edge, a widening of glass occurs. Use of only the NMR tube from the set for stretching

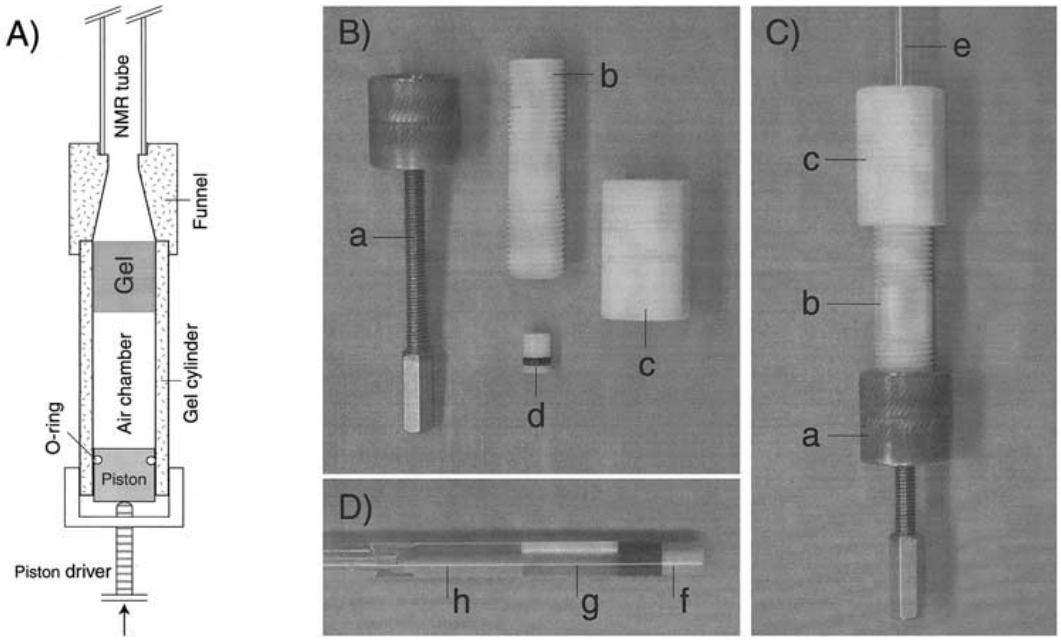

Figure 4.2: Apparatus for preparation of strained PAM [59].
Scheme of apparatus for polymerization and insertion of hydrogel into NMR tube (A), individual parts for insertion (B), assembled parts with NMR tube (C), and sample in NMR tube ready for measurement (D). Components: a - piston driver, b - teflon chamber, c - funnel, d - piston, e - NMR tube from set, f - end plug, g - stretched hydrogel, and h - top plug.

a hydrogel is recommended. With flame-treated NMR tubes, there was an issue with the tightness of teflon funnel, or rupture could occur. During pushing of hydrogel water-filled teflon chamber improved ratio of successful stretching, water is incompressible, and no pressure build-up occurred. Use of end plug to push hydrogel inside NMR tube to get rid of the isotropic solution below sample. Water was added to prevent the drying of the hydrogel in case of long-term storage.

4.3 Poly(*N*-isopropylacrylamide) samples

Arcylamide, *N*-isopropylacrylamide, and amonium persulfate (APS) were purchased from Sigma-Aldrich. *N,N"*-methylenebis(acrylamide) (BIS) and *N,N,N',N'*-Tetramethylethylenediamine (TEMED) were obtained from ACROS organics.

Two types of PNIPAM samples were prepared. The first was PNIPAM with a cross-linker prepared similarly as PAM for stretching. The second type was PNIPAM and linear PAM with a cross-linker, which created a semi-interpenetrating polymer network for faster response.

Poly(*N*-isopropylacrylamide)(PNIPAM) was prepared in two different ways. The first was hydrogel for stretching prepared similarly as PAM. The main difference was the usage of nitrogen bubbling to remove dissolved oxygen from the solution with monomers. Furthermore, instead of teflon chamber, thick-walled glass tubes were used. It was observed that in teflon chamber, the polymerization of PNIPAM samples was not homogeneous. Oxygen presence influences the outcome of PNIPAM polymerization. Polymerization was done in glass tubes

that could be sealed by flame with nitrogen atmosphere. A way to get rid of oxygen was to bubble nitrogen through the mixture for 20 min before TEMED solutions were added. As narrow glass tubes had thick walls, it was not easy to seal them by flame, and parafilm was used to seal the tubes. Glass tubes were stored vertically in a beaker and put inside a plastic bag flushed with nitrogen. After attempts to remove oxygen, the top of PNIPAM hydrogel prepared this way showed a different degree of polymerization.

As tubes were prepared in a way for flame sealing, the narrow part had to be crushed with a hammer. It was not convenient if thick walls crush the glass tube because of the potential rupture of a hydrogel. When hydrogel needed to be stretched, it had to be prepared with a specific diameter and without any surface imperfections that could cause a rupture during stretching. An issue with thick wall tubes was how to get the sample out. A method was to use a needle with a syringe to push water under the hydrogel to get it out of the glass tube. Another way to get a sample out of a thick wall glass tube was to collapse the sample inside by heating. The addition of different solvents in the cononsolvency ratio could cause collapse. With the temperature-induced collapse, an issue is the reversibility of the observed process. The final PNIPAM preparation was to bubble the solution by nitrogen gas for 20 minutes to get rid of oxygen that would react with radicals. Preparation of samples was done by two ways of polymerization. Polymerization of PAM at 70 °CC with APS for 2 hours [83]. Semi-interpenetrating networks of linear PAM with PNIPAM and cross-linker were prepared by thermally triggered polymerization of PAM with APS. A glass vial with acrylamide and APS was inserted in a water bath heated. For testing purposes, two semi-interpenetrating hydrogels with different amounts of linear PAM were prepared, with 50 µl and 100 µl of linear PAM solution by radical polymerization with PNIPAM and cross-linker. Reversible phase transition of semi-interpenetrating hydrogels was done by several cycles of heating and cooling prior to measurement.

5. Partial orientation of carnosine

5.1 Setting of NMR measurements

Measurements of samples in 5 mm tube were done by Bruker Avance NMR spectrometer (Bruker Biospin, Germany) operating at 11.7 T (500 HMz for ^{1}H, 125 MHz for ^{13}C, and 77 MHz for ^{2}H). TBI probe head suitable for inverse detected measurement was used. The 90 deg pulse lengths were 7.5 μs, 120 μs, and 14.5 μs for ^{1}H, ^{2}H, and ^{13}C, respectively. NMR spectra were acquired and processed in Topspin 1.3. The temperature was set to 298 K and maintained by temperature unit BVT 3000. Measurement of ^{1}H and ^{2}H NMR spectra at 11.7 T were done by non-shaped radio-frequency pulses. ^{2}H spectra were acquired with a 20 deg pulse due to the use of a low power channel designed for the lock. ^{13}C non-decoupled spectra were measured for comparison to ^{13}C measurement from 4.7 T. Two ^{1}H-^{13}C HSQC spectra were used to determine magnitude of an additional splitting. The first was CLIP-HSQC spectra [87], CLIP mean Clean In-Phase signal that provides both peaks of the doublet to have the same phase, both are positive. The second was P.E.HSQC [9] which also enables determination of the magnitude and sign ^{1}H-^{1}H RDCs from HSQC spectra, but only for a case of a weak coupling. The polarization transfer period was set to correspond to a total coupling of 140 Hz, 1024 data points were acquired in the indirect (^{13}C) dimension and 8192 data points were acquired in the direct (^{1}H) dimension. Automatic baseline correction and manual phase adjustment of NMR signal were made. The large sample was measured by Bruker Biospec 4.7/20 operating at 200 MHz for ^{1}H and 50 MHz for ^{13}C. The 90 deg pulse lengths were 100 μs and 50 μs for ^{1}H and ^{13}C, respectively. NMR spectra at 4.7 T were acquired with ParaVision 4.0. Spectra were processed in matNMR [88] for visualization. Localized and nonlocalized ^{1}H and nonlocalized ^{13}C NMR spectra were measured to obtain as many RDCs as possible at 4.7 T. ^{1}H localized NMR spectrum was measured by pulse sequence PRESS [89], with TE 6.12 ms (1st echo period 3.78 ms and 2nd echo period 2.34 ms), TR 2500 ms and with 16 averages. Before the localization sequence an outer volume suppression and water suppression using the VAPOR scheme were run with a total duration of 650 ms [90]. ^{13}C nonlocalized spectrum was acquired in 4096 scans. Martin Burian acquired data in IKEM, NMR spectra processing in MATLAB was done by the author.

Magnetic field homogeneity for liquid samples had been usually set by a manual search of maximal intensity in lock window for ^{2}H signal of deuterated solvent. The observed intensity in the case of isotropic liquid corresponds to field homogeneity. However, there is not one signal in a case of partial orientation, but there are two signals very close to each other, that overlap can occur. The most intensive signal from solvent in the case of two overlapping signals would not correspond to the best homogeneity of the magnetic field. The solution to this issue was to adjust a local magnetic field on CH_2 group of a molecule of interest by 'gs' command. Even better option would be to have CH_3 group that provides narrower signal due to averaging induced by motion. In the case of two ^{2}H signals near each other, an issue occurred when the lock was changing during the acquisition of HSQC spectra resulting in useless data. This situation was solved

by setting a larger magnitude of the lock sweep rate so that lock is on one peak of doublet and frequency was not shifted in ^{1}H NMR spectra.

5.2 Remarks on sample preparation

Mixing and stretching of gelatin is described in Chapter 4. Stretched gelatin has been used as orienting media for very small molecules, such as monopeptide alanine [57], partial orientation was directly proportional to stretching. Gelatin is easy to manipulate in the liquid state. It can be poured into a form of the desired shape and subsequently uniformly stretched. An advantage of gelatin after a rupture is heating and stretching again to provide a similar partial orientation. The main concern with the preparation of gelatin was the presence of bubbles that could create a rupture during stretching in a silicone hose. Removal of bubbles was done by cutting hydrogel with a scalpel, top part of a sample with foam was thrown away, and clear gelatin was heated and poured into glass funnel connected to a silicon hose. To fully melt 40 % (w/w) gelatin, the temperature of the water bath was set up to 70 °C. The sample requires several days to reach equilibrium after stretching. In case of an expensive or temperature sensitive molecule of interest, it is better to add the solution to uniform orienting media already characterized by ^{2}H additional splitting of solvent. Sample of stretched gelatin in 5 mm NMR tube for measurement at 11.7 T is shown in Figure 5.1 (a).

A large sample of stretched gelatin was prepared to detect the partial orientation of carnosine in a 4.7 T NMR spectrometer used to measure rodents. The goal was to measure localized ^{1}H NMR spectra from volume of about 1x1x1 cm^{3} and nonlocalized ^{13}C spectra for potential evaluation of ^{1}H-^{1}H and ^{1}H-^{13}C RDCs respectively. Unlike a small sample, a much wider gelatin cylinder with a diameter of 27 mm has more significant nonuniform regions created by stretching at both ends. Localized measurement from the central part of the sample should provide signal from the most homogeneous part of the large sample. Large sample of stretched gelatin for measurement at 4.7 T is shown in Figure 5.1 (b).

An issue with gelatin was also long-term stability as the flexible tube is not completely sealed. Drying a sample could change the uniformity of stretching and line widths of observed signals. Most samples were measured only once in the stretched state after several days required for equilibration. Since a mold occurred on the top of several gelatin samples, the addition of a drop of water with several milligrams of sodium azide was routinely done. Stretched gelatin samples were stored in a fridge at 5 °C and left at room temperature for a day before NMR measurement. The temperature range of orienting media made from gelatin could be an issue in case of temperature above 25 °C when hydrogen bonds start to break down by thermal motion. Chemical cross-linking of gelatin that would enable measurement at elevated temperatures can be obtained by chemical reaction with radicals or by irradiation of gelatin by accelerated electrons [58]. The motivation for the usage of chemically cross-linked gelatin would be a measurement of the partial orientation of carnosine at the temperature of the human body. Mechanical properties are favorable above 10 % (w/w) gelatin up to 50 % (w/w). For hydrogels with a lower amount of gelatin, a rupture occurred.

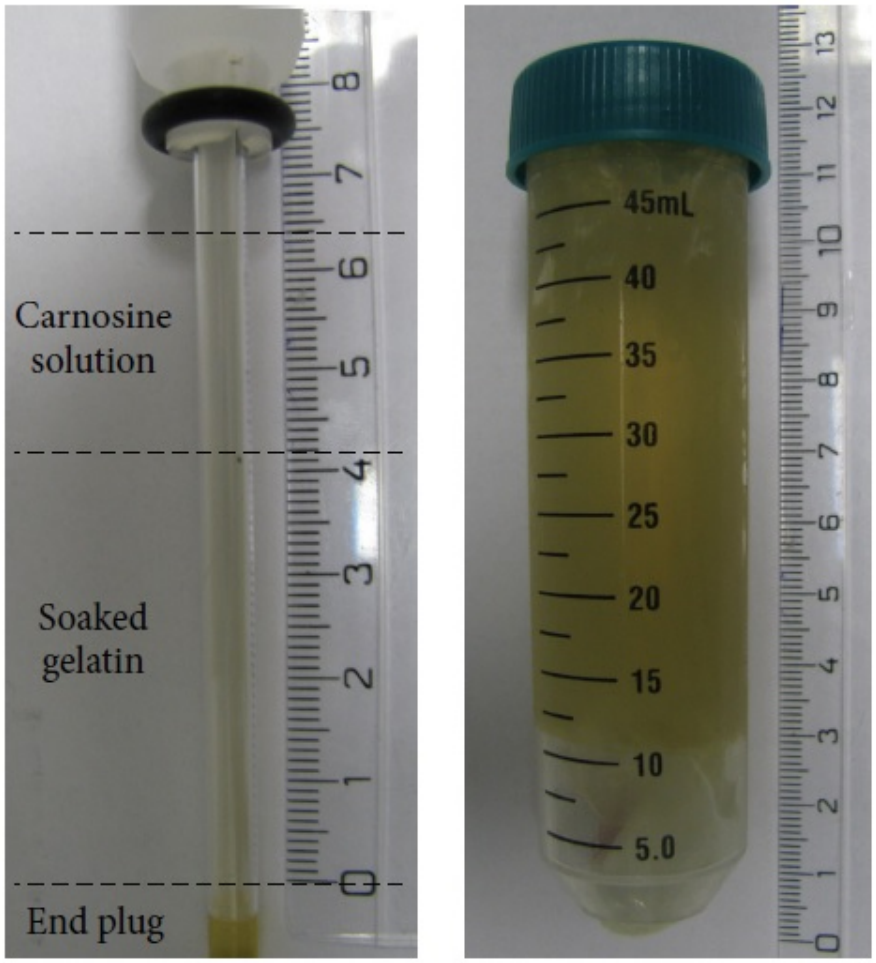

Figure 5.1: Gelatin samples
Sample of stretched gelatin for 11.7 T (a) and larger sample for 4.7 T (b) [39].

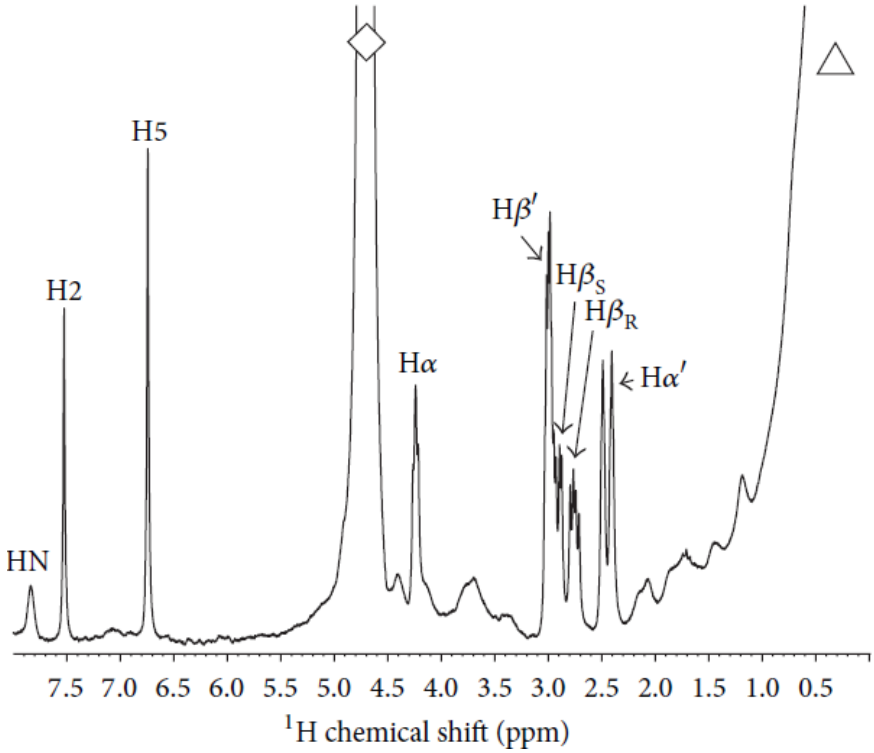

Figure 5.2: Sample with 20 % gelatin
^{1}H NMR spectrum of carnosine in 20 % gelatin [39]. Observable signals of carnosine are shown, assignment is in the text. β-alanine signals are denoted Hα' and Hβ'.

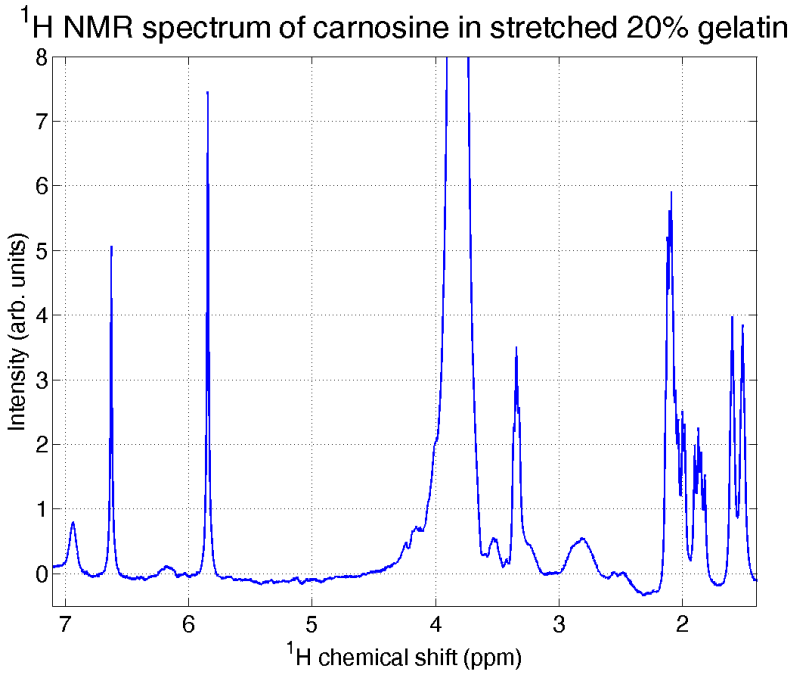

Figure 5.3: Carnosine in 20 % gelatin
^{1}H NMR spectrum of carnosine in 20 % stretched gelatin.

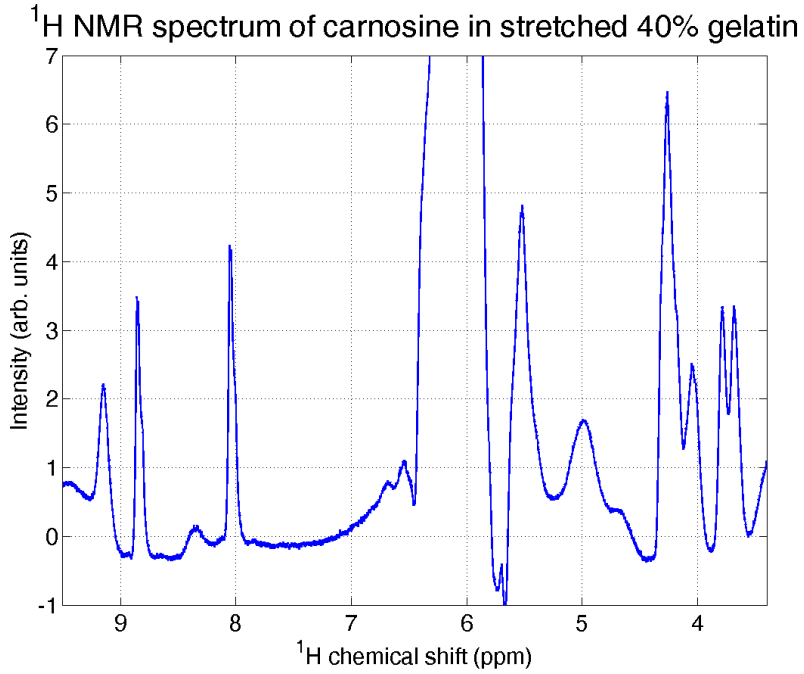

Figure 5.4: Carnosine in 40 % gelatin
^{1}H NMR spectrum of carnosine in 40 % stretched gelatin.

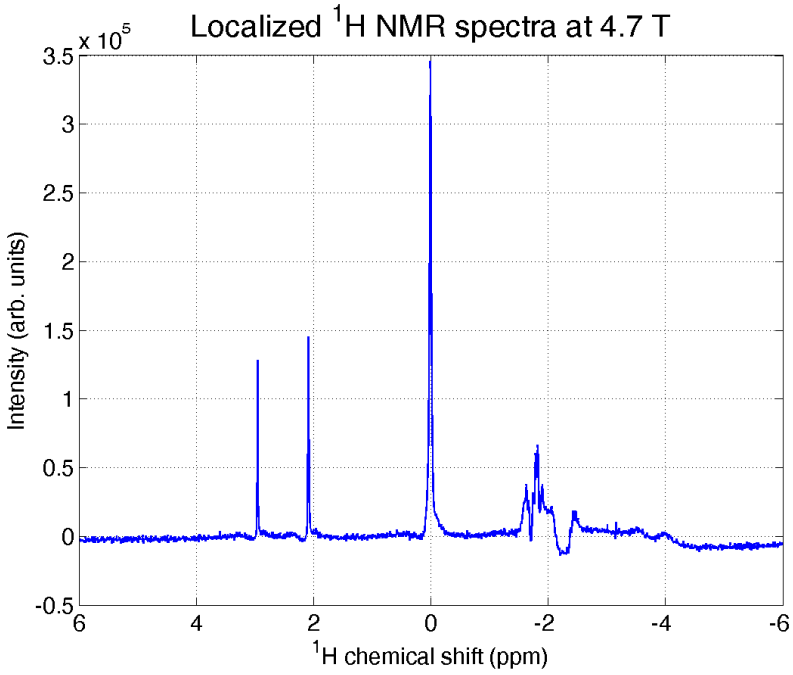

Figure 5.5: Localized ^{1}H NMR spectrum from 4.7 T

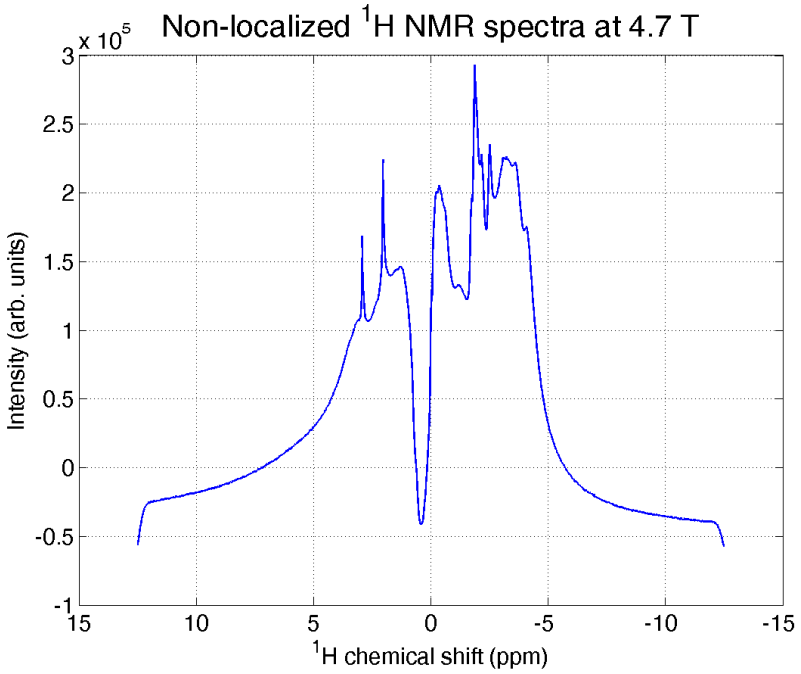

Figure 5.6: ^{1}H NMR spectrum from entire sample at 4.7 T

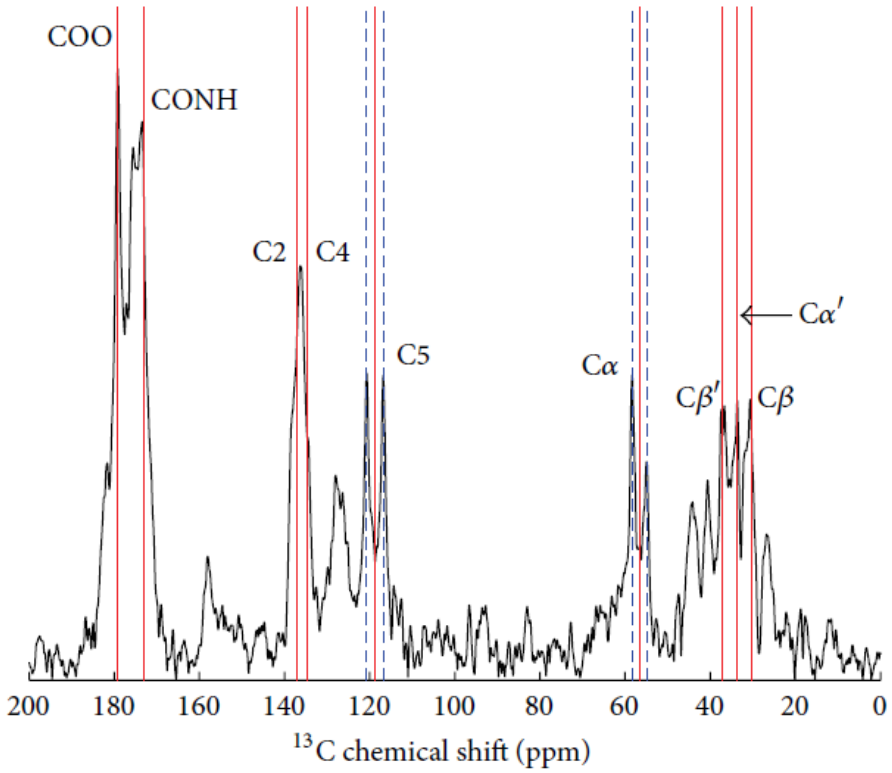

Figure 5.7: ^{13}C NMR spectrum at 4.7 T
Spectrum was acquired from entire sample, the first 50 points of FID were removed, processing in magnitude mode was done in Matlab [39].

5.3 Properties of the orienting media for NMR

Several aspects of orienting media have to be considered to obtain desired results, especially uniformity of partial orientation and strong interaction between a molecule of interest and orienting media. Interactions of the molecule with orienting media should be only steric. Specific interaction with orienting media could induce structural changes on the molecule of interest, especially for very flexible molecules. Special attention is required in a case of charged groups of orienting media and molecules of interest as opposite charges attract each other. No specific interaction was observable between gelatin and carnosine, only steric interaction was considered for alignment tensor estimation. The main factor for the magnitude of partial orientation in gelatin is the elongation factor, the ratio of the length of a hydrogel before and after stretching. Elongation factors were 120 %, 140 %, and 130 % for 20 %, 30 %, and 40 % gelatin, respectively. Uniform stretching was validated by measuring the splitting of ^{2}H signal of deuterated water. Measured splitting was 130 Hz, 285 Hz, and 189 Hz for 20 %, 30 %, and 40 % gelatin with line widths 16 Hz, 34 Hz, and 25 Hz, respectively.

5.4 Determination of RDCs and partial orientation

^{1}H and ^{1}H-^{13}C HSQC NMR spectra of stretched gelatin were measured for determination of RDCs of carnosine. ^{1}H spectrum of 20 % gelatin and carnosine with assignment is shown in Figure 5.2. The most intensive signals are from water (diamond) and silicone hose (triangle). The interesting part is in range with H2 and H5 of histidine. There is minimal overlap with gelatin. The difference in the H2 and H5 signals intensity is attributed to an exchange of ^{1}H to ^{2}H isotope as deuterium is present in the solvent, especially at elevated temperatures. The other signals from histidine are also observable CH of Hα and CH_2 group is differentiated to HβS and HβR. The signal from alanine are two CH_2 groups denoted as Hβ' and Hα', both CH_2 group are motionally averaged. At higher gelatin weight ratio, the linewidth of signals is much larger as can be seen in Figure 5.4 for 40 % gelatin compared to 20 % gelatin with the same spectral width in Figure 5.3. The most reliable way to obtain RDCs for evaluation of partial orientation was to measure ^{1}H-^{13}C RDCs by P.E.HSQC spectra. P.E.HSQC spectra provide separated signals where coupling can be easily determined for given ^{1}H-^{13}C pair. The magnitude and sign of RDCs can be determined simply by subtraction of J-coupling in the isotropic environment from total splitting on stretched sample. It would be helpful to obtain as many RDCs as possible, especially of such a small molecule as carnosine. Magnitude of ^{1}H-^{13}C RDCs (one chemical bound) and ^{1}H-^{1}H RDCs (through space) were comparable. The main advantage is that ^{1}H-^{13}C ^{1}J-coupling are much larger than ^{1}H-^{1}H ^{1}J-couplings. The difference between ^{1}H-^{13}C and ^{1}H-^{1}H RDCs determination is that in the case of HSQC spectra only coupling in chemically bound ^{1}H and ^{13}C is extracted, in case of ^{1}H-^{1}H RDCs determined from ^{1}H spectra a fitting of complete proton spin system is necessary. Determination of ^{1}H-^{1}H RDCs from simple ^{1}H was not as straightforward as initially expected. ^{1}H-^{1}H RDCs from simple ^{1}H NMR spectra

for 20 %, 30 %, and 40 % samples were approximately fitted by PERCH NMR software and later by gNMR software.

^{1}H and ^{13}C NMR spectra were acquired for large sample at 4.7 T. Localized ^{1}H spectrum measured by PRESS is shown in Figure 5.5. Several multiplets from Hβ', HβS, HβR, and Hα' are visible, but can not be precisely fitted. Hα signal is not observable. Nonlocalized ^{1}H spectrum is shown in Figure 5.6. It could be possible to estimate Hα' splitting, but other signals are severely overlapped. At 4.7 T only nonlocalized ^{13}C NMR spectra were evaluated for determination of ^{1}H-^{13}C RDCs. Several spectra with the same setting were measured without signal lock, and the resulting ^{13}C NMR spectrum was the sum. Individual NMR spectra were plotted and no shift due to change of the magnetic field in time was observed. Figure 5.7 show the assigned signals, C5 and Cα. The magnitude of additional splitting was determined from maximum of intensity, it is rough estimate due to signal overlap. The plastic tube has a strong NMR signal from ^{13}C and ^{1}H in nonlocalized NMR spectra. There were two main issues with a larger sample to consider. The alignment magnitude depends on the stretching of hydrogel that does not have to be uniform for a hydrogel with such a larger diameter. The best option was to measure localized spectra from the middle part of the hydrogel. Nevertheless, due to the significant background signal caused by utilization of surface coil, high field part of localized ^{1}H NMR spectrum could not be fitted appropriately. The other issue was using a plastic polypropylene centrifuge tube as a holder, which can create a severe distortion of the magnetic field, as was later observed by MRI measurement of piece of polyethylene submerged in water at 11.7 T, data not shown. Plastic is solid and has much faster T_2 relaxation and can be suppressed by the acquisition of signal by spin echo or by removing several FID points. However, this removal creates severe phase mismatch, and it is necessary to evaluate signal in magnitude mode in such a way ^{13}C NMR spectrum was obtained. Another issue with the measurement at 4.7 T could be the setting of field homogeneity that was done by observing the shape and intensity of ^{1}H signal of water in the stretched sample. NMR spectra of ^{1}H show no usable signals even after processing with the removal of fast relaxing signal from plastic, values of ^{1}H-^{1}H RDCs could not be fitted due to severe overlap and phase distortion. Processing of NMR data from 4.7 T was done in MATLAB by MatNMR toolbox.

Carnosine could provide enough observable RDCs to obtain alignment tensor that characterizes partial orientation. The model aimed to characterize partial orientation by ^{1}H-^{13}C RDCs and to compare measurable ^{1}H-^{1}H RDCs from the model with situation *in vivo*. Partial orientation was determined by obtaining alignment tensor by PALES [15], the principle is described in Chapter 1. Mode '-bestFit' was used as the most suitable option for small molecules in gelatin. The necessary condition for evaluating partial alignment by PALES is a rigid nature of molecule of interest, otherwise experimental RDCs would be smaller than expected. For a flexible molecule, molecular dynamics have to be done to evaluate the influence of averaging due to motion [91]. Alignment tensor was determined by input in the form of measured RDCs and a set of all possible structures downloaded from Pubchem [92]. An approximation of only one possible structure and thus one alignment tensor was adopted. The rigid parts, especially the L-histidine imidazole ring, were crucial for alignment tensor estimation. The

atoms	isotropic	20% uns	20% str	30% uns	30% str	40% uns	40% str
Cα-Hα	142.2	142.1	167.2	144	191	142	176
Cβ-HβS	131	131.1	113.25	131	104	125	108
Cβ-HβR	130.5	130.3	132.9	131	149	126	135
Cα'-Hα'	129.3	129.6	154.7	131	166	130	160
Cβ'-Hβ'	145.8	145.6	158.8	147	169	143	158
C2-H2	208.8	209.2	206.1	209	208	200	202
C5-H5	189.8	190.5	191.4	190	196	186	189

Table 5.1: Total splitting from ^{1}H-^{13}C P.E.HSQC spectra of unstretched gelatin in Hz.

atoms	20% gel (Hz)	30% gel (Hz)	40% gel (Hz)	Phantom (Hz)
C2-H2	-1.55	-0.5	1	-
C5-H5	0.45	3	1.5	3.5
Cα-Hα	12.55	23.5	17	16.5
Cβ-HβR	1.3	9	4.5	-
Cβ-HβS	-8.9	-13.5	-8.5	-
HβR-HβS	-6	-8	-5	-
HβR-Hα	-10	-14	-13	-
HβS-Hα	-8	-11	-9	0
Cα'-Hα'	12.5	17.5	15	-
Cβ'-Hβ'	6.6	11	7.5	-
Hα'-Hα'	13	25	17	-
Hβ'-Hβ'	5 or -6	12 or -14	7 or -9	-

Table 5.2: Measured RDCs of carnosine in gelatin samples. Magnitude of RDCs correspond to stretching ratio of 1.2, 1.4, 1.3, and 1.3 for 20%, 30%, 40%, and phantom, respectively

best fit was for structures with a common motif of L-histidine corresponding to the most populated structure in solution [41]. It was reported that L-histidine has three main structural motives with populations ratio of 60:20:20 and β-alanine is flexible. MATLAB script was used to sent data to PALES, process results, and visualize alignment tensor components for a set of structures in case of several gelatin elongation factors and weight concentrations. Visualization of overlap for carnosine structures with the best correlation for L-histidine was done in VMD [93]. A conformational analysis with averaged structure should be done to evaluate results properly in a molecule with internal motions. Data from molecular dynamics should provide averaged intermolecular distances that affect observed values of RDCs [94]. Measured ^{1}H-^{13}C RDCs enabled estimation of the alignment tensor of carnosine in stretched gelatin. Alignment tensor components for 20%, 30%, and 40% gelatin.

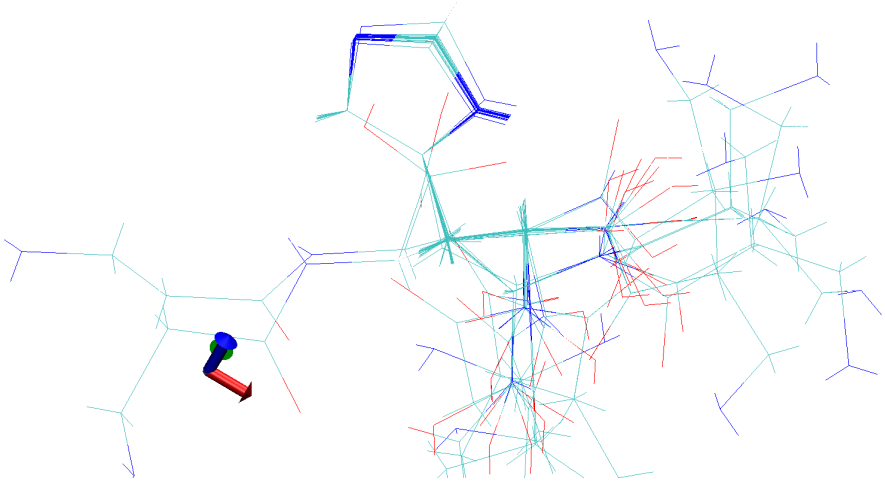

Figure 5.8: Carnosine conformation
Overlap of the best fitting conformations in VMD [93].

5.5 Comparison of *in vitro* model and *in vivo* data

Comparison of results for *in vitro* model and *in vivo* data available from literature for carnosine is provided. The stretching of a hydrogen network causes steric interaction of the solvent with gelatin, similar to muscle cells, the origin is associated with ordered collagen structures. Partial orientation is temperature-dependent, for flexible parts of molecules smaller RDCs are detected due to motional averaging. The temperature of human body is about 37 °C. There were reports that temperature in mitochondria can reach up to 50 °C [95]. Presented model from stretched gelatin was measured at 25 °C. *In vivo* spectra provide only two signals, denoted as H2 and H4 in Figure 2.5. By IUPAC they are denoted H2 and H5, as is used in this work. In the model, there is lower intensity observed on the H2 signal caused by an exchange of ^{1}H to ^{2}H from deuterated water, possibly by preparation at elevated temperature. *In vivo* H5 carnosine signal has a different relaxation time associated with the function of carnosine in muscle tissue as a chelator [44]. *In vivo* NMR data show possibility of presence of two compartments for carnosine [45]. The more intensive is monomer with small anisotropy observable as line broadening. The other shows large additional splitting that could be RDCs between two carnosine molecules. Although in other works there are no additional signals observable at carnosine H2 or H5 signal in ^{1}H localized NMR spectra [50], [29]. There was no study of diffusion of carnosine in muscle tissue to estimate the size of compartments to the author's knowledge. The influence of susceptibility has to be considered as localization of carnosine molecules in muscle cell is still unknown [26].

An exciting option is to detect localized correlated ^{1}H spectra (L-COSY), cross-peaks between signals of carnosine were detected. Measured ^{1}H L-COSY spectra from muscle tissue at 3 T [55] show signal with very low intensity and thus be not visible as could be a case for data from 7 T [56]. *In vivo* L-COSY spectra of muscle tissue [55] show off-diagonal cross-peak. There is also effect of an exchange with paramagnetic complex (Cu^{2+} ions) that shows faster relaxation

[96]. Measurement of *in vivo* localized ^{1}H NMR spectra is not as simple task due to low concentration of metabolites, an overlap of signals, and broadening caused by different magnetic properties of neighboring tissue. Evaluation of carnosine data *in vivo* is complicated as L-COSY ^{1}H NMR spectra show the cross peak indicating coupling between imidazole hydrogens. *In vitro* model made from stretched gelatin showed presence of only monomer carnosine.

It would be of interest to detect more signals of carnosine *in vivo* to gain additional information about partial orientation of this interesting molecule. ^{1}H-^{13}C RDCs detection could gain precise information about partial orientation, but it is of a way of how to get them *in vivo*. Better evaluation of additional splitting for carnosine was achieved for lower magnetic field of 1.5 T [54] than at 7 T [29]. ^{13}C isotopic labeling of carnosine could enable measurement of ^{1}H-^{13}C RDCs. Isotopic labeling of entire carnosine or only L-histidine would not be practical due to metabolic pathways. Carnosine is not metabolized as a dipeptide, but an enzyme carnosinase separates carnosine to L-histidine and β-alanine. But by ^{13}C labeling, only β-alanine would be enhanced, L-histidine would be metabolized and could be incorporated in various other macromolecules. Carnosine concentration in muscle tissue can be doubled by oral supplementation of β-alanine [51]. From the point of partial orientation, β-alanine is flexible, and averaged signals were observed. It is also known that carnosine is only inside cells, a presence of carnosine in serum or blood is a pathological state. Noninvasive determination of pH by carnosine ^{1}H signal was used to diagnose Duchenne muscular dystrophy [49].

5.6 Summary of chapter

The carnosine can provide more RDCs than other observable small metabolites and includes L-histidine with a rigid imidazole ring. However, only the signal from the imidazole ring is observable *in vivo*. Gelatin can be considered similar to the animal cell environment, as collagen is the most abundant material in animal cells. In the case of the *in vitro* model based on stretched gelatin, the main parameters are homogeneity of hydrogel and uniform stretching. Homogenous hydrogels were achieved by melting gelatin without bubbles and slow cooling to room temperature in a given form. Stretching of gelatin was done by elongation of silicon tube, and samples were left to equilibrate for several days. The elongation factor determines observed directed anisotropy and line widths of NMR signals. Setting field homogeneity using the continuous mode of acquisition (TopSpin command 'gs') is recommended for getting the best field homogeneity for stretched samples.

In vitro model measurement focus was on data from high-resolution HSQC NMR spectra where ^{1}H-^{13}C RDCs were determined directly from measured NMR spectra. Based on measured RDCs, L-histidine is partially rigid, and β-alanine is flexible. Structures of carnosine determined by PALES with the approximation of one structure correspond to previously reported data from solution [41]. Carnosine in presented *in vitro* model is in the form of monomer even at concentration of 0.5 mol/dm^{-3}. Results of carnosine measurement in *in vitro* model based on stretched gelatin were published in [39]. For exact evaluation of flexible parts, molecular dynamics with assumption of effective RDC magnitude due to

motion would be necessary. Stretched gelatin provide suitable orienting media for observation of partial orientation for very small molecules such as monopeptides and dipeptide detected in *in vivo* ^{1}H NMR spectra from muscle tissue.

6. Response of hydrogel by localized NMR

6.1 Setting of NMR measurement

Stretched PAM samples undergoing volume phase transition (VPT) in 5 mm NMR tubes were measured by Bruker Avance III HD spectrometer (Bruker Biospin, Germany) operating at 11.7 T (500 MHz for ^{1}H and 76 MHz for ^{2}H). BBFO 5 mm probe head and TopSpin 3.2 were used to acquire localized and non-localized ^{1}H and ^{2}H NMR data. Magnetic field lock and homogeneity were set by automatic TopShim on a sample of Gd doped deuterated water. The sample position was set by pushing NMR tubes to the bottom of the sample gauge for every sample and measurement. NMR spectra from the entire coil area were measured for ^{1}H with a 90 deg pulse duration of 5 μs at 22 W and ^{2}H with a 20 deg pulse with the duration of 100 μs at 4 W. Acquisition of ^{2}H NMR signal in different layers to evaluate the uniformity of partial orientation by phase encoding was utilized to observe processes in hydrogel undergoing VPT [19]. Calibration of gradient strength was done by measurement of water diffusion coefficient at 298 K. The maximum available gradient strength was determined to be 50 gauss/cm. The gradient was set to the maxim value of 95 %, 32 steps of phase encoding were acquired with FOV of 30 mm. The shape of the gradient pulse was set to SMSQ32. The center of ^{2}H spectra was set between water and acetone signals. Measured NMR spectra were transformed to magnitude mode by 'mc' command. Interactive manual fitting and visualization of measured RQS time dependence were done in MATLAB.

Temperature responsive semi-interpenetrating hydrogels based on PNIPAM were measured by Bruker Avance III HD spectrometer operating at 11.8 T (500 MHz for ^{1}H) equipped with a GREAT 60 triple gradient amplifier (maximum gradient amplitude 300 G/cm), Micro-5 micro-imaging probe head, and ^{1}H coil for 10 mm NMR tubes. Setup and acquisition of MRI data were made in ParaVision 6.0 and TopSpin 3.1 PV. The vertical area with uniform signal intensity is about 15 mm long. The sample was placed that the bottom of the 8 mm NMR tube was still observable. The setting of tuning and matching was done manually and was not adjusted after the change of temperature. Determination of resonance frequency, adjustment of shims, pulse calibration, and receiver gain were made by ParaVision 6.0 procedures. Slice of 0.5 mm was measured, the position was set for the lower part of a hydrogel. Gradient strength for diffusion filter was set to b=1000 s/mm^2. Processing of spatially resolved NMR data was done by ParaVision 6.0 and MATLAB. Custom MATLAB scripts were used to determine SNR, visualize measured diffusion-weighted data, and estimate the apparent diffusion coefficient.

6.2 Remarks on sample preparation

The stretched PAM samples were made by procedures described in Chapter 4. Experience with sample preparation was obtained during work on the author's master work. The set for polymerization and stretching of hydrogels was used [59], commercially available from New Era [86]. Hydrogels were made with PAM and a cross-linker BIS with molar ratio of 50:1. When the ratio of cross-linker was varied, observed splitting was smaller, possibly due to lower swelling of hydrogels. There are three regions of possible outcome for network morphology associated with the ratio of monomer and cross-linker [97]. A low amount of cross-linker will produce a dense homogeneous network with junctions created from individual molecules of cross-linker. An intermediate amount of cross-linker produces hydrogel with an inhomogeneous network as cross-linker creates dense structures connected by polymer fibers. A high amount of cross-linker will create long fibers with very dense junctions created mainly from molecules of cross-linker. The high amount region could also be of interest. A response is faster as less solvent is trapped inside collapsing network as the network is created from long chains. Use of fresh solution of APS and TEMED prepared a few minutes before sample polymerization was done, especially in case of highly evaporating TEMED. Conditions during polymerization of monomers with cross-linker create a network with a given morphology. The main issue with the preparation of PAM was the proper mixing of reactants during polymerization. Fast mixing of the solution undergoing polymerization was done by 1 ml pipette tip cut with scissors to enable faster mixing of a solution undergoing polymerization. The temperature during polymerization was also considered a factor. When a hydrogel was prepared in an ice bath and left to polymerize overnight in a fridge, the splitting in ^{2}H spectra were similar or lower than for hydrogel prepared at room temperature. There is some influence of oxygen on PAM polymerization. A hydrogel prepared in a nitrogen atmosphere was not fully transparent, swell less, and was more brittle upon compression. For the NMR study of temperature response, a usual way of hydrogel preparation used by other groups was polymerization between two glass plates without access to oxygen. However, in the case of partial orientation, a sample in the form of a compressible cylinder was required. PAM samples were kept at the room temperature set to 296 K by air-conditioning and were measured in the NMR spectrometer at the temperature of 298 K. Although VPT in water-acetone mixtures was presented as a solvent-based process, the temperature can influence the onset of observed phenomena.

PNIPAM samples were prepared by two procedures. The first was PNIPAM only with a cross-linker suitable for stretching, as in the case of PAM. The second was semi-interpenetrating networks from linear PAM and PNIPAM with a much faster response upon stimulus. Severe negative effects of oxygen presence during PNIPAM polymerization were observed. PNIPAM made without nitrogen atmosphere showed a bubble structure observed on the surface after a temperature change above VPT. For the preparation of homogeneous hydrogel, the bubbling of stock solution for 20 minutes with nitrogen and the use of glass tubes for polymerization instead of the teflon chamber was necessary. By recommendation of Hana Kouřilová, cooling of PNIPAM stock solution with nitrogen bubbling through solution was done in an ice water bath to obtain a homogeneous hydro-

gel. The author concluded that oxygen presence is the main issue of PNIPAM polymerization and the use of an ice bath is not necessary to obtain homogeneous sample. There was an issue with how to get polymerized hydrogel out of a thick glass tube without damaging a hydrogel. One way is to use a steel needle with a syringe filled with water, slide the needle along the glass wall to the bottom and push out hydrogel by water from the syringe. Hydrogels were very often scratch by the needle, and during stretching, such samples ruptured. Another option is to use ethanol or salt (NaCl) solution to force PNIPAM to collapse. However, there would be residues of used chemicals that can influence the measurement of partial orientation. The method was to put a glass tube in hot water to collapse the hydrogel and flush or pull collapsed hydrogel into cold distilled water. Several times collapsed gel adhered at the top to the glass tube, and a steel chemical spoon had been used to detach hydrogel from the wall. As a glass tube was sealed only by parafilm, oxygen presence caused the difference in polymerization at the top of the hydrogel. Irreversible changes in the polymer network could occur during several collapses of a hydrogel when mechanical forces during VPT can disintegrate polymer fibers, but after several VPT the observed process should be reversible. The main difference in the preparation of PAM was using nitrogen gas to remove oxygen from the solution about 20 minutes before polymerization and usage of glass tube because PNIPAM is very sensitive to oxygen.

As hydrogel density is set by weight percentage of monomer, it has to be noted, that the weight ratio of the monomer of PAM and PNIPAM is 1:1.6 due to the presence of large isopropyl moiety. An issue with cross-linker faster incorporation during polymerization could be even more significant for PNIPAM. For the weight ratio higher than 5 % (w/w), PNIPAM hydrogels did not swell enough to fill the teflon chamber and could not be stretched inside the NMR tube. This hydrogel can be compared to 3.1 % (w/w) PAM, which is a lower limit for stretching, such PAM gel also often ruptured during pushing to NMR tube. For both stretched hydrogels, care was taken to get rid of air at the bottom, which would be inside the NMR coil area. Open NMR tube was turned upside down and filled with water to be above the glass. The ultem plug was moved from a side on the glass to prevent air from getting inside the NMR tube and slowly pushed inside to seal the bottom end of the NMR tube. Care was taken to slowly push the ultem plug to avoid the rupture of a hydrogel. From the author perspective, it was better to have more liquid at the bottom than to push hydrogel directly by ultem end-plug.

Samples for MRI observation of PNIPAM response were prepared in two steps. At first, the linear PAM was prepared by mixing the monomer with APS in a water bath at 60 °C for 30 min. Hydrogels were prepared by mixing linear PAM solution with NIPAM monomers, cross-linker, and APS. This solution was bubbled with nitrogen gas for 20 minutes to get rid of oxygen. Free radical polymerization of the network was initialized by the addition of 10 % (v/v) TEMED that was not bubbled with nitrogen due to the very high evaporation of this chemical. Two samples with different amounts of linear PAM were prepared to provide teh observable differences. Samples were placed in an 8 mm NMR tube to enable complete swelling and a lower possibility for tilting of hydrogel during collapse or swelling than in a 10 mm tube, although measurements were done in NMR coil for 10 mm tubes. The most important parameter is the concentration of linear PAM, how many channels are created for water to flow from a hydrogel.

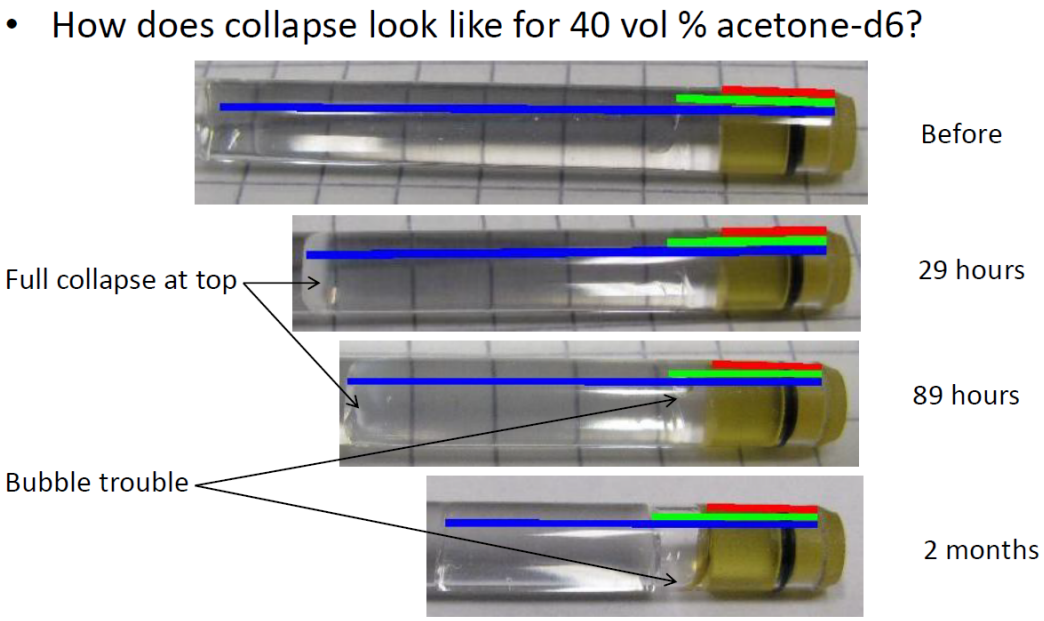

Figure 6.1: Photographs of PAM sample with 40 % (v/v) of acetone-d6 After acetone-d6 addition on the top a collapsed layer is observable. After acetone-d6 reaches bottom a bubble is observed due to difference in gas solubility in water-acetone-d6 mixtures.

6.3 Partial orientation and stimuli-responsive hydrogels

For PAM-based hydrogels, the partial orientation is determined by monomer concentration and aspect ratio [59]. It was of interest to observe what would happen to partial orientation of a suitable molecule in a stretched hydrogel undergoing VPT. Uniaxial elongation causes RDCs that were used to measure partial orientation to determine the molecular structure of the compound. Particular alignment tensor is not significant for structure determination. When uniaxial deformation by elongation is introduced, additional splitting can be observed in the NMR spectra of the molecule of interest. Additional splitting is also observed on deuterated solvent that is used to quickly estimate the magnitude and uniformity of partial orientation. Some hydrogels show a response to certain stimuli observable of an abrupt change of volume. The change of alignment tensor in hydrogel undergoing VPT could gain new knowledge about this exciting phenomenon. Time to reach equilibrium after stimuli depend on the morphology, size, and shape of the cross-linked polymer network. VPT can be a long process, especially in the presence of skin effect or barrier effect when solvent cannot flow through the collapsed layer of a macroscopic hydrogel. Observed phenomena can be influenced by the presence of other solvents, or addition of solutes, or the change of temperature. Molecular-level changes depend on the interaction of several polymer fibers. For PAM the phenomenon is based on the solubility of polymer chains in water, although even monomers are not soluble in acetone. PNIPAM shows more interesting temperature dependent change governed by cooperative hydration of polymer chain. For PAM as a monomer or short chains,

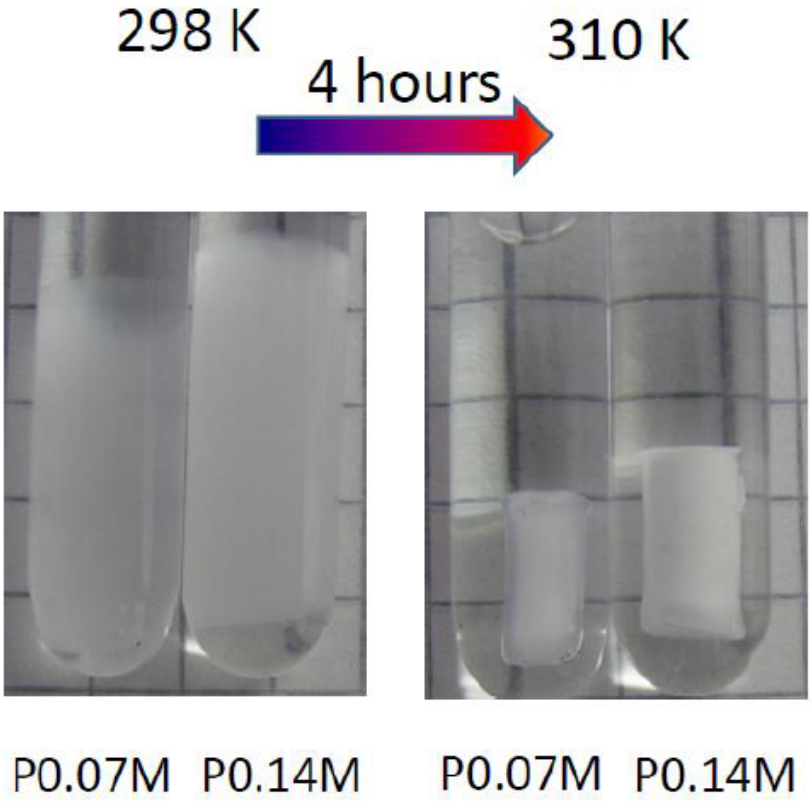

Figure 6.2: Samples of cross-linked PNIPAM with linear PAM
Photo of two samples in 8 mm NMR tubes at room temperature of 298 K and after 4 hours at 310 K in dry bath.

the same behavior is observed. However, the cooperative hydration of PNIPAM requires a certain length of chains. VPT is viewed as process on a macroscopic scale as the response to solvent trapped inside collapsed hydrogel.

The stretching induces linear dependence of anisotropic NMR interactions [59]. The idea was to use a suitable rigid molecule to observe the temperature-driven VPT of a stretched hydrogel made from cross-linked PNIPAM. After the first observation by non-localized measurement, changes were detected on signal of deuterated water for several days for one sample after heating. By de Gennes scaling concepts [98] a change propagates from atomic-level interactions up to macroscopic dimensions upon a specific time. During temperature-induced VTP, a change propagates in hydrogel from the surface to the middle of a sample. Also PAM shows the response from the surface to the core in case of the addition of another solvent [8]. There were reported several pools of deuterated water trapped in collapsing PNIPAM [81]. Temperature dependence was also observed, pools with different relaxation and populations were observed.

There is a difference in signal intensities of doublets in ^{2}H spectra associated with the setting of shims [19]. VPT can be influenced by the uniaxial elongation of the cross-linked PNIPAM network [83]. As observed for small metabolite molecule precise and easy way to obtain RDCs is to measure ^{1}H-^{13}C HSQC spectra. Several hours are required to obtain high-resolution HSQC spectra, and during this period, a signal would be averaged. In case of changes in orienting media, such a localized measurement would be very time-consuming. Small water-soluble molecules do not show high partial orientation in stretched PAM. An issue is also the influence of molecular probe on VPT of a hydrogel, an additive could change the onset or progress of the response. Measurement of ^{2}H signal of solvent was used to verify the presence of anisotropy and also provide information about the magnitude of partial orientation in a given orienting media.

PAM was chosen due to the volume phase transition in water-acetone mixtures. Stretched PAM hydrogel was initially used as orienting media for muscle metabolites where partial orientation was not observed. Carnosine was used as a probe for evaluation of partial orientation due to previous experience. PAM was the first orienting media used to achieve partial orientation used in the author's master work. For carnosine in stretched PAM, only two imidazole signals showed ^{1}H-^{13}C RDCs of about 3 Hz. The other RDCs were not larger than 1 Hz, which was set as experimental error. One sample of PNIPAM was not ruptured after stretching, at least part of a sample. Sample show ^{2}H RQS of 2.5 Hz at 298 K. A similar observation for carnosine was also on the sample of stretched PNIPAM where ^{1}H-^{13}C RDCs on both imidazole signals were about 2.5 Hz. The rest of the carnosine showed RDCs less than the error of measurement. After the change of temperature to 303 K, the RQS was 2.78 Hz, and during several weeks, observed RQS at room temperature in the entire sample was changing to 1.4 Hz. Although PAM provided partial orientation for proteins [59] no reliable additional splitting was observable in ^{1}H-^{13}C HSQC spectra of carnosine in stretched PAM. Without the possibility to determine alignment tensor from RDCs, the focus was on RQS of solvent visible in ^{2}H spectrum, which is commonly used to evaluate magnitude and uniformity of partial orientation in given orienting media. The response of hydrogel to change of stretching, how the lower level of a hydrogel is deformed when the upper level collapsed. It was assumed that skin effect and barrier ef-

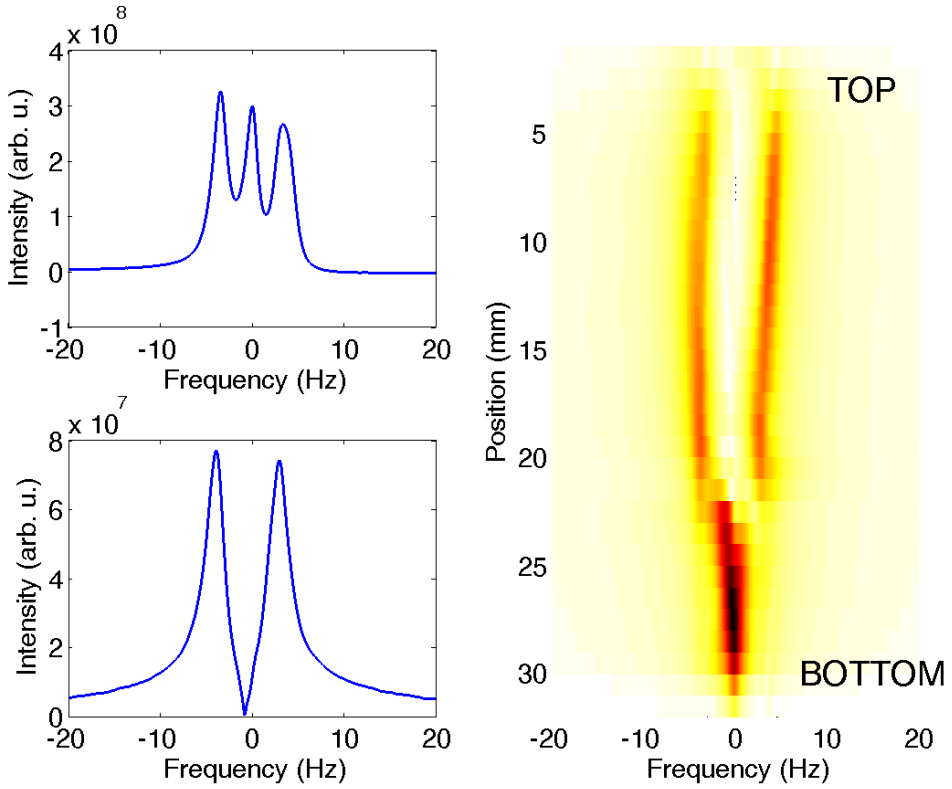

Figure 6.3: RQS observation after addition of acetone to PAM
^{1}H NMR spectra from entire sample of stretched hydrogel. The left part of doublet is taken as a reference.

fect hinder acetone flow through layers of a hydrogel. Characterization of stimuli response of hydrogel based on PAM was done by observation of partial orientation of solvent. For stimuli based on temperature, the response of a hydrogel is imminent, but as a solvent cannot flow freely through the collapsed network. Characterization of a macroscopic sample by MRI enables observation of collapse and swelling of hydrogel upon temperature stimuli in a specific layer from the top to the bottom of a hydrogel. Relaxation-weighted and diffusion-weighted images enable observation of dimensions and characterization of the amount of restricted water during collapse and swelling induced by a change of temperature.

6.4 VPT of PAM by localized partial orientation

It was decided to observe solvent, large rigid molecule soluble in water would have to be in higher concentration for HSQC measurement at natural abundance. Also localized HSQC measurement would be very time consuming. The presence of large molecules could affect the progress of VPT in water-acetone mixture. Interest was in water molecules that interact with the polymer network but also with acetone. The focus was on partial orientation only. Measurement of ^{2}H signal is commonly utilized in macromolecular science due to favorable quadrupolar interaction. Restricted ^{2}H has splitting about 10 times larger than ^{1}H. In ^{1}H spectra,

Gel	62	63	64	66	67	68
Acetone-d6 added (ml)	0.188	0.193	0.240	0.223	0.277	0.283
Ace con whole (vol %)	30	32	34	36	38	40
Ace con gel (vol %)	35	34	39	38	43	42
Length (mm)	26	28	28	27	27	29
RQS (Hz)	6.6	7.5	7.5	7.0	7.6	8.5

Table 6.1: Details about the samples and addition of acetone-d6.

information can be gained by acetone and water signal line-width and intensity where effects of susceptibility are also observed in ^{2}H spectra. The mobility and local magnetic field of observed molecules are changing during VPT. The focus was on localized ^{2}H NMR spectra that provide a signal of partially deuterated water and acetone-d6 in the different layers of solution and hydrogel. PAM samples with acetone were not stored in a refrigerator as change of temperature can influence VPT propagation in a hydrogel. The difference in the use of acetone-d6 and acetone for the introduction of VPT was not concerned. The addition of acetone to the top of the hydrogel caused the collapse of hydrogel exposed to pure acetone. There are three spatial compartments, liquid above, inside, and below hydrogel. This way of VPT was chosen that changes can be observed in layers of hydrogels. Due to solvent hinderance effect, it takes quite a long time for PAM to reach equilibrium due to hindrance of solvent exchange by a collapsed polymer fiber network. The exact temperature for measurement and sample storage, 298 K, was kept. No change of sample due to temperature dependence of volume phase transition should occur.

The first series of PAM samples in range from 20 to 62 % (v/v) was prepared and showed that there are distinct differences of splitting of ^{2}H NMR signal in about a week after the addition of acetone. After acetone addition, the complete collapse of the top of the hydrogel was observed, and the author decided that longer samples reaching out of the observable area would be more suitable. The top is influenced so that more interesting would be to observe the passage of acetone through the longer hydrogel. Hydrogels were pushed further inside the NMR tube to have enough water to provide a pressure buffer for slow pushing of the end plug. Samples for acetone-d6 measurement were in two groups by the amount of water below hydrogel. The position of the hydrogel in the NMR tube is by counting piston rotations. A hydrogel is transparent, and the end was observable only as a very thin line. The funnel and NMR tube was fixed by parafilm, any movement during pushing could cause rupture of a hydrogel, but the end of gel could not be observed. At the bottom of a hydrogel, a bubble is observable after acetone mixed with water. No gas bubbles were observable inside hydrogels, bubbles occurred above or below hydrogel. In hydrogel undergoing a volume phase transition, water-rich and polymer-rich regions are created. PNIPAM measurement of T_1-T_2 2D ^{2}H NMR spectra at different temperatures showed several regions of water [81]. ^{2}H was used as it exhibits wider relaxation range due to presence of quadrupolar interaction. It has to be noted that studied samples consist of 15 % (w/w) linear chains of two different lengths. The shape and dimensions of such regions in a cross-linked network are unknown.

Measurement of length in Figure 6.4 show distinct change on the begging

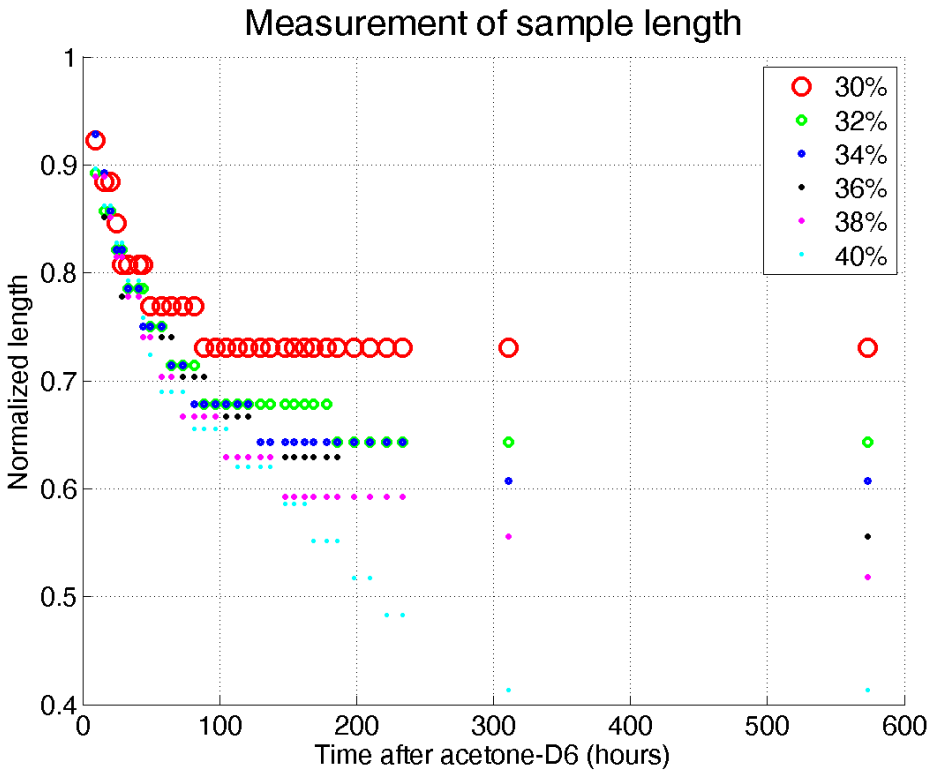

Figure 6.4: Hydrogel length dependence on acetone-d6 concentration
Time dependence of hydrogel normalized length after addition of acetone-d6 at the top. Initial length of hydrogels are in table

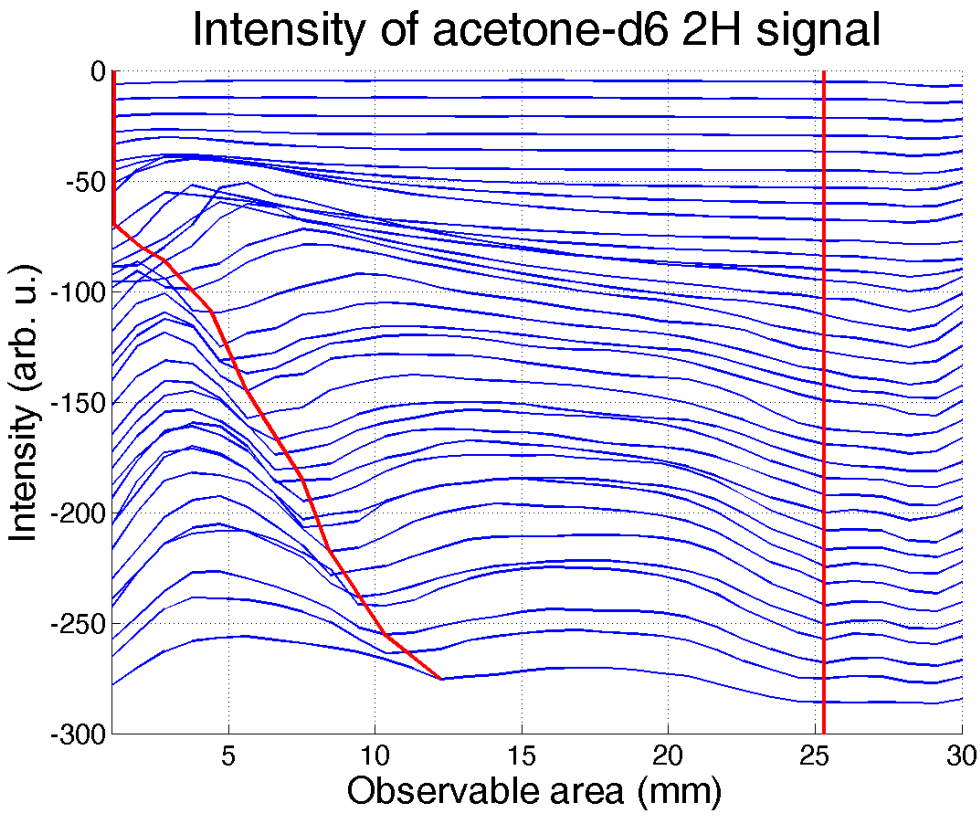

Figure 6.5: Intensity of ^{2}H acetone-d6 signal in time
Observation of top of hydrogel by intensity from integral from ppm to ppm in region of acetone-d6 signal. Red line indicates hydrogel boundary.

when the top of hydrogel that was exposed to pure acetone-d6 and fully collapsed. Swelling of dried hydrogel prepared in teflon chamber in NMR tube with an excessive amount of water, a hydrogel was shorter than hydrogel swelled in teflon chamber and did not show any additional splitting. Stretched PAM VPT in water-acetone mixtures mechanical properties of PAM should be of concern because collapse induced on top of the hydrogel can influence stretching of hydrogel below. The upper part exposed to high acetone-d6 concentration entirely collapsed and shrunk to such an extent that hydrogel does not fill the entire NMR tube, and acetone can reach the lower hydrogel layer. As acetone-d6 is mixed with water, hydrogel response changes, and polymer network show volume change proportional to the local acetone-d6 concentration in a particular layer. Another question is how deuterated water in a mixture with ordinary water influences the volume phase transition of PAM. Isotope effect due to usage of acetone-d6 was not considered. The first series of PAM hydrogels were measured with acetone concentration from 20 to 60 % (v/v). The hydrogel was considered as 95 % (w/w) water. Some polymer was not incorporated into the network, and additional water was soaked into a hydrogel in the chamber before stretching. In the first series, acetone was added at the top to have the concentration of 20, 30, 32.5, 35, 37.5, 40, 42.5, 45, and 60 % (v/v). Samples in the first series were short, and FOV was set to 20 mm. In series of localized ^{1}H and ^{2}H NMR spectra, an overlap occurred as outer volume suppression was not used and the signal was acquired in the whole area of the NMR coil. The position of the sample in the NMR coil was set in the middle of a hydrogel by the sample gauge.

In the second series, acetone-d6 was used with the concentrations of 30, 32, 34, 36, 38, and 40 % (v/v). Measurement of samples started after the addition of acetone (acetone-d6). Two series of PAM samples were prepared, one with acetone and the main one with acetone-d6. Acetone-d6 ^{2}H NMR signal was observed to gain information on the interaction of water, whether orienting media influence dynamic complexes of water and acetone. PAM is not soluble in acetone (acetone-d6). The presence of acetone causes VPT, above 40 % (v/v) solvent change properties. It is a question of water-rich and polymer-rich regions, where acetone could be only in water-rich regions.

Measurement of RQS in layers and length of the entire hydrogel was used to observe the response. Phase encoding is not sensitive to chemical shift artifacts in images and was used to obtain localized ^{2}H NMR spectra of orienting media [19]. Results of water RQS time dependence for a different amount of acetone-d6 added to the top of hydrogels are shown. As stretched hydrogel fills the NMR tube, acetone is added at the top. Observation by localized NMR in layers of the particular sample in time provides information about the partial orientation of solvent inside the hydrogel. A uniaxial deformation introduced by stretching of orienting medium creates a hindrance for solvent molecules or possible clusters. It would be ideal that acetone flows only through a hydrogel to observe consecutive changes associated only with dependence on acetone concentration. The study aimed to investigate the potential of observation of macroscopic changes in a cross-linked network by using spatial separation of NMR signal. Most NMR probe heads are equipped with Z-gradient, enabling measurement of signal with spatial resolution along the z-axis. Acetone was poured at the top of the hydrogels and the time dependence of localized NMR spectra from different layers was measured

and evaluated. Localized ^{2}H NMR spectra were measured by phase encoding, and changes of partial orientation were detected.

Acrylamide and PAM are not soluble in acetone. Partial orientation was not detected on ^{2}H signal of acetone-d6. There was no RQS observed on the acetone-d6 signal, as acetone-d6 does not interact with polymer, acrylamide is not soluble in acetone. The influence of a change of chemical shift induced by the addition of acetone was not evaluated. Acetone-d6 ^{2}H NMR signal in stretched hydrogels did not show any splitting due to RQS. There was no decrease of NMR signal intensity as observed for water for a minimal magnitude of additional splitting. Changes during phase transition phenomena in hydrogels are associated with a change in the number of water molecules interacting with polymer fibers.

By comparison of RQS magnitude and hydrogel length, an interesting observation was done. Monotonous dependence of the final length of hydrogel on acetone-d6 concentration was observed. It was stated that RQS is related to the diameter of hydrogel thus to the volume, but there is an observable rise of RQS magnitude for samples with low acetone content (30 and 32 % (v/v)). Similar dependence can be observed by the measurement of RQS of deuterated water. Several effects should be considered to describe observed phenomena. The first is the mechanical relaxation of a hydrogel after changes introduced by the addition of acetone. In the hydrogel immediately after stretching, a change of RQS is observed as the hydrogel reaches mechanical equilibrium. Another more exciting process could be an exchange of water molecules interacting with polymer and acetone. Polymer does not interact with acetone. The apparent increase of RQS could be associated with decreasing concentration of acetone-d6 as it is mixed with water below hydrogel.

6.5 MRI of PNIPAM response to temperature stimuli

MRI can provide unique quality control for hydrogels as it can see polymer signal of solvent signal inside the hydrogel. MRI provides localized information about interaction on a molecular level with spatial resolution. Samples presented in this work were characterized by NMR and visual observation. Two test samples of semi-interpenetrating PNIPAM with linear chains of PAM were prepared. PNIPAM has concentration of 0.54 mol/kg, the first sample has 0.07 mol/kg and the second 0.14 mol/kg of linear PAM. PNIPAM at the temperature above VPT shows a change from the surface to the core. NMR provides a unique way to measure self-diffusion coefficients. An attractive property of water is the temperature dependence of self-diffusion coefficients [99]. MRI can measure 2D slices with contrast induced by a difference in relaxation and diffusion. Cylindrical hydrogels were suitable for observation of radial change of hydrogel after a stimulus. Although it would be desirable to observe the same sample volume, as hydrogel undergoes VPT amount of polymer in the observable area is changing. The slice position was kept constant at the bottom of the NMR tube. An influence of oxygen is observable as a change of polymer network at the surface of a hydrogel cylinder. Diffusion-weighted NMR measurement enabled observation of water macroscopic mobility and as the self-diffusion coefficient of water is

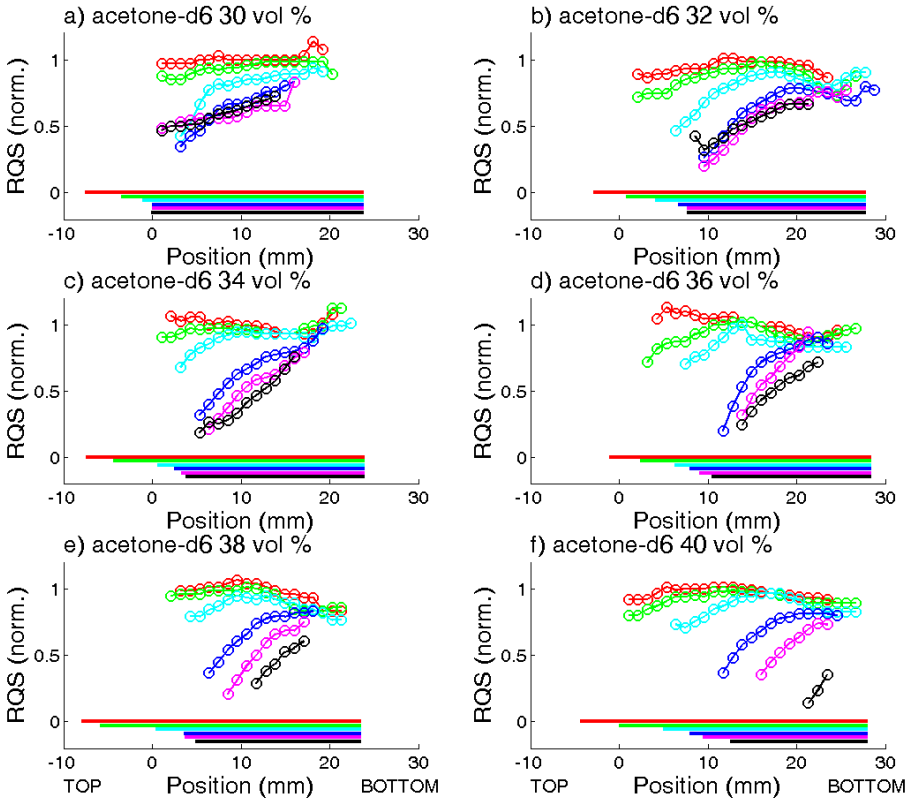

Figure 6.6: RQS of ^{2}H water signal in 6 time intervals
Values of normalized RQS and sample position for 6 acetone-d6 concentrations in selected intervals after addition of acetone-d6.

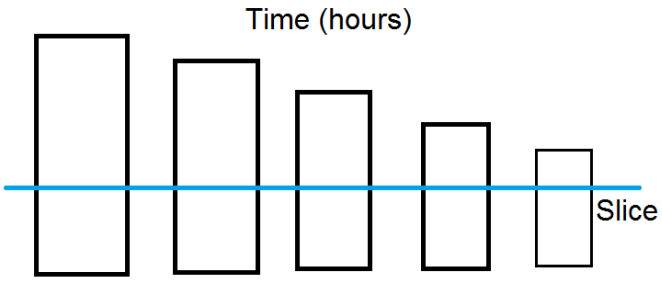

Figure 6.7: Slice position during volume phase transition.
Scheme of volume observed by MRI. The lower middle part was chosen to observe the smallest influence of surface related change. The shape of collapsing hydrogel is idealized, usually gel can bent of is tilted inside NMR tube.

temperature-dependent. Measurement could also be done on the whole sample. The main advantage of localization is the characterization of skin effect or barrier effect when the surface has radial symmetry in 2D measurement. Measurement of T_2 of HDO signal in 5% (w/w) linear PNIPAM solution showed interesting behavior [100]. After initial heating in about 75 hours a change in T_2 relaxation of HDO started to occur. T_2 magnitude is rising a reaching possibly an equilibrium in about 130 hours after stimulus. The authors provide an explanation for this behavior as the bound water is excluded from globular-like structures that are created after stimulus. Measurement of ^{1}H HRMAS PFG NMR spectra of PNIPAM undergoing VPT showed free, restricted and trapped water [70]. Spatial localization requires more scans in order to get information in reasonable time relaxation delay 5 times T_1. Although the response of polymer could be observable by MRI measurement with a selective pulse to observe the signal of isopropyl, the response of polymer was observed immediately. The macroscopic response is of interest, especially the effect of the hindrance of solvent inside collapsing hydrogel. Any additive can influence observed dependence. The setting of the NMR experiment was done on fully swelled or fully collapsed hydrogel at temperature before the change was introduced on the sample. It was observed that relaxation fitted from images is much shorter. The observed phenomenon is described in [20], where a method for relaxation determination from an image was shown. Pulse sequence for fast measurement of slices Rapid Acquisition with Relaxation Enhancement (RARE).

A particular interest was in diffusion-weighted imaging that provides a source of contrast that does not require the introduction of a contrast agent, as a signal from solvent is observed. The study was done on semi-interpenetrating hydrogels, the previous hydrogel was made from PNIPAM and cross-linker only, and the response took about two weeks. Linear PAM chains are rapidly tumbling during polymerization of the PNIPAM network and thus provide channels for faster solvent movement. Such channel effectively suppression skin effect or barrier effect in temperature stimuli-responsive hydrogel. The author decided to observe a semi-interpenetrating network created from linear PAM and cross-linked PNIPAM. As was reported for homogeneous PNIPAM that show skin effect, a collapse takes up to several weeks. For the entire period, the measured sample has to be kept at the same temperature inside the NMR magnet. It is a very demanding

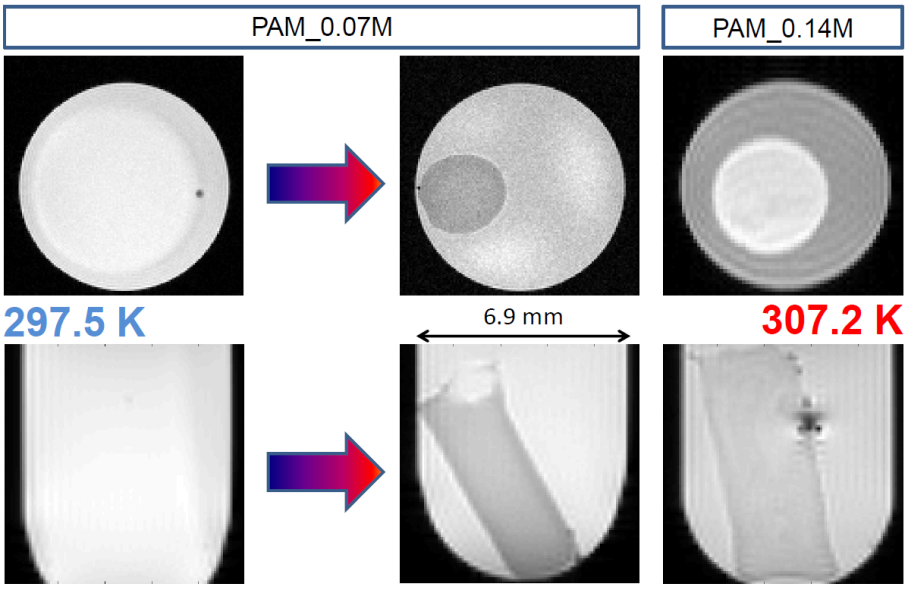

Figure 6.8: Proton density MRI of responsive hydrogel.
Horizontal and vertical slices of two observed samples at 297.5 K and 307.2 K. PAM 0.14 M horizontal slice was measured with RARE, other images were acquired with FLASH pulse sequence. Horizontal image of PAM 0.14 M show artifact in the middle part caused by presence of piece of plastic.

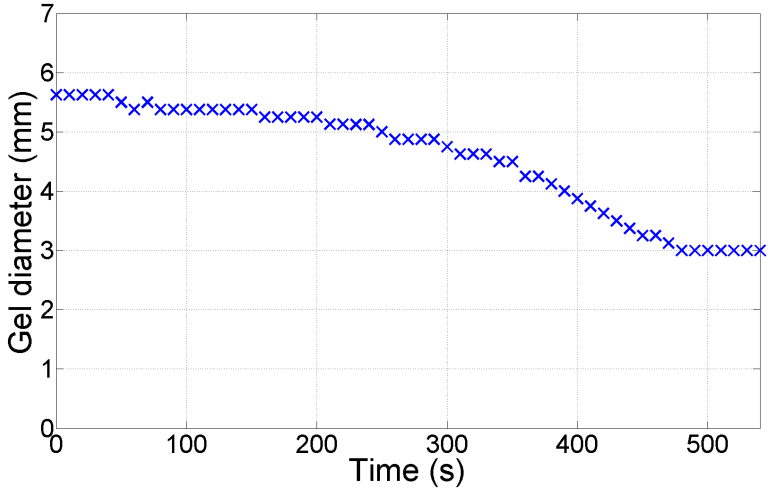

Figure 6.9: Diameter of gel from MRI image.
Time dependence of gel diameter from the middle part. Scheme of slice setting during hydrogel measurement. The same part of a hydrogel, but as it is collapsing or swelling, layer would have to change size in order to observe the same amount of polymer. In order to observe the same layer of hydrogel during volume phase transition by slice selective MRI plane of measurement was chosen.

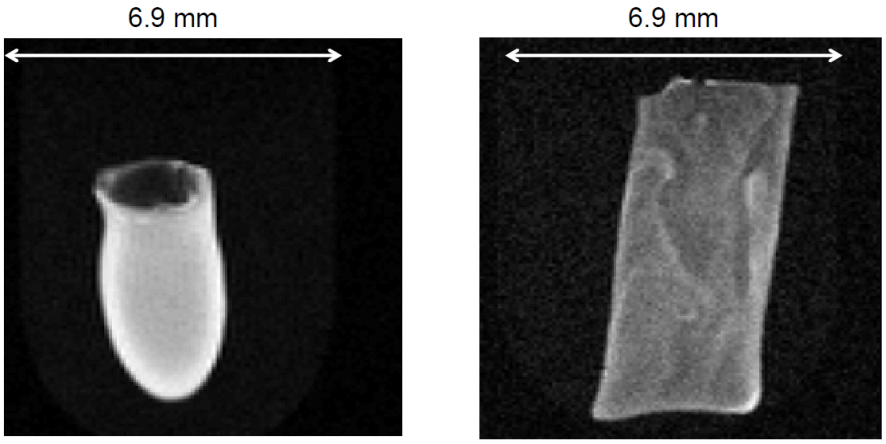

Figure 6.10: Collapsed hydrogels measured with diffusion weighted MRI. Diffusion weighted image can be used for quality control. Hydrogel with 0.07 mol/kg of linear PAM is homogeneous with distinct surface layer, that polymerized differently due to presence of oxygen. Hydrogel with 0.14 mol/kg of linear PAM is not homogeneous, solution with more linear PAM was viscous in such an extend that was not mixed properly.

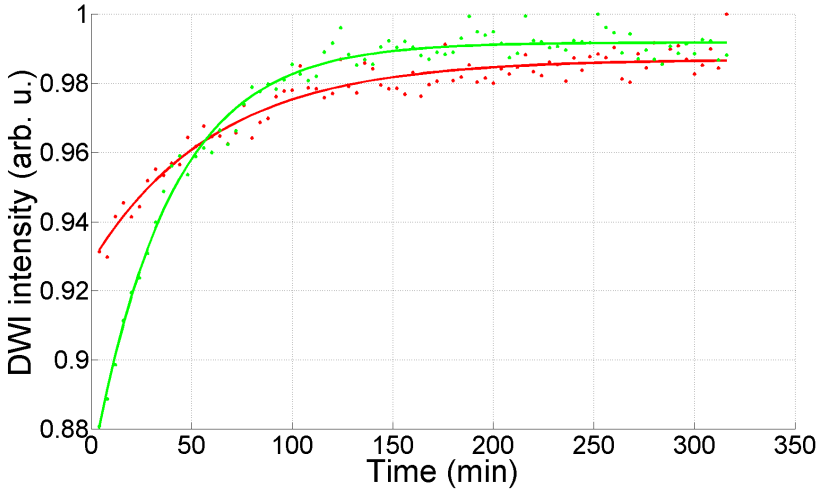

Figure 6.11: Collapsed hydrogels measured with diffusion weighted MRI. Sum of intesity of water signal in series of diffusion weighted images can be used to determine when hydrogel reaches equilibrium. For 0.07 mol/kg linear PAM sample equilibrium is reached in 3.5 hours. For 0.14 mol/kg linear PAM sample equilibrium is reached in 2.5 hours. Intensity time dependence after change of temperature from 298 K to 307 K.

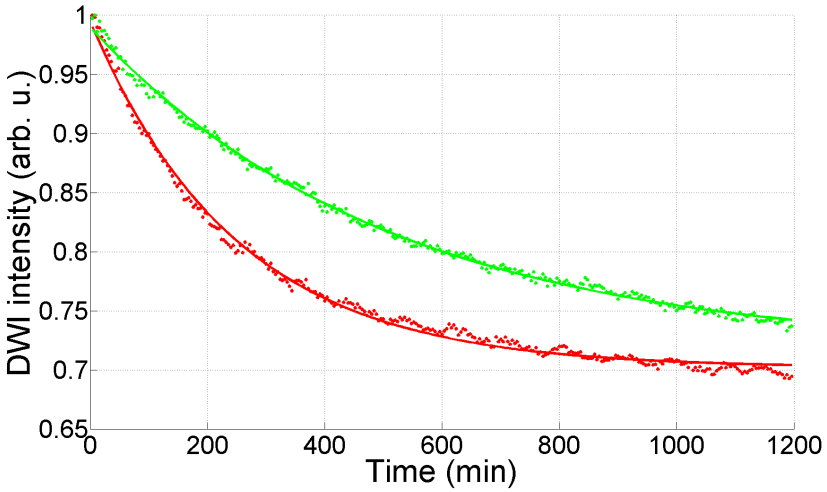

Figure 6.12: Collapsed hydrogels measured with diffusion weighted MRI. Normalized sum of intensity show how hydrogels reaches equilibrium in case of swelling. For 0.07 mol/kg linear PAM sample equilibrium is reached in 22 hours. For 0.14 mol/kg linear PAM sample equilibrium is reached in 45 hours. Intensity time dependence after change of temperature from 307 K to 298 K.

measurement for spectrometer usage.

An essential factor for PAM samples was measurement and storage at the temperature of 298 K. For PNIPAM hydrogel, a sample has to be in the NMR spectrometer for the entire observation. Linear PAM provides channels that enable fast transport of solvent after stimuli, and skin effect is not observed in such hydrogels. Observation of hydrogel homogeneity by MRI for quality control of prepared samples. The reversible response was created by several cycles of collapse and swelling. The first is a restriction of motion of individual polymer units, and the second is the hindrance of solvent molecules inside the collapsed hydrogel. The first response occurs in a whole sample and is imminent after the temperature is equilibrated in a sample, about 3 min in a distilled water sample. A flow around cylindrical hydrogel associated with temperature equilibration was observed in the NMR tube. The severe disadvantage of measurement of VPT by NMR is an effect of change of signal intensity caused by a difference in magnetic field homogeneity.

The semi-interpenetrating hydrogels were collapsed in several hours, took swelling took about two days. Measurement of diameter of hydrogel cylinder. MRI enables to gain contrast in localized measurement by using diffusion filter to observe water interacting with polymer, the motion of solvent hindered by polymer structure. Although non-localized measurement would also gain information, localization provides an additional view on the behavior of hydrogel undergoing VPT. For measurement of hydrogels, even one gradient strength of diffusion filter is enough to determine sample equilibrium to characterize collapse and swelling of particular hydrogel. The apparent diffusion coefficient, a fit for one average component, was done. It showed lower values for the surface of hydrogel, but inside a plateau was observed, it is known that there are several pools of water in the polymer network undergoing VPT [81]. A change in the NMR signal of solvent molecules was used to determine equilibrium.

The observed signal is a product of the magnitude of pool population and diffusion coefficient. A particular diffusion strength is used as a filter to suppress water that does not interact with the polymer network. The experiment was set up to utilize a change of diffusion coefficient with temperature. The equilibrium is evaluated that there is only a tiny change in the difference of signal intensity. The signal is mainly for diffusion coefficient above the specific threshold given by the gradient magnitude used for diffusion filter. Although information gained by diffusion can correspond to dimensions of obstacles, the VPT in the hydrogel is evaluated only to determine the time to reach an equilibrium. NMR spectrometer enables precise control of sample temperature. The change of temperature was chosen to be fast, and it was measured on the water by diffusion-weighted imaging that equilibrium was reached after 3 minutes for water in an 8 mm NMR tube, data not shown. Change of temperature influence intensity of the signal in diffusion-weighted measurement not only by Boltzmann factor but also a change of water properties could be observed. The mechanism of the temperature-induced VPT is still not fully understood. The main focus is an interaction of CH_3 moieties with water, that change of movement of polymer fibers at a specific temperature. Characterization of volume phase transition based on MRI of a cross-section of PNIPAM based hydrogel in the form of a free swollen cylinder was done.

The observed intensity in images with a change of TE does not scale by T_2 [20]. To measure the image, several iterations with different gradient strengths have to measure. In case of waiting for the spin system to get to equilibrium, acquiring an image would take much longer for just one image. Diffusion-weighted images are used as a way to characterize water inside macroscopic cross-linked semi-interpenetrating hydrogel based on temperature-responsive PNIPAM during reversible phase transition. The knowledge about water in PNIPAM under VPT was measured in [81], where several pools of water were detected, and temperature dependence was observed. Study of linear chains by small angle X-ray and ^{1}H NMR diffusion showed some insight into phenomena [69]. Measurement of relaxation time T_2 of ^{1}H in HDO with linear chains showed that certain processes occur even a week after change of temperature [100]. 2D ^{2}H T1-T2 correlation measurement showed several pools of water inside PNIPAM linear chains after collapse [81]. It has to be noted that cited studies used different preparation procedure for polymerization of linear PNIPAM and the last also change utilized a difference in tacticity of polymer fibers. In case of cross-linked PNIPAM a situation is more complicated as cross-links do not allow free motion of polymer chains.

6.6 Summary of chapter

The project initially aimed to observe VPT of PNIPAM by partial orientation of a suitable molecular probe. The experiments showed that response of 5 % (w/w) PNIPAM occurred from the surface to the middle and could take about 2 weeks. The focus of characterization of VPT by partial orientation shifted towards already proven stretched PAM where stimuli can be introduced by the addition of acetone at the top of stretched hydrogel. An issue of rupture of hydrogel due to pressure build-up was solved by filling a teflon chamber with water while

pushing a hydrogel into the NMR tube. Water is incompressible, and no pressure build-up in the air-filled chamber did occur, although hydrogel still shows sometimes cracks at the bottom. Localized ^{2}H NMR spectra of the first series of PAM samples provided observation of hydrogel response to acetone in the range of 20 to 60 % (v/v). Equilibration was reached in about two weeks. The second series presented in this work was in the range of 30 to 40 % (v/v) and deuterated acetone was used. The additional splitting of deuterated water showed a change after addition of deuterated acetone. As the top of a hydrogel was exposed to pure acetone and gel collapsed to such an extent that hydrogel does not fill entire NMR tube acetone could reach lower hydrogel layers without flowing only through the hydrogel. Observed dependence is interesting, but proper understanding requires separation of the interaction of water with polymer fibers and water with acetone and knowledge about hydrogel mechanical properties. The observed dependence was dependent on the amount of acetone added at the top rather than predicted equilibrium concentration of acetone. Interpretation of NMR measurement for characterizing volume phase transition of PAM in water-acetone mixtures is needed by a proper theoretical model that would account for stretching effects on hydrogel volume phase transition. Even very low RQS of about 7 Hz for 5 % (w/w) PAM hydrogel enable characterization of the polymer network response.

MRI was utilized to observe response of semi-interpenetrating PNIPAM hydrogels. The small angle X-ray and diffusion studies show cavities with a Gaussian distribution inside PNIPAM undergoing collapse. The connectivity of the cavities implies that the hydrogel structure is an irregular sponge phase with smooth interfaces and a submicrometer cross section. MRI of suitable slice show how hydrogel reaches equilibrium after stimulus.

7. MRI of ^{19}F molecular probe and IONPs

7.1 Setting of NMR measurement

The new ^{19}F molecular probe described in [101] and 2,2,2-trifluoroethanol (TFE) were measured by Bruker Avance III HD NMR spectrometer (Bruker Biospin, Germany) operating at 11.8 T (500 MHz for ^{1}H and 470 MHz for ^{19}F). The spectrometer was equipped with a GREAT 60 triple gradient amplifier, Micro-5 imaging probe head with x,y,z gradient coils (maximum gradient amplitude 300 G/cm), and ^{1}H radio-frequency coil tunable to ^{19}F for 5 mm NMR tubes. TopSpin 3.1 PV was used for the acquisition of relaxation data by inversion recovery and spin echo pulse sequences for the fit of T_1 and T_2 of ^{19}F containing chemicals, respectively. For comparison of imaging methods, two capillaries with inner diameter 1.1 mm were filled with molecular probe (concentration 16.7 mM) and TFE (concentration 33.1 mM). Relaxation measurement was done on a sample consisting of a capillary in an empty 5 mm NMR tube. The ^{19}F resonance frequencies were 470.884 MHz for the contrast agent and 470.858 MHz for the TFE solution. ParaVision 6 with TopSpin 3.1 PV were used to acquire pulse sequences ^{19}F UTE, ^{19}F RARE, and ^{1}H FLASH. Images of capillaries for comparison of ^{19}F acquisition of two compounds were obtained with the following settings. ^{19}F UTE was measured with 90 deg pulse duration 0.105 ms, TR 5.5 ms, TE 0.091 ms, BW 25 kHz, FOV 5 x 5 mm, slice thickness 4 mm, 202 projections, 512 averages, image resolution 64 x 64 points in 9.5 min. Calibration of UTE sequence was done on a sample of TFE and water (volume ratio 1/3) because of very short T_2 of contrast agent as is recommended in ParaVision 6 manual. ^{19}F RARE was measured with 90 deg pulse duration 2.1 ms, TR 3000 ms, TE 7 ms, BW 15 kHz, FOV 5 x 5 mm, slice thickness 4 mm, RARE factor 64, 190 averages, image resolution 64 x 64 points in 9.5 min. ^{1}H FLASH for determination of the position of capillaries was measured with 15 deg pulse duration 0.84 ms, TR 100 ms, TE 2.5 ms, BW 50 kHz, FOV 5 x 5 mm, slice thickness 1 mm, 4 averages, image resolution 128 x 128 points in 51.2 s. Sample of labeled cells in medium with concentration 50 and 100 mM of ^{19}F were measured in 5 mm Shigemi NMR tube with following settings. ^{1}H FLASH was measured with 90 deg pulse, TR 100 ms, TE 2.1 ms, FOV 20 x 20 mm, slice thickness 1 mm, 8 averages, image resolution 128 x 128 points. Horizontal ^{19}F UTE images were measured with 90 deg pulse duration 0.158 ms, TR 4.5 ms, TE 0.111 ms, BW 20 kHz, FOV 10 x 10 mm, slice thickness 5 mm, 1200 averages, 106 projections, image resolution 34 x 34 points in 9.5 min. Vertical ^{19}F UTE images were measured with 90 deg pulse duration 0.158 ms, TR 6.5 ms, TE 0.111 ms, BW 20 kHz, FOV 20 x 20 mm, slice thickness 5 mm, 20000 averages, 208 projections, image resolution 64 x 64 points in 7.5 hours. Calibration of UTE sequence was done on the sample of TFE and water (volume ratio 1/3) because of very short T_2 of molecular probe as is recommended in ParaVision 6 manual.

Iron oxide nanoparticles (IONPs) T_1 and T_2 relaxation times were measured by Bruker Avance III HD NMR spectrometer operating at 11.7 T (500 MHz for

^{1}H). BBFO probe head and TopSpin 3.2 were used to acquire T_1 data by inversion recovery and T_2 data by CPMG pulse sequences. CMPG pulse sequence was measured with 90 deg pulse of the duration of 10.4 μs and echo time of 420 μs. Measurement of relaxation experiments was done by setting temperature calibrated by methanol and ethylene glycol, wait for 15 min, automatic tuning and matching by ATMA, automatic setting of field homogeneity by TopShim, and acquire NMR spectra for the fitting of T_1 and T_2 dependencies. The sample consisted of two NMR tubes, the inner tube was filled with 1,1,2,2-tetrachloroethane-D_2 (99.5 % D, Merck) for the lock, and 70 μl of suspension with IONPs in distilled water was placed between NMR tubes. The intensity and integral dependencies were fitted in TopSpin for T_1 and MATLAB for T_2. ^{1}H images of IONPs were acquired by Bruker Avance III HD NMR spectrometer (Bruker Biospin, Germany) operating at 11.8 T (500 MHz for ^{1}H). The spectrometer was equipped with a GREAT 60 triple gradient amplifier, Micro-5 imaging probe head with x,y,z gradient coils (maximum gradient amplitude 300 G/cm), and ^{1}H radio-frequency coil for 10 mm NMR tubes. ^{1}H MSME images were acquired with 90 deg pulse with duration 0.15 ms, TR 2 s, BW 50 kHz, FOV 8x8 mm, slice thickness 0.5 mm, 4 averages, image resolution 128 x 128 points in 17 minutes. TE values were set to 3.3 ms, 5 ms, and 6.5 ms.

7.2 MRI of ^{19}F molecular probe

MRI enables unique observation of the structure of tissue *in vivo*. Unique information can be acquired by enhancing contrast with the addition of specific molecules. Most contrast agents used for MRI are based on a paramagnetic center that alters the relaxation of nearby water molecules that are detected. An exciting option is to observe NMR signals directly from a molecule with a paramagnetic center without overlap with metabolites. That can be achieved by detection of ^{19}F labeled molecules as ^{19}F in a body is usually fixed in bones and contribute to NMR spectra as a broad background. A suitable pulse sequence can provide sufficient sensitivity and specificity for a given molecular probe in reasonable time [102]. Short T_1 relaxation time caused by the presence of a paramagnetic center enables rapid repetition of pulse sequence to gain signal by a high number of scans. Relaxation T_1 is associated with T_2 relaxation, and only sequences with very short TE or acquisition of FID can measure sufficient signal for very fast relaxing signals. Ultrashort echo time (UTE) [22], [23] and zero echo time (ZTE) [103] are able to measure FID and reach ultrashort TE defined in the range of 50 μs to 500 μs. ^{19}F has 100 % natural abundance, and the resonance frequency is not far away from ^{1}H.

Pulse sequence inversion recovery and spin-echo were used for the determination of T_1 and T_2 of molecular probe and TFE, respectively. The concentration of ^{19}F was 100 mM for both compounds, molecular probe has 6 ^{19}F atoms, and TFE has 3 ^{19}F atoms. The samples were in flame-sealed capillaries. Relaxations were determined by measurement of particular capillary in a 5 mm NMR tube. ^{19}F relaxation values for molecular probe were $T_1 = 1.52(3)$ ms and $T_2 = 0.78(2)$ ms at 11.8 T. Baseline correction for the molecular probe was done manually due to a very broad ^{19}F signal with a line width of about 400 Hz. TFE ^{19}F relaxation values were $T_1 = 3.46(7)$ s and $T_2 = 2.96(15)$ s.

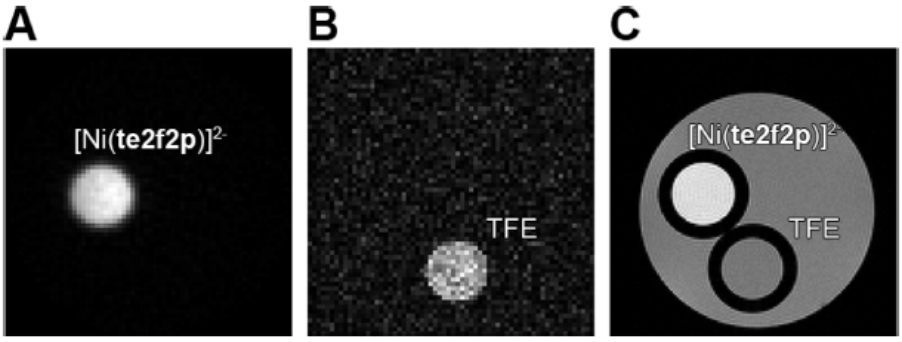

Figure 7.1: ^{19}F and ^{1}H images of phantom.
^{19}F images with frequency setting on ^{19}F molecular probe by UTE (A) and TFE with RARE (B) measured with resolution 64 x 64 points in 9.5 min, and ^{1}H image for localization (C). Published in [101].

^{1}H FLASH images were measured to confirm localization. The paramagnetic center does not influence only ^{19}F NMR signal but also has a strong effect on relaxation of ^{1}H in water as was observed in Figure 7.1. Comparison of two ^{19}F containing compound was done by UTE for molecular probe, and RARE [21] for TFE set to have the same duration, 9.5 minutes. UTE pulse sequence is suitable for compounds with extremely short T_2 and can provide significant T_1 contrast by rapid repetition. RARE is suitable for compounds with T_2 relaxation time. Both imaging sequences were measured with resolution 64 x 64 points in 9.5 min. The UTE image is reconstructed from the sum of projections. The intensity of the RARE image is determined by the measured signal at the center of the k-space, which is one experiment in the middle of the train of echoes. Comparison of imaging sequences was done by SNR that was calculated as $[2 \times ((signal)^2 - (noise)^2)/(noise)^2]^{1/2}$. The signal and noise data were chosen from areas of the same size. Processing was done in MATLAB. In the case of the molecular probe with UTE SNR of 35 was achieved, for TFE measured with RARE SNR was 5.9. The combination of ^{19}F molecular probe with UTE provides about 6 times higher SNR than the same ^{19}F concentration of TFE acquired with RARE pulse sequence. It was estimated that for SNR of 2, the required ^{19}F concentration for the molecular probe was 5.6 mM.

UTE was used for measurement of ^{19}F images of cells that were exposed to two concentrations of ^{19}F molecular probe, counted, and fixed. Only the molecular probe that was inside living cells after fixation was present in the measured samples. ^{19}F UTE and ^{1}H FLASH MRI images of cells in 5 mm NMR tubes are shown in Figure 7.2. Horizontal images were done in 9.5 min, and ^{19}F molecular probe in cells was observed. The molecular probe was supposed to be only inside cells, but there was also observed ^{19}F signal with lower intensity in the solution above the cell pellet. NMR measurements were started the next day after fixation, and the presence of ^{19}F outside could be caused by the efflux of a tiny molecular probe through the cell membrane.

Improvement of the intensity of the observed signal in case that TR is not longer than 5 times T_1 could be gained by use of Ernst angle [1]. For UTE and compound with very short T_2, it was reported that maximum intensity with 2D slice is achieved even for longer pulses than at Ernst angle [104]. The intensity im-

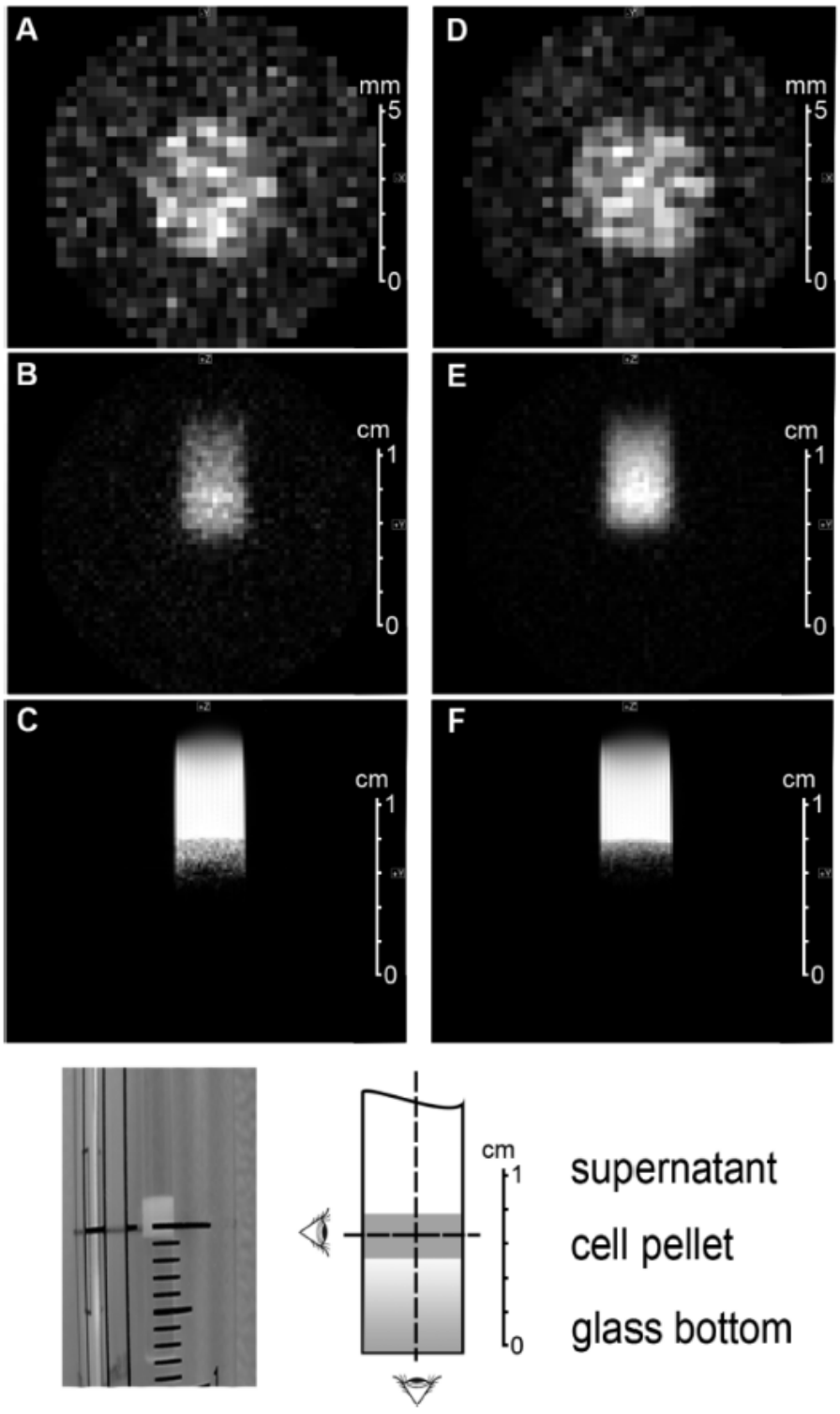

Figure 7.2: ^{19}F and ^{1}H images of labeled cells.
Two samples of labeled fixed cells were measured. The lower concentration: (A) ^{19}F horizontal profile, (B) ^{19}F vertical profile, and (C) ^{1}H for comparison. The higher concentration: (D) ^{19}F horizontal profile, (E) ^{19}F vertical profile, and (F) ^{1}H for comparison. At the bottom there is the photo and scheme of the sample with indicated center of MRI coil. Published in [101].

provement with Ernst angle was observed for compounds with longer T_1 and T_2. The phenomenon could be caused by relaxation during selective radio-frequency excitation pulse with a duration of 0.105 ms, as relaxation times of molecular probe are very short $T_1 = 1.52(3)$ ms and $T_2 = 0.78(2)$ ms at 11.8 T. For UTE with lower than 90 deg pulse in case of very short relaxation times, the effect on SNR would be not such pronounced, although energy deposited would be lower. Ernst angle could provide higher SNR for TFE measured by RARE, which was not obvious to the author at the time of measurement. The main focus far the author was measurement of ^{19}F molecular probe.

It was observed that NMR signal intensity is not improved at lower imaging gradient strength as observed with echo methods. A decrease of SNR was observed for gradient strength for UTE below 25 kHz (data not shown). Acquisition times and signal sampling given by resolution were set proportional to gradient strength used for frequency encoding. The lower strength of gradient NMR signal was supposed to be more intense, but as sampling starts later, the T_2 affects the intensity of the first point that determines the magnitude of the NMR signal. For higher SNR, it would be necessary to adapt the Bruker method UTE to set a fixed acquisition time for several gradient strengths for very fast relaxing compounds. Acquisition time duration also influences the setting of TR. For gradient strength lower than 30 kHz, a minimum of TR 4.5 ms could not be achieved due to parameter adjustment of original Bruker method.

7.3 Measurement of novel IONPs

The contrast in MRI images can be gained by the usage of iron-oxide nanoparticles (IONPs) that shorten T_2 relaxation of nearby water molecules. An exciting option for application is to get nanoparticles inside living cells and observe presence in a specific time after transplantation, as in the case of pancreatic islets [106]. Measurement of T_1 and T_2 of water with IONPs was done by inversion recovery and CPMG pulse sequence, respectively. Acquisition of data and fitting of T_1 and T_2 at 11.7 T was done by Petr Dvořák. Aqueous suspensions of coated IONPs were measured. T_1 was measured to ensure 5 times T_1 relaxation delay that was necessary for the determination of relaxation delay for T_2 data acquisition. T_2 measurement has an issue with the intensity of the first point of measurement, after the second echo of the CPMG pulse sequence, that was omitted for the fitting.

MSME pulse sequence was used for the acquisition of images to observe and compare T_2 contrast of new IONPs with commercially available ferucarbotran (Resovist). Images are shown in Figure 7.3 with TE of 3.3, 5, and 6.5 ms show similar T_2 contrast. T_2 values estimated from MRI images by the fit of SNR are much shorter than measured by CPMG. Phase encoding used for spatial localization of NMR signals influences NMR signal intensity [20]. MRI image of the cross-section of sample for relaxation measurement is in Figure 7.4. An issue with bubbles occurred after sealing of capillary in MRI images. Bubbles were created after some time when the sample stand still. Even after using ultrasound, tiny air bubbles were still observed in capillaries, especially with images acquired by gradient echo (FLASH). Several different slices were acquired to obtain one with only water to evaluate influence of iron-oxide nanoparticles. Bubbles distort

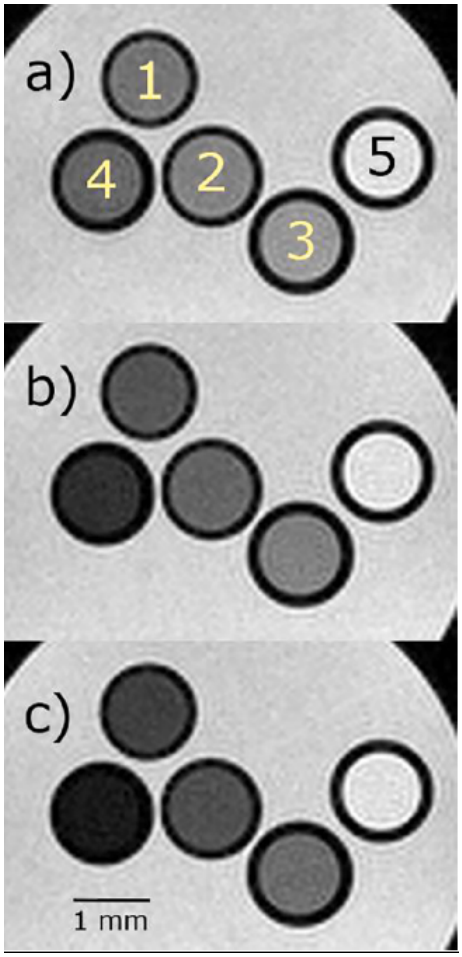

Figure 7.3: T_2 weighted ^{1}H images of water with iron-oxide nanoparticles ^{1}H MSME image of capillaries acquired at 11.8 T with a) TE=3.3 ms, b) TE=5 ms, and c) TE=6.5 ms. The samples were: 1-ϵFe_2O_3 s08, 2-ϵFe_2O_3 s12, 3-ϵFe_2O_3 s19, 4-ferucarbotran (Resovist), and 5-water. Images were published in [105].

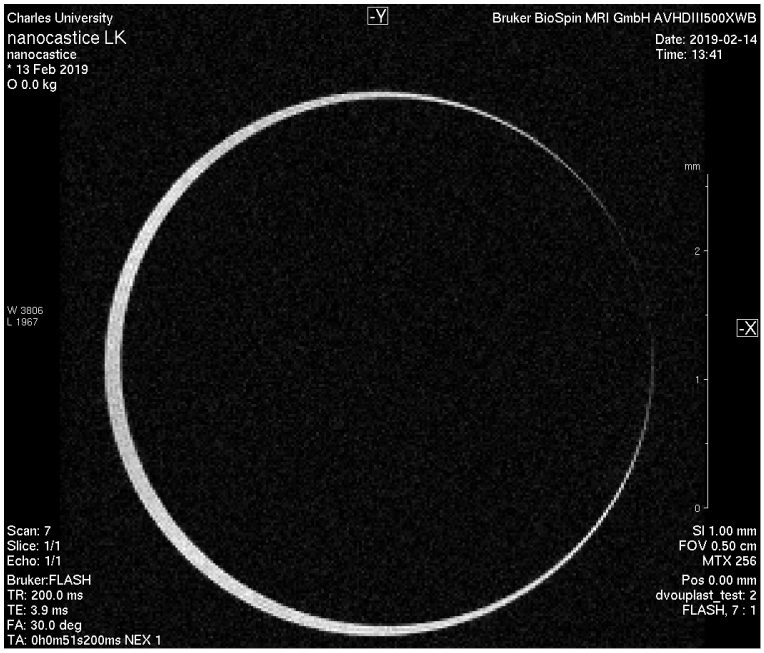

Figure 7.4: ^{1}H image of water with IONPs in 5 mm NMR tube
Slice made from a sample used for determination of relaxation times.

the magnetic field, and at higher echo times, this effect can be observable up to several millimeters far away from a bubble.

Performance of novel IONPs was compared to commercially available Resovist. Commonly used pulse sequence based on gradient echo (FLASH) in Figure 7.5 and spin echo (MSME) in Figure 7.6 were measured with several TE values. Resovist still provide better T_2 contrast than studied IONPs. A higher initial intensity is also caused by faster T_1 relaxation of Resovist.

7.4 Summary of chapter

^{19}F molecular probe was compared with TFE by measurement of SNR for the same ^{19}F concentration, image resolution, and experimental time. Relaxation

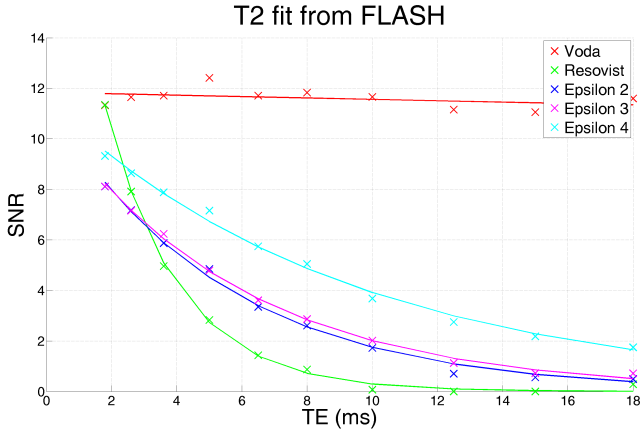

Figure 7.5: Dependence of SNR on TE for FLASH.

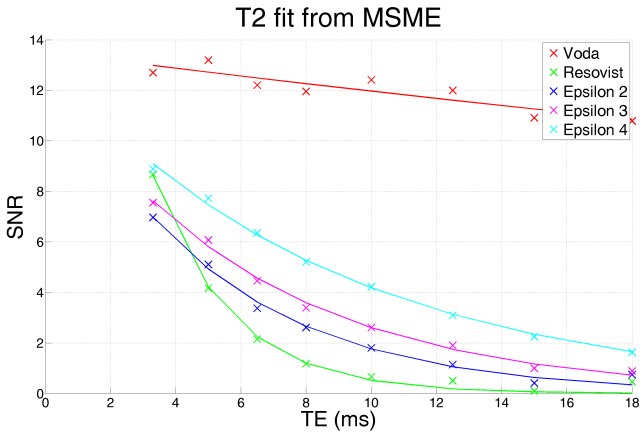

Figure 7.6: Dependence of SNR on TE for MSME.

times T_1 and T_2 were determined for molecular probe and TFE at 11.8 T. Suitable pulse sequences were used for the given relaxation times of two compounds. The UTE pulse sequence acquired the images of the molecular probe. TFE was visualized by the RARE. SNR was 6 times higher for molecular probe measured with UTE. It was estimated that SNR of 2 could be achieved in 9.5 min for the molecular probe with ^{19}F concentration just of 5.6 mmol. ^{19}F UTE of labeled cells measured in 9.5 min showed clearly the presence of molecular probe. There is a possibility to improve SNR for a compound with very short T_2 by adjusting the Bruker ParaVision methods to set acquisition time and sampling independently on the setting of gradient strength used for imaging.

Relaxation times T_1 and T_2 were measured at 11.7 T. NMR images of novel IONPs were acquired by gradient echo (FLASH) and spin echo (MSME) pulse sequences with several different TEs. Images by spin-echo based MSME were acquired with TE of 3.3 ms, 5 ms, and 6.5 ms. Three novel IONPs with different thicknesses of silica show comparable T_2 contrast with commercially available ferucarbotran (Resovist).

Conclusion

This dissertation was focused on the utilization of NMR to study three topics. Chapter 5 describe the measurement of the partial orientation of carnosine in stretched gelatin as an *in vitro* model of muscle tissue. Chapter 6 provide insight into volume phase transition in hydrogels by partial orientation of water in PAM that collapse after acetone addition and PNIPAM temperature-induced stimuli detected by diffusion-weighted MRI. Chapter 7 is about MRI measurement of ^{19}F molecular probe and IONPs utilized as contrast agents. The conclusions of the three topics are in separate sections:

Partial orientation of carnosine

Carnosine is an exciting target for *in vivo* localized NMR measurement. ^{1}H signals from histidine are used for the noninvasive determination of pH in muscle tissue. *In vitro* model based on stretched gelatin was used to obtain RDCs characterizing partial orientation of muscle metabolite carnosine at 4.7 T and 11.7 T. Data from 4.7 T were only non-localized ^{13}C NMR spectra where two ^{1}H-^{13}C RDCs could be estimated, other signals show severe overlap in magnitude mode. *In vitro* model showed that the best approach for characterization of partial orientation is to obtain ^{1}H-^{13}C RDCs. Although basic ^{1}H spectra where additional splitting caused by ^{1}H-^{1}H RDCs is observed can be acquired in a localized way in a reasonable time. In the case of ^{1}H-^{1}H RDCs, there is a severe issue of strong coupling that requires fit for the entire ^{1}H spin network to determine the magnitude of coupling constant. Larger magnitude of ^{1}H-^{13}C J-coupling and larger chemical shift dispersion of ^{13}C enabled more precise RDC data for alignment tensor fitting by PALES. Additional splitting in ^{1}H and ^{1}H-^{13}C HSQC spectra of carnosine were observed. Measurement of carnosine NMR signals provides enough RDCs for the estimation of alignment tensor in PALES. The structure with the best fit of RDCs corresponds to monomer carnosine detected in solution, even at 0.5 M concentration. Data obtained from carnosine in stretched gelatin were compared with *in vivo* measurements reported by several groups in different magnetic fields (1.7 T to 7 T). The current evaluation of muscle metabolism is based on localized ^{31}P NMR spectra that provide an estimation of phosphate-containing molecules that serve as storage of energy for muscle tissue. Although additional splitting observable in *in vivo* NMR spectra is an exciting phenomenon, from the perspective of the author, there is no potential for utilization as a new diagnostic parameter.

Volume phase transition of hydrogels by MRI

Partial orientation was used to observe the volume phase transition of hydrogel after the stimulus. The original studied system was PNIPAM that shows VPT with a change of temperature. Observation of partial orientation was done on PAM samples that collapsed after the addition of acetone after several attempts with PNIPAM. For the temperature response of PNIPAM a shrinkage occurs from the surface to the center of the hydrogel. In the case of PAM and acetone, a response is observable in the layers as acetone diffuses into PAM. Additional splitting observable in ^{2}H NMR spectra of the solvent provided information about

the response of PAM. The initial idea was to use a suitable probe molecule to determine the alignment tensor during a temperature-induced phase transition of a hydrogel made from PNIPAM. Large molecules, such as proteins, can be partially oriented in a stretched PAM and also PNIPAM. A probe molecule has to be rigid, non-symmetrical, and provide enough ^{1}H-^{13}C or ^{1}H-^{15}N RDCs to determine alignment tensor. ^{1}H-^{1}H RDCs are not desirable due to severe overlap caused by strong coupling. Splitting of ^{2}H NMR signal of deuterated water in stretched PAM was affected by the addition of acetone, gradual changes can be seen in layers. In the case of 5 % (w/w), PAM with a molar ratio of cross-linking 50:1 observed changes of RQS occurs in about two weeks after acetone-d6 addition. The final measurement was made with acetone-d6 with a range of concentration in equilibrium from 30 % to 40 % (v/v). Acetone-d6 signal intensity in ^{2}H NMR spectra can also be used for evaluation of equilibrium of observed process. As expected by the fact that acrylamide and PAM are not soluble in acetone (acetone-d6), there was no additional splitting observed on ^{2}H signal. Splitting was created by the initial stretching of a swollen hydrogel, and as hydrogel undergoes VPT, a change of splitting into individual layers in time is observed. Splitting is not dependent on relaxation or chemical shift change due to water-acetone mixing and could be used to observe the phase transition in a new way. Stretched PAM had a splitting of about 7 Hz, line-width of the signal was about 2 Hz, observable RQS above 3 Hz could be determined. A gas bubble at the bottom of hydrogels due to different solubility of air in water-acetone mixtures severely affects NMR signals, as severe broadening and change of chemical shift due to different susceptibility was observed. Deeper insight into observed processes is required to fully understand observed processes and utilized the observation of partial orientation in hydrogel undergoing VTP.

The response of PNIPAM hydrogel was measured by MRI after temperature stimulus. Observation of slice of hydrogel provides a way to observe changes in hydrogel during VPT, at least determination of reaching equilibrium. As the phenomena of VPT correspond to the interaction between polymer network and solvent, change of NMR signal of solvent could elucidate processes undergoing in the polymer network. Another advantage for MRI is that solvent would have a much larger T_2 than polymer undergoing VPT, the NMR images would be mainly solvent. A rate of some change leading to equilibrium was observable in spatially encoded NMR data. However, similar information could be gained by utilizing a z-gradient only NMR probe, as in the case of PAM localized measurement. Diffusion filter utilization was particularly of interest due to the temperature dependence of the water diffusion coefficient, which provides additional contrast for observation of response. Semi-interpenetrated cross-linked networks based on PNIPAM were made to observe collapse and swelling in several days instead of several weeks. The first response is the immediate change on the molecular level caused by the cooperative hydration of polymer fibers. The second is induced by the hindrance of solvent inside collapsed hydrogel, which propagates from the surface to the center with time depending on dimensions, shape, and hydrogel cross-linking morphology. The second process is observed by localized NMR. Linear PAM serves as a channel network to enable the fast movement of solvent in and out of macroscopic hydrogel. To obtain the same response after the stimulus, hydrogel undergoes several cycles of collapse and swelling before measurement.

Relaxation-weighted and especially diffusion-weighted images of hydrogel enable the evaluation of homogeneity of the prepared hydrogel. Series of images from a middle part of cylindrical hydrogel was used to observe how long it takes for solvent inside hydrogel to get to equilibrium.

MRI of ^{19}F molecular probe and IONPs

MRI provides a unique non-destructive way to observe living tissues. Usage of suitable compounds that influence NMR relaxation can provide additional contrast or directly localize abnormal tissue. Novel ^{19}F molecular probe and IONPs were studied at 11.7 T. Relaxation T_1 and T_2 of new ^{19}F molecular probe with paramagnetic center and TFE were measured. Comparison of ^{19}F molecular probe measured by UTE with TFE acquired by RARE was made by determination of SNR from the images of capillaries of the same ^{19}F concentration with resolution 64 x 64 points obtained in 9.5 min. The novel molecular probe acquired by UTE showed about 6 timer higher SNR than TFE measured by RARE.

Images acquired with spin-echo-based MSME pulse sequence were used to compare T_2 contrast. Novel silica-coated IONPs provided similar T_2 contrast as commercially available ferucarbotran Resovist.

Bibliography

[1] Richard R. Ernst, Geoffrey Bodenhausen, and Alexander Wokaun. *Principles of Nuclear Magnetic Resonance in One and Two Dimensions*. Oxford University Press, 1987.

[2] M. H. Levitt. *Spin Dynamics, 2nd eddition*. Wiley 2009, ISBN 978-0-470-51117-6, 2009.

[3] V. Ntziachristos, R. Kreis, C. Boesch, and B. Quistorff. Dipolar resonance frequency shifts in h-1 mr spectra of skeletal muscle: Confirmation in rats at 4.7 t in vivo and observation of changes postmortem. *Magnetic Resonance In Medicine*, 38(1):33–39, July 1997.

[4] C. Boesch and R. Kreis. Dipolar coupling and ordering effects observed in magnetic resonance spectra of skeletal muscle. *Nmr In Biomedicine*, 14(2):140–148, April 2001.

[5] E. Brunner. Residual dipolar couplings in protein nmr. *Concepts In Magnetic Resonance*, 13(4):238–259, 2001.

[6] Hans Wolfgang Spiess. 50th anniversary perspective: The importance of nmr spectroscopy to macromolecular science. *Macromolecules*, 50(5):1761–1777, March 2017.

[7] M. C. Koetting, J. T. Peters, S. D. Steichen, and N. A. Peppas. Stimulus-responsive hydrogels: Theory, modern advances, and applications. *Materials Science & Engineering R-reports*, 93:1–49, July 2015.

[8] T. TANAKA. Collapse of gels and critical endpoint. *Physical Review Letters*, 40(12):820–823, 1978.

[9] P. Tzvetkova, S. Simova, and B. Luy. Pehsqc: A simple experiment for simultaneous and sign-sensitive measurement of ((1)j(ch)+d-ch) and ((2)j(hh)+d-hh) couplings. *Journal of Magnetic Resonance*, 186(2):193–200, June 2007.

[10] F. Kramer, M. V. Deshmukh, H. Kessler, and S. J. Glaser. Residual dipolar coupling constants: An elementary derivation of key equations. *Concepts In Magnetic Resonance Part A*, 21A(1):10–21, March 2004.

[11] G. Kummerloewe and B. Luy. Residual dipolar couplings for the configurational and conformational analysis of organic molecules. *Annual Reports On Nmr Spectroscopy, Vol 68*, 68:193–230, 2009.

[12] C. M. Thiele. Residual dipolar couplings (rdcs) in organic structure determination. *European Journal of Organic Chemistry*, (34):5673–5685, December 2008.

[13] M. Blackledge. Recent progress in the study of biomolecular structure and dynamics in solution from residual dipolar couplings. *Progress In Nuclear Magnetic Resonance Spectroscopy*, 46(1):23–61, March 2005.

[14] J. R. Tolman and K. Ruan. Nmr residual dipolar couplings as probes of biomolecular dynamics. *Chemical Reviews*, 106(5):1720–1736, May 2006.

[15] Markus Zweckstetter. Nmr: prediction of molecular alignment from structure using the pales software. *Nature Protocols*, 3(4):679–690, 2008.

[16] A. D. Elster. Mri questions and answers.

[17] Antonin Skoch, Filip Jiru, and Juergen Bunke. Spectroscopic imaging: Basic principles. *European Journal of Radiology*, 67(2):230–239, August 2008.

[18] Bernhard Blumich. *NMR Imaging of Materials*. Oxford University Press, 2000.

[19] P. Trigo-Mourino, C. Merle, M. R. M. Koos, B. Luy, and R. R. Gil. Probing spatial distribution of alignment by deuterium nmr imaging. *Chemistry-a European Journal*, 19(22):7013–7019, May 2013.

[20] A. HAASE, M. BRANDL, E. KUCHENBROD, and A. LINK. Magnetization-prepared nmr microscopy. *Journal of Magnetic Resonance Series A*, 105(2):230–233, November 1993.

[21] J. HENNIG, A. NAUERTH, and H. FRIEDBURG. Rare imaging - a fast imaging method for clinical mr. *Magnetic Resonance In Medicine*, 3(6):823–833, December 1986.

[22] C. J. BERGIN, J. M. PAULY, and A. MACOVSKI. Lung parenchyma - projection reconstruction mr-imaging. *Radiology*, 179(3):777–781, June 1991.

[23] M. D. Robson, P. D. Gatehouse, M. Bydder, and G. M. Bydder. Magnetic resonance: An introduction to ultrashort te (ute) imaging. *Journal of Computer Assisted Tomography*, 27(6):825–846, November 2003.

[24] F. Hofling and T. Franosch. Anomalous transport in the crowded world of biological cells. *Reports On Progress In Physics*, 76(4):046602, April 2013.

[25] *Disorders of Voluntary Muscle, 8th Edition*. Cambridge University Press, 2009. ISBN: 9780521876292.

[26] P. W. Kuchel, B. E. Chapman, W. A. Bubb, P. E. Hansen, C. J. Durrant, and M. P. Hertzberg. Magnetic susceptibility: Solutions, emulsions, and cells. *Concepts In Magnetic Resonance Part A*, 18A(1):56–71, May 2003.

[27] C. Boesch. Musculoskeletal spectroscopy. *Journal of Magnetic Resonance Imaging*, 25(2):321–338, February 2007.

[28] R. Kreis and C. Boesch. Spatially localized, one- and two-dimensional nmr spectroscopy and in vivo application to human muscle. *Journal of Magnetic Resonance Series B*, 113(2):103–118, November 1996.

[29] I. J. Kukurova, L. Valkovic, J. Ukropec, B. de Courten, M. Chmelik, B. Ukropcova, S. Trattnig, and M. Krssak. Improved spectral resolution and high reliability of in vivo h-1 mrs at 7 t allow the characterization of the effect of acute exercise on carnosine in skeletal muscle. *Nmr In Biomedicine*, 29(1):24–32, January 2016.

[30] Y Sharf, T Knubovets, D Dayan, A Hirshberg, S Akselrod, and G Navon. The source of NMR-detected motional anisotropy of water in blood vessel walls. *BIOPHYSICAL JOURNAL*, 73(3):1198–1204, SEP 1997.

[31] Y. Xia, J. B. Moody, and H. Alhadlaq. Orientational dependence of t-2 relaxation in articular cartilage: A microscopic mri (mu mri) study. *Magnetic Resonance In Medicine*, 48(3):460–469, September 2002.

[32] H. J. A. I. 't Zandt, D. W. J. Klomp, F. Oerlemans, B. Wieringa, C. W. Hilbers, and A. Heerschap. Proton mr spectroscopy of wild-type and creatine kinase deficient mouse skeletal muscle: Dipole-dipole coupling effects and post-mortem changes. *Magnetic Resonance In Medicine*, 43(4):517–524, April 2000.

[33] R. Kreis, B. Jung, J. Slotboom, J. Felblinger, and C. Boesch. Effect of exercise on the creatine resonances in h-1 mr spectra of human skeletal muscle. *Journal of Magnetic Resonance*, 137(2):350–357, April 1999.

[34] V. A. Selivanov, P. de Atauri, J. J. Centelles, J. Cadefau, J. Parra, R. Cusso, J. Carreras, and M. Cascante. The changes in the energy metabolism of human muscle induced by training. *Journal of Theoretical Biology*, 252(3):402–410, June 2008.

[35] W. K. J. Renema, D. W. J. Klomp, M. E. P. Philippens, A. J. van den Bergh, B. Wieringa, and A. Heerschap. Magnetization transfer effect on the creatine methyl resonance studied by cw off-resonance irradiation in human skeletal muscle on a clinical mr system. *Magnetic Resonance In Medicine*, 50(3):468–473, September 2003.

[36] M. J. Kruiskamp, R. A. de Graaf, J. van der Grond, R. Lamerichs, and K. Nicolay. Magnetic coupling between water and creatine protons in human brain and skeletal muscle, as measured using inversion transfer h-1-mrs. *Nmr In Biomedicine*, 14(1):1–4, February 2001.

[37] H. J. A. I. Zandt, A. J. C. de Grooft, W. K. J. Renema, F. T. J. J. Oerlemans, D. W. J. Klomp, B. Wieringa, and A. Heerschap. Presence of (phospho)creatine in developing and adult skeletal muscle of mice without mitochondrial and cytosolic muscle creatine kinase isoforms. *Journal of Physiology-london*, 548(3):847–858, May 2003.

[38] P. W. Kuchel, K. Kirk, and D. Shishmarev. The nmr 'split peak effect' in cell suspensions: Historical perspective, explanation and applications. *Progress In Nuclear Magnetic Resonance Spectroscopy*, 104:1–11, February 2018.

[39] Karel Bernášek, Marián Grocký, Martin Burian, and Jan Lang. Stretched gelatin phantom for detection of residual dipolar couplings in mr spectra and data analysis of carnosine. *Journal of Spectroscopy*, 2016:7, 2016.

[40] Boesch C. Kreis, R. Orientational dependence is the rule, not the exception in 1h-mr spectra of skeletal muscle: the case of carnosine. *Proceeding of International Society for Magnetic Resonance in Medicine*, 8:31, 2000.

[41] J. O. FRIEDRICH and R. E. WASYLISHEN. A h-1 and c-13 nuclear-magnetic-resonance study of carnosine. *Canadian Journal of Chemistry-revue Canadienne De Chimie*, 64(11):2132–2138, November 1986.

[42] A. A. Boldyrev, G. Aldini, and W. Derave. Physiology and pathophysiology of carnosine. *Physiological Reviews*, 93(4):1803–1845, October 2013.

[43] W. Derave, B. De Courten, and S. P. Baba. An update on carnosine and anserine research. *Amino Acids*, 51(1):1–4, January 2019.

[44] C. E. BROWN and W. E. ANTHOLINE. Chelation chemistry of carnosine - evidence that mixed complexes may occur invivo. *Journal of Physical Chemistry*, 83(26):3314–3319, 1979.

[45] L. Schroder, C. Schmitz, and P. Bachert. Molecular dynamics and information on possible sites of interaction of intramyocellular metabolites in vivo from resolved dipolar couplings in localized h-1 nmr spectra. *Journal of Magnetic Resonance*, 171(2):213–224, December 2004.

[46] K. Nagai, Y. Misonou, Y. Fujisaki, R. Fuyuki, and Y. Horii. Topical application of l-carnosine to skeletal muscle excites the sympathetic nerve innervating the contralateral skeletal muscle in rats. *Amino Acids*, 51(1):39–48, January 2019.

[47] J. W. PAN, J. R. HAMM, D. L. ROTHMAN, and R. G. SHULMAN. Intracellular ph in human skeletal-muscle by h-1-nmr. *Proceedings of the National Academy of Sciences of the United States of America*, 85(21):7836–7839, November 1988.

[48] B. M. Damon, A. C. Hsu, H. J. Stark, and M. J. Dawson. The carnosine c-2 proton's chemical shift reports intracellular ph in oxidative and glycolytic muscle fibers. *Magnetic Resonance In Medicine*, 49(2):233–240, February 2003.

[49] H. Reyngoudt, S. Turk, and P. G. Carlier. H-1 nmrs of carnosine combined with p-31 nmrs to better characterize skeletal muscle ph dysregulation in duchenne muscular dystrophy. *Nmr In Biomedicine*, 31(1):e3839, January 2018.

[50] Mahir S. R. Ozdemir, Harmen Reyngoudt, Yves De Deene, Hakan S. Sazak, Els Fieremans, Steven Delputte, Yves D'Asseler, Wim Derave, Ignace Lemahieu, and Eric Achten. Absolute quantification of carnosine in human calf muscle by proton magnetic resonance spectroscopy. *Physics In Medicine and Biology*, 52(23):6781–6794, December 2007.

[51] R. C. Harris, M. J. Tallon, M. Dunnett, L. Boobis, J. Coakley, H. J. Kim, J. L. Fallowfield, C. A. Hill, C. Sale, and J. A. Wise. The absorption of orally supplied beta-alanine and its effect on muscle carnosine synthesis in human vastus lateralis. *Amino Acids*, 30(3):279–289, May 2006.

[52] V. H. Carvalho, A. H. S. Oliveira, L. F. de Oliveira, R. P. da Silva, P. Di Mascio, B. Gualano, G. G. Artioli, and M. H. G. Medeiros. Exercise and beta-alanine supplementation on carnosine-acrolein adduct in skeletal muscle. *Redox Biology*, 18:222–228, September 2018.

[53] D. Spelnikov and R. C. Harris. A kinetic model of carnosine synthesis in human skeletal muscle. *Amino Acids*, 51(1):115–121, January 2019.

[54] L. Schroder and P. Bachert. Evidence for a dipolar-coupled am system in carnosine in human calf muscle from in vivo h-1 nmr spectroscopy. *Journal of Magnetic Resonance*, 164(2):256–269, October 2003.

[55] S. S. Velan, S. Ramamurthy, S. Ainala, C. Durst, S. K. Lemieux, R. R. Raylman, R. G. Spencer, and M. A. Thomas. Implementation and validation of localized constant-time correlated spectroscopy (lct-cosy) on a clinical 3t mri scanner for investigation of muscle metabolism. *Journal of Magnetic Resonance Imaging*, 26(2):410–417, August 2007.

[56] S. Ramadan, E. M. Ratai, L. L. Wald, and C. E. Mountford. In vivo 1d and 2d correlation mr spectroscopy of the soleus muscle at 7t. *Journal of Magnetic Resonance*, 204(1):91–98, May 2010.

[57] C. Naumann, W. A. Bubb, B. E. Chapman, and P. W. Kuchel. Tunable-alignment chiral system based on gelatin for nmr spectroscopy. *Journal of the American Chemical Society*, 129(17):5340–+, May 2007.

[58] G. Kummerlowe, M. U. Kiran, and B. Luy. Covalently cross-linked gelatin allows chiral distinction at elevated temperatures and in dmso. *Chemistry-a European Journal*, 15(45):12192–12195, 2009.

[59] J. J. Chou, S. Gaemers, B. Howder, J. M. Louis, and A. Bax. A simple apparatus for generating stretched polyacrylamide gels, yielding uniform alignment of proteins and detergent micelles. *Journal of Biomolecular Nmr*, 21(4):377–382, December 2001.

[60] V. M. Gun'ko, I. N. Savina, and S. V. Mikhalovsky. Properties of water bound in hydrogels. *Gels*, 3(4):37, December 2017.

[61] K. Saalwachter. Proton multiple-quantum nmr for the study of chain dynamics and structural constraints in polymeric soft materials. *Progress In Nuclear Magnetic Resonance Spectroscopy*, 51(1):1–35, August 2007.

[62] N. A. Hadjiev and B. G. Amsden. An assessment of the ability of the obstruction-scaling model to estimate solute diffusion coefficients in hydrogels. *Journal of Controlled Release*, 199:10–16, February 2015.

[63] Y. E. Shapiro. Structure and dynamics of hydrogels and organogels: An nmr spectroscopy approach. *Progress In Polymer Science*, 36(9):1184–1253, September 2011.

[64] B. Amsden. Solute diffusion within hydrogels. mechanisms and models. *Macromolecules*, 31(23):8382–8395, November 1998.

[65] K. T. Yung. Mri measurements of t-1, t-2 and d for gels undergoing volume phase transition. *Magnetic Resonance Imaging*, 21(2):PII S0730–725X(02)00639–2, February 2003.

[66] Yulia B. Monakhova, Mikhail V. Pozharov, Tamara V. Zakharova, Evgeniya K. Khvorostova, Aleksej V. Markin, Dirk W. Lachenmeier, Thomas Kuballa, and Svetlana P. Mushtakova. Association/Hydrogen Bonding of Acetone in Polar and Non-polar Solvents: NMR and NIR Spectroscopic Investigations with Chemometrics. *JOURNAL OF SOLUTION CHEMISTRY*, 43(11):1963–1980, NOV 2014.

[67] H. G. SCHILD. Poly (n-isopropylacrylamide) - experiment, theory and application. *Progress In Polymer Science*, 17(2):163–249, 1992.

[68] J. Spevacek. Nmr investigations of phase transition in aqueous polymer solutions and gels. *Current Opinion In Colloid & Interface Science*, 14(3):184–191, June 2009.

[69] K. Laszlo, A. Guillermo, A. Fluerasu, A. Moussaid, and E. Geissler. Microphase structure of poly(n-isopropylacrylamide) hydrogels as seen by small- and wide-angle x-ray scattering and pulsed field gradient nmr. *Langmuir*, 26(6):4415–4420, March 2010.

[70] T. M. Alam, K. K. Childress, K. Pastoor, and C. V. Rice. Characterization of free, restricted, and entrapped water environmentsin poly(n-isopropyl acrylamide) hydrogels via 1h hrmas pfg nmrspectroscopy. 52:15211527, 2014.

[71] K. Makino, J. Hiyoshi, and H. Ohshima. Kinetics of swelling and shrinking of poly (n-isopropylacrylamide) hydrogels at different temperatures. *Colloids and Surfaces B-biointerfaces*, 19(2):197–204, December 2000.

[72] R. Pelton. Poly(n-isopropylacrylamide) (pnipam) is never hydrophobic. *Journal of Colloid and Interface Science*, 348(2):673–674, August 2010.

[73] H. Kojima and F. Tanaka. Cooperative hydration induces discontinuous volume phase transition of cross-linked poly(n-isopropylacrylamide) gels in water. *Macromolecules*, 43(11):5103–5113, June 2010.

[74] S. HIROTSU and A. ONUKI. Volume phase-transition of gels under uniaxial tension. *Journal of the Physical Society of Japan*, 58(5):1508–1511, May 1989.

[75] E. Kutnyanszky, A. Embrechts, M. A. Hempenius, and G. J. Vancso. Is there a molecular signature of the lcst of single pnipam chains as measured

by afm force spectroscopy? *Chemical Physics Letters*, 535:126–130, May 2012.

[76] M. Duskova-Smrckova and K. Dusek. How to force polymer gels to show volume phase transitions. *Acs Macro Letters*, 8(3):272–278, March 2019.

[77] S. Ganapathy, P. R. Rajamohanan, M. V. Badiger, A. B. Mandhare, and R. A. Mashelkar. Proton magnetic resonance imaging in hydrogels: volume phase transition in poly(n-isopropylacrylamide). *Polymer*, 41(12):4543–4547, June 2000.

[78] S. Kariyo, M. Kuppers, M. V. Badiger, A. Prabhakar, B. Jagadeesh, S. Stapf, and B. Blumich. Morphology and chain dynamics during collapse transition of pnipam gels studied by combined imaging, relaxometry and xe-129 spectroscopy techniques. *Magnetic Resonance Imaging*, 23(2):249–253, February 2005.

[79] M. Knorgen, K. F. Arndt, S. Richter, D. Kuckling, and H. Schneider. Investigation of swelling and diffusion in polymers by h-1 nmr imaging: Lcp networks and hydrogels. *Journal of Molecular Structure*, 554(1):69–79, October 2000.

[80] H. Shirota, N. Kuwabara, K. Ohkawa, and K. Horie. Deuterium isotope effect on volume phase transition of polymer gel: Temperature dependence. *Journal of Physical Chemistry B*, 103(47):10400–10408, November 1999.

[81] Shunsuke Kametani, Sokei Sekine, Takahiro Ohkubo, Tomohiro Hirano, Koichi Ute, H. N. Cheng, and Tetsuo Asakura. NMR studies of water dynamics during sol-to-gel transition of poly (N-isopropylacrylamide) in concentrated aqueous solution. *POLYMER*, 109:287–296, JAN 27 2017.

[82] A. Schuetz, T. Murakami, N. Takada, J. Junker, M. Hashimoto, and C. Griesinger. Rdc-enhanced nmr spectroscopy in structure elucidation of sucro-neolambertellin. *Angewandte Chemie-international Edition*, 47(11):2032–2034, 2008.

[83] S. Hirotsu. Anomalous kinetics of the volume phase transition in poly-n-isopropylacrylamide gels. *Japanese Journal of Applied Physics Part 2-letters*, 37(3A):L284–L287, March 1998.

[84] M. VALTIER, P. TEKELY, L. KIENE, and D. CANET. Visualization of solvent diffusion in polymers by nmr microscopy with radiofrequency field gradients. *Macromolecules*, 28(12):4075–4079, June 1995.

[85] G. Kummerlowe, E. F. McCord, S. F. Cheatham, S. Niss, R. W. Schnell, and B. Luy. Tunable alignment for all polymer gel/solvent combinations for the measurement of anisotropic nmr parameters. *Chemistry-a European Journal*, 16(24):7087–7089, 2010.

[86] New Era. New era enterprizes, inc.

[87] Andreas Enthart, J. Christoph Freudenberger, Julien Furrer, Horst Kessler, and Burkhard Luy. The clip/clap-hsqc: Pure absorptive spectra for the measurement of one-bond couplings. *Journal of Magnetic Resonance*, 192(2):314–322, June 2008.

[88] J. D. van Beek. matnmr: A flexible toolbox for processing, analyzing and visualizing magnetic resonance data in matlab((r)). *Journal of Magnetic Resonance*, 187(1):19–26, July 2007.

[89] P. A. Bottomley. Spatial localization in nmr spectroscopy in vivo. *Annals of the New York Academy of Sciences*, 508:333–348, 1987.

[90] I. Tkáč, Z. Starčuk, I.-Y. Choi, and R. Gruetter. In vivo 1h nmr spectroscopy of rat brainat 1 ms echo time. *Magnetic Resonance in Medicine*, 41:649656, 2008.

[91] H. Thiele, G. McLeod, M. Niemitz, and T. Kuhn. Structure verification of small molecules using mass spectrometry and nmr spectroscopy. *Monatshefte Fur Chemie*, 142(7):717–730, July 2011.

[92] S. Kim, J. Chen, T. J. Cheng, A. Gindulyte, J. He, S. Q. He, Q. L. Li, B. A. Shoemaker, P. A. Thiessen, B. Yu, L. Zaslavsky, J. Zhang, and E. E. Bolton. Pubchem 2019 update: improved access to chemical data. *Nucleic Acids Research*, 47(D1):D1102–D1109, January 2019.

[93] W. Humphrey, A. Dalke, and K. Schulten. Vmd: Visual molecular dynamics. *Journal of Molecular Graphics & Modelling*, 14(1):33–38, February 1996.

[94] A. Kolmer, L. J. Edwards, I. Kuprov, and C. M. Thiele. Conformational analysis of small organic molecules using noe and rdc data: A discussion of strychnine and alpha-methylene-gamma-butyrolactone. *Journal of Magnetic Resonance*, 261:101–109, December 2015.

[95] D. Chretien, P. Benit, H. H. Ha, S. Keipert, R. El-Khoury, Y. T. Chang, M. Jastroch, H. T. Jacobs, P. Rustin, and M. Rak. Mitochondria are physiologically maintained at close to 50 degrees c. *Plos Biology*, 16(1):e2003992, January 2018.

[96] L. Schorder, C. H. J. Schmitz, and P. Bachert. Carnosine as molecular probe for sensitive detection of cu(ii) ions using localized h-1 nmr spectroscopy. *Journal of Inorganic Biochemistry*, 102(2):174–183, February 2008.

[97] T.-P. Hsu, D. S. Ma, and C. Cohen. Effects of inhomogeneities in polyacrylamidegels on thermodynamic and transportproperties. 24:1273–1278, 1983.

[98] P. G. De Gennes. *Scaling Concepts in Polymer Physics*. Cornell University Press, Ithaca, NY, 1979.

[99] M. Holz, S. R. Heil, and A. Sacco. Temperature-dependent self-diffusion coefficients of water and six selected molecular liquids for calibration in

accurate h-1 nmr pfg measurements. *Physical Chemistry Chemical Physics*, 2(20):4740–4742, 2000.

[100] L. Starovoytova and J. Spevacek. Effect of time on the hydration and temperature-induced phase separation in aqueous polymer solutions. h-1 nmr study. *Polymer*, 47(21):7329–7334, October 2006.

[101] J. Blahut, K. Bernasek, A. Galisova, V. Herynek, I. Cisarova, J. Kotek, J. Lang, S. Matejkova, and P. Hermann. Paramagnetic f-19 relaxation enhancement in nickel(ii) complexes of n-trifluoroethyl cyclam derivatives and cell labeling for f-19 mri. *Inorganic Chemistry*, 56(21):13337–13348, November 2017.

[102] F. Schmid, C. Holtke, D. Parker, and C. Faber. Boosting f-19 mri-snr efficient detection of paramagnetic contrast agents using ultrafast sequences. *Magnetic Resonance In Medicine*, 69(4):1056–1062, April 2013.

[103] M. Weiger, K. P. Pruessmann, and F. Hennel. Mri with zero echo time: Hard versus sweep pulse excitation. *Magnetic Resonance In Medicine*, 66(2):379–389, August 2011.

[104] M. Carl, J. T. A. Chiang, and J. Du. Maximizing mr signal for 2d ute slice selection in the presence of rapid transverse relaxation. *Magnetic Resonance Imaging*, 32(8):1006–1011, October 2014.

[105] L. Kubickova, P. Brazda, M. Veverka, O. Kaman, V. Herynek, M. Vosmanska, P. Dvorak, K. Bernasek, and J. Kohout. Nanomagnets for ultrahigh field mri: Magnetic properties and transverse relaxivity of silica-coated epsilon-fe2o3. *Journal of Magnetism and Magnetic Materials*, 480:154–163, June 2019.

[106] Z. Berkova, D. Jirak, K. Zacharovova, J. Kriz, A. Lodererova, P. Girman, T. Koblas, E. Dovolilova, M. Vancova, M. Hajek, and F. Saudek. Labeling of pancreatic islets with iron oxide nanoparticles for in vivo detection with magnetic resonance. *Transplantation*, 85(1):155–159, January 2008.

List of Figures

1.1 P.E.HSQC pulse sequence. 7
1.2 The z imaging pulse sequences. 11

2.1 Structure of muscle unit. 15
2.2 Localized NMR spectra of muscle tissue for ^{1}H, ^{13}C, and ^{31}P . . . 16
2.3 Types of muscles defined by pennation angle. 16
2.4 Schematic molecular structure of carnosine 18
2.5 Localized NMR spectra of muscle. 19
2.6 L-COSY spectra of muscle tissue *in vivo*. 20

3.1 Dependence of additional splitting on stretching of gelatin. 21
3.2 PAM alignment by composition and stretching. 22
3.3 The swelling ratio for two PAM gels. 24

4.1 Stretching apparatus for 5 mm NMR tubes. 28
4.2 Apparatus for preparation of strained PAM [59]. 29

5.1 Gelatin samples 33
5.2 Sample with 20 % gelatin 34
5.3 Carnosine in 20 % gelatin 34
5.4 Carnosine in 40 % gelatin 35
5.5 Localized ^{1}H NMR spectrum from 4.7 T 35
5.6 ^{1}H NMR spectrum from entire sample at 4.7 T 36
5.7 ^{13}C NMR spectrum at 4.7 T 36
5.8 Carnosine conformation 40

6.1 Photographs of PAM sample with 40 % (v/v) of acetone-d6 . . . 46
6.2 Samples of cross-linked PNIPAM with linear PAM 47
6.3 RQS observation after addition of acetone to PAM 49
6.4 Hydrogel length dependence on acetone-d6 concentration 51
6.5 Intensity of ^{2}H acetone-d6 signal in time 52
6.6 RQS of ^{2}H water signal in 6 time intervals 55
6.7 Slice position during volume phase transition. 56
6.8 Proton density MRI of responsive hydrogel. 57
6.9 Diameter of gel from MRI image. 57
6.10 Collapsed hydrogels measured with diffusion weighted MRI. . . . 58
6.11 Collapsed hydrogels measured with diffusion weighted MRI. . . . 58
6.12 Collapsed hydrogels measured with diffusion weighted MRI. . . . 59

7.1 ^{19}F and ^{1}H images of phantom. 64
7.2 ^{19}F and ^{1}H images of labeled cells. 65
7.3 T_2 weighted ^{1}H images of water with iron-oxide nanoparticles . . 67
7.4 ^{1}H image of water with IONPs in 5 mm NMR tube 68
7.5 Dependence of SNR on TE for FLASH. 68
7.6 Dependence of SNR on TE for MSME. 69

List of Tables

5.1 Total splitting from ^{1}H-^{13}C P.E.HSQC spectra of unstretched gelatin in Hz. 39
5.2 Measured RDCs of carnosine in gelatin samples. Magnitude of RDCs correspond to stretching ratio of 1.2, 1.4, 1.3, and 1.3 for 20%, 30%, 40%, and phantom, respectively 39

6.1 Details about the samples and addition of acetone-d6. 50

List of Abbreviations

1D	one-dimensional
2D	two-dimensional
ADC	apparent diffusion coefficient
AM	acrylamide
APS	ammonium persulfare
BB	broadband
BIS	*N,N"*-methylenebis(acrylamide)
BW	bandwidth
CA	contrast agent
CEST	chemical exchange saturation transfer
COSY	correlated spectroscopy
CPMG	Carr-Purcell-Meiboom-Gill
D_2O	heavy water
DTI	diffusion tensor imaging
DWI	diffusion weighted imaging
EPI	echo-planar imaging
Eq.	equation
et al.	et alia
FID	free induction decay
Fig.	figure
FLASH	fast low-angle shot
FOV	field of view
FT	Fourier transform
FWHM	full width at half maximum
Gd	gadolinium
H_2O	light water (no deuterium enrichment)
HDO	semi-heavy water
HSQC	heteronuclear single quantum coherence
i.e.	id est
IPAP	in-phase anti-phase
IKEM	Institute of clinical and experimental medicine
IONPs	iron oxide nanoparticles
IUPAC	International union of pure and applied chemistry
LCST	lower critical solution temperature
MAS	magic angle spinning
MFF UK	Faculty of Mathematics and Physics Charles University
MRI	magnetic resonance imaging
MRS	magnetic resonance spectroscopy
MRSI	magnetic resonance spectroscopy imaging
MSME	multi slice multi echo
NIPAM	*N*-isopropylacrylamide
NMR	nuclear magnetic resonance
PALES	prediction of alignment from structure
PAM	polyacrylamide
PFG	pulse field gradient

PNIPAM	poly(*N*-isopropylacrylamide)
RARE	rapid acquisition with relaxation enhancement
RF	radio-frequency
SAG	Strain-induced alignment in gels
SAR	specific absorption rate
SNR	signal to noise ratio
$\mathbf{T}_1$	longitudinal relaxation time
$\mathbf{T}_2$	transversal relaxation time
Tab.	table
TE	time echo
TFE	2,2,2-trifluoroethanol
TEMED	*N*,*N*,*N'*,*N'*-tetramethylethylenediamine
UTE	ultrashort time echo
VPT	volume phase transition
ZTE	zero time echo

List of Conference Contributions

I. Bernášek, K., Grocký, M., Lang, J., RDC of muscle metabolites in a gel model, talk, NMR Valtice 2012, 27th Central European NMR Meeting, Valtice, Czech Republic (2012)

II. Bernášek, RDC of muscle metabolites in a gel model, talk, 21st Annual Student Conference, Week of Doctoral Students 2012, Prague, Czech Republic (2012)

III. Bernášek, K., Grocký, M., Lang, J., Gelatin phantom for carnosine's RDC, poster, Ampere NMR School, Zakopane, Polland (2013)

IV. Bernášek, K., Hanyková, L., Lang J., ^{2}H chemical shift imaging of phase transition in polyacrylamide network, talk, NMR Valtice 2016, 31st Central European NMR Meeting, Valtice, Czech Republic (2016)

V. Bernášek, K., Hanyková, L., Lang, J., MRI study of temperature responsive hydrogel networks based on *N*-isopropylacrylamide, talk, NMR Valtice 2017, 32nd Central European NMR Meeting, Valtice, Czech Republic (2017)

VI. Bernášek, K., Hanyková, L., Lang, J., MRI study of temperature responsive hydrogel networks based on *N*-isopropylacrylamide, poster, EUROMAR 2017, Warsaw, Polland (2017)

VII. Bernášek, K., *N*-isopropylacrylamide based cross-linked hydrogel stimuli-responsive behavior observed by MRI, poster, MMCE 2019, Prague (2019)

List of Publications

Articles associated with this thesis:

1 Bernášek Karel, Grocký Marián, Burian Martin, Lang Jan. *Stretched gelatin phantom for detection of residual dipolar couplings in MR spectra and data analysis for carnosine*, Journal of Spectroscopy, Volume 2016, Article ID 4596542, DOI 10.1155/2016/4596542

2 Blahut Jan, Bernášek Karel, Gálisová Andrea, Herynek Vít, Císařová Ivana, Kotek Jan, Lang Jan, Matějková Stanislava, and Hermann Petr. *Paramagnetic ^{19}F relaxation enhancement in nickel(II) complexes of N-trifluoroethyl cyclam derivatives and cell labeling for ^{19}F MRI* Inorganic Chemistry, 2017, 56, 13337-13348, DOI 10.1021/acs.inorgchen.7b02119

3 Kubíčková Lenka, Brázda Petr, Veverka Miroslav, Kaman Ondřej, Herynek Vít, Vosmanská Magda, Dvořák Petr, Bernášek Karel, Kohout Jaroslav. *Nanomagnets for ultra-high field MRI: Magnetic properties and transverse relaxivity of silica-coated ϵ-Fe_2O_3* Journal of magnetism and magnetic materials 480 (2019) 154-163, DOI 10.1016/j.jmmm.2019.02.067

Other articles of the author:

1 Kubíčková Lenka, Kaman Ondřej, Veverka Pavel, Herynek Vít, Brázda Petr, Bernášek Karel, Veverka Miroslav, Kohout Jaroslav *Magnetic properties, ^{57}Fe Mössbauer spectroscopy and ^{1}H NMR relaxometry of ϵ-$Fe_{2-x}Ga_xO_3$ nanoparticles: the effect of galium doping on magnetism and MRi performance* Journal of Alloys and Compounds 856 (2021) 158187, DOI 10.1016/j.jallcom.2020.158187

A. Attachments

A.1 First Attachment